Development of Evanescent wave based Sensor platforms for use in Immunosensing.

By

Colm McAtamney B.Sc. (Hons)

A thesis presented

To

Dublin City University

For the degree of Master Of Science

October 1999

School of Physical Sciences

Dublin City University

Ireland

Declaration

I hereby certify that this material, which I now submit for assessment on the program of study leading to the award of Master of Science is entirely my own work and has not been taken from the work of others save and to the extent that such work has been cited and acknowledged within the text of my work.

Signed: _____ Date: 3/2/00

Dedication

To Mam, Dad, Hugh, Ruth and Amy

Acknowledgements

I would like to thank the members of the Optical Sensors Group past and present, especially Paud, Aidan, Mick, Antoinette, Penny and Sarah-Jane for all those nights in the bar. Thanks also to Marian and Katrina in the office. How you put up with us is a mystery to me.

Thank you to Dr Colette McDonagh, Professor Martin Henry and Dr Brian Lawless for their valuable assistance during the course of this thesis.

I would also like to thank the physics technicians Alan Hughes, Al Devine and especially Des Lavelle. Des thanks for making me see that the Neville brothers are rubbish, Oh and for all the work you did for me aswell. Thank you to Dr John Quinn for all the help with the biology.

Last but not least, thanks to my supervisor Professor Brian MacCraith. The last three years have been very enjoyable. Thanks for the guidance throughout and the opportunity to do this Masters.

Abstract

Two optical sensor platforms based on evanescent wave interactions for detection of biomolecules are presented. The first, a sol-gel derived planar waveguide, employs a grating coupler to couple light into a guided mode. The evanescent field of the mode interrogates the sensing layer. The platform employing mono-mode waveguides is described and applied to the imaging of fluorescently labelled antibodies which are immobilised on the waveguide surface. The antibodies, immunoglobulin G, are immobilised via an avidin-biotin bridge. First avidin is coated onto a silanized waveguide via a crosslinker. Then the surface is incubated with biotinylated fluorescently labelled antibodies. Compact optics image the evanescently excited fluorescence onto a large area, cooled CCD array. The image data is processed and corrected for local background levels.

The second, a Surface Plasmon Resonance (SPR) refractive index sensor comprises of an integrated miniature SPR device interfaced to a computer. The sensor combines all of the necessary electro-optical components to excite a surface plasmon wave and quantify the resonance condition, within a single platform. This sensor is applied to liquid refractive index sensing and the monitoring of biomolecular interactions. Finally, work leading to the development of disposable sensor chips for use on the TI SPR sensor is presented.

Table of Contents

Chapter 1 Introduction

1.1 Introduction

Biosensors have generated wide interest in both scientific and industrial communities owing to their wide range of application in areas such as medical diagnostics, process control and environmental monitoring.

Biosensors are analytical devices, which use a biological detection or recognition system for a target molecule in association with a physicochemical transducer, which converts the biological recognition event into a usable output signal. The biomolecules used in biosensors are chosen mainly for their specificity, which is employed to recognise a particular analyte. Biomolecules used in biosensors include receptors such as antibodies, enzymes, chelators, DNA probes and ionophores. Immunosensors are those sensors which use antibodies as recognition elements.

The basic principles of immunosensing have been adopted from the well-established technique of immunoassays, the origin of which was founded on the research performed by Yalow and Benson in the late fifties[1]. Their analysis of human insulin, using information obtained from its binding with insulin-specific antibody, provided one of the earliest successes in solution phase radioimmunoassay (RIA). The first biosensor followed soon after in the form of the Clark and Lyons electrochemical sensor for glucose and urea[2].

Since immunoassays tend to be labour intensive and are not designed for continuous monitoring, a lot of work has been directed toward the fabrication of simpler immunosensor devices. The development of optical transducers and the availability of cheaper instrumentation have helped this development.

All immunsensors can be characterised by two essential components: (1) The biochemical component which may include one or more antibodies and additional signal generating molecules. (2) The transducer component which actually measures the antibody binding event.

1.2 Optical Immunosensors

One of the major advantages of optical sensors is their ability to probe surfaces and films in a non-destructive manner. Additionally they offer advantages in terms of safety, sensitivity and speed as well as permitting *in situ* sensing and real time measurements. Optical sensors are the next most commonly used transducers after amperometric and potentiometric devices. Optical phenomena exploited in the various types of optical transducers include light absorption, fluorescence/phosphorescence, bio/chemiluminescence, reflectance, Raman scattering and refractive index.

Optical immunosensors are receiving attention as alternatives to conventional immunoassay techniques, due to their promise of enhanced sensitivity and the elimination of expensive and time-consuming separation and incubation procedures. An optical immunosensor consists of either an antibody or antigen immobilised on a suitable surface. Its function, upon interaction with a biospecific immunological component, is to produce a measurable optical signal.

If binding occurs between an immobilised antibody and an antigen on a transducer surface, the properties of the solid phase are altered. The increase in layer thickness or surface coverage can be measured in terms of a change in refractive index, mass increase, or reflective properties. A device capable of measuring such parameters directly associated with the immunoreaction on the surface can be referred to as a direct immunosensor. Direct optical immunosensing techniques include surface plasmon resonance[3] and ellipsometry[4]. Planar waveguides have also been employed as direct immunosensors[5].

Indirect immunosensors employ labels tagged to one of the components of an immunoreaction (antibody or antigen). The label is capable of signal generation due to some secondary reaction. Typical labels employed in immunoassays are radioactive markers, enzymes, electroactive compounds or fluorophores. In the case of indirect optical immunosensors, fluorophores are the predominant label used. Evanescent wave techniques, such as mono-mode or multi-mode dielectric waveguides, are often employed as the interrogation mechanism in indirect[6,7,8] immunosensors

An important limitation of direct immunosensors, is non-specific binding on the transducer surface, since the working principle is based on the measurement of alterations on the transducer surface. Non-specific binding leads to generation of a signal response independent of the antibody/antigen interaction. This non-specific binding increases the limit of detection, and the signal to noise ratio tends to be smaller compared to a sensor using specific signal enhancement by labelling. In an indirect optical immunosensor, only non-specific binding with labelled components can increase background signal. Non-specific binding of other sample components, not labelled, does not produce a signal as long as the chosen label does not exhibit spectral overlap with other sample components. For this reason, indirect methods generally produce better signal to noise ratios.

This thesis reports work on direct (surface plasmon resonance) and indirect (evanescent wave planar waveguide fluoro-immunosensors) techniques.

1.2.1 Evanescent wave fluorescence immunosensors

An evanescent field is generated whenever light is totally internally reflected at an interface[9]. Figure 1.1 illustrates light propagating in an optical waveguide. For all angles greater than the critical angle, θ_c, light is internally reflected and travels the length of the waveguide.

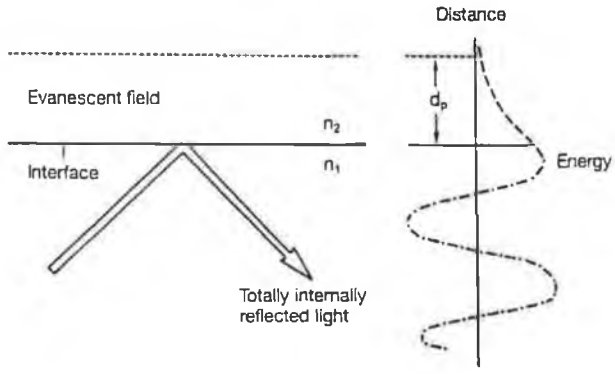

Figure 1.1 Propagation of light along an optical waveguide.

The critical angle is defined as

$$\theta_c = \sin^{-1} \frac{n_2}{n_1} \qquad 1.1$$

As the optical energy propagates along a waveguide, a small fraction extends a short distance beyond the guiding layer and into the surrounding media of lower refractive index. This is usually characterised by its electric field strength and is known as the evanescent field. This evanescent field decays exponentially from the waveguide surface. The distance over which the electric field decays by a factor of e^{-1} of its value at the interface is known as the penetration depth and is given by

$$d_p = \frac{\lambda}{2\pi\left(n_1^2 \cdot \sin^2 \theta_1 - n_2^2\right)^{1/2}} \qquad 1.2$$

Evanescent wave immunosensing can be either direct or indirect. In direct sensing, binding of an analyte to an antibody immobilised on the waveguide surface can alter the dielectric properties of the surface layer, producing a modified reflected signal, which can then be measured. A wider scope of applications can be realised if a fluorescent reagent is introduced to the antibody-analyte complex. The evanescent wave can excite the fluorescent molecule causing it to emit radiation. This emitted radiation can be detected by a variety of detectors, e.g., photomultiplier tubes or CCD cameras. Fluorophores outside the evanescent field are not excited and their presence does not interfere with the signal, thus eliminating the need for a washing step and reducing both the time and complexity of the assay. Furthermore, nonspecific adsorption of sample components that are not fluorescent does not generate a signal and is not therefore a source of interference.

Evanescent wave immunosensors have utilised both planar waveguides[6,7,8] and optical fibres[10]. Planar waveguides can be plain glass microscope slides but often the glass slides are used as a support for a light guiding layer with a higher refractive index.

Techniques for depositing these thin films onto planar surfaces include reactive low-voltage ion plating, spin coating and dip-coating. Compared with optical fibres the substrate surface is easier to coat with a reagent layer. This ease in coating and the surface area provided by the substrate allow for the construction of multianalyte sensors[12,13] onto a single waveguide. In addition planar waveguides can be easily handled and are less expensive to mass produce.

In this work, the fabrication of high refractive index sol-gel waveguiding layers, via a dip coating technique is reported. The sol-gel process is a method of preparing glasses and ceramics at low temperatures by hydrolysis and condensation reactions using organic or inorganic precursors[14]. The waveguides produced by this process are used to develop a platform for multi-analyte fluoro-immunosensors

1.2.2 Surface Plasmon Resonance Sensors

The technique of surface plasmon resonance (SPR) has been applied extensively to immunological sensing, due to its high sensitivity for monitoring optical changes at interfaces between a thin metal film and a dielectric fluid.

SPR is an optical reflectance procedure, which is sensitive to dielectric properties of the medium close to a metal surface[15]. A surface plasmon is an electromagnetic field charge density oscillation that can exist at a metal-dielectric interface. It propagates as a bound non-radiative surface electromagnetic mode along the metal-dielectric interface, and is resonantly excited by p-polarised light once the surface wavevectors of the incident radiation and the surface plasmon waves are matched. Upon excitation, an electromagnetic field is formed which decays exponentially with distance from the metal film surface into the interfacing medium. When resonance occurs, the reflected light intensity from the metal surface goes through a minimum at a defined angle of incidence. The plasmon resonance angle depends on optical properties of the medium under the metal layer, the type and thickness of the metal, the wavelength of the incident light and changes in the refractive index layer above the metal surface. It is this last factor which is important for sensing.

SPR was first demonstrated in 1968 by Otto[15] using the prism/air-gap/metal configuration shown in figure 1.2a. Otto showed that, at a specific angle of incidence, the internal reflection of the light beam from the inner surface of a prism was significantly attenuated if a silver film was brought close to the prism surface. The problem with this configuration, however, is the difficulty of maintaining a small and precise separation between prism and metal[2] . A more favoured configuration is the Attenuated Total Reflection (ATR) method, proposed by Kretschmann and Raether[16], shown in figure 1.2b, in which the air gap is replaced by the metal itself.

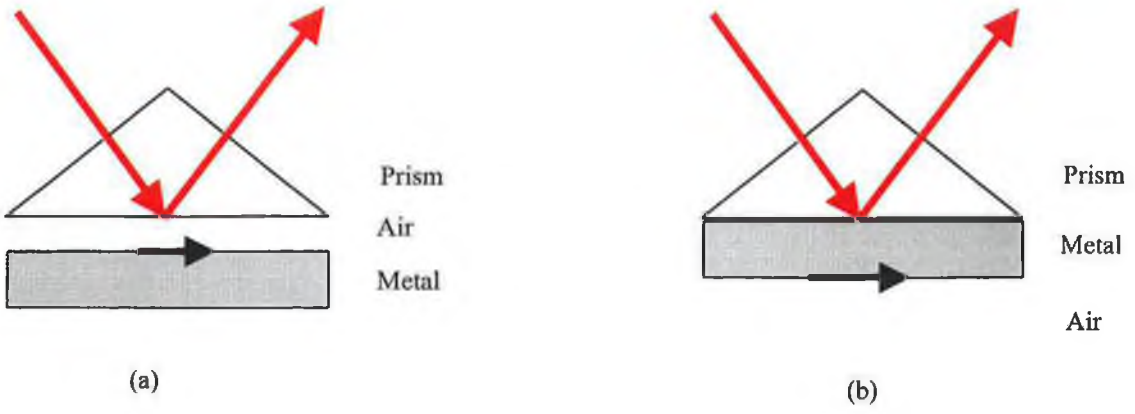

Figure 1.2 (a) Otto configuration; (b) Kretschmann and Raether configuration

In 1983 Liedberg proposed SPR as a technique to monitor antigen-antibody interactions at the surface of a silver film[3]. The interactions between gamma globulin IgG antibodies adsorbed on the silver surface and anti-gamma globulin IgG antibodies were evaluated. The resultant change in thickness and local dielectric constant of the reacting surface as the interaction took place changed the SPR angle and this was seen in the reflectivity. This work prompted considerable research interest in the study of immunoreactions using SPR.

Despite these extensive studies, a real-time immunosensor has become commercially available only recently (BIAcore™, Pharmacia Biosensor AB, Uppsala,

Sweden). The Biosensor group in Pharmacia in Sweden described the detection of various proteins on a sensor chip consisting of a thin gold film deposited on a glass slide and covered with a carboxymethyl-dextran hydrogel matrix[17].

Miniaturised SPR sensors using the ATR method have been developed as an alternative to laboratory based SPR systems such as the BIAcore™ SPR sensor. These have been developed as compact and cost effective sensing devices with potential for field applications. One such sensor, developed by Texas Instruments[18], integrates a light source, a detector and an optical system for excitation and interrogation of surface plasmon waves into a single sensor chip. The system relies on the detection of the angular position of surface plasmon resonance by measuring the reflection of a divergent light beam, using a 128 pixel linear Si detector array. It includes a temperature sensor and exhibits a resolution of 1×10^{-5} refractive index units (RIU) [13].

Part of this thesis deals with the use of the Texas Instruments (TI) surface plasmon resonance sensor for both liquid refractive index sensing, and monitoring of biomolecule interactions. Work was also carried out on the fabrication of gold-coated glass slides for use as disposable sensor chips on the TI SPR sensor.

1.3 Biomolecule Immobilisation

The usual aim in biosensor construction is to produce a thin film of immobilised biologically active material on a transducer surface. This material should only respond to the presence of one or a group of materials requiring detection. For an immobilisation technique to be of practical use, a number of requirements need to be satisfied:

1. The biological layer must remain bound tightly to the sensor surface whilst retaining its structure and function.
2. The biological component must retain its activity when attached to the sensor surface.
3. The biological component needs to have long term stability.
4. The biological component needs to retain its specificity

The principal methods of immobilisation are: (1) Non-specific adsorption. (2) Entrapment within a membrane. (3) Direct covalent linkage. (4) Indirect covalent linkage via a spacer or a carrier protein already linked to the surface.

Non-specific adsorption of antibodies onto solid surfaces can proceed via either physical or chemical interactions[19]. Physical adsorption involves van der Waals forces, ionic binding or hydrophobic forces, whereas in chemisorption there is a sharing or transfer of electrons to form a chemical bond. It is the simplest method of antibody immobilisation. While a reasonable density of antibodies can be immobilised in this way, the activity is usually variable and dissociation and denaturing of the protein may occur.

In contrast, covalent binding is the preferred method of attaching an antibody to a surface due to the strong, stable linkage. Antibodies have functional groups present for covalent immobilisation onto surfaces, these include amino-acid side chains, carboxyl groups and thiol groups. Covalent coupling between the antibody and the sensor surface is best achieved through functional groups on the antibody, which are not required for biological activity. Covalent binding also has the advantage that the biomolecule is generally strongly immobilised on the surface and therefore unlikely to detach from the surface during use.

Suitable functional groups, which are available for covalent attachment, are also on some transducer surfaces (e.g. hydroxyl groups on silica). However, most surfaces are modified in order to produce a functionality, which may be covalently coupled with an antibody[20]. Silica surfaces have been reacted with amino silanes, like trimethyl-silanes, to produce a surface-bearing amino functionality[2]. Proteins can then be coupled to these surfaces through cross-linking chemistry. Bhatia *et al*[2] described in detail the immobilisation chemistry for direct covalent binding of antibodies to a silica surface. The procedure involves three steps: (1) Coating of a clean silica surface with a silane film. (2) Coupling of heterobifunctional crosslinker, with different reactive groups on each end, to the thiol group on the silane, through its maleimide region. (3) Formation of an amide bond by the free succinimide end of the crosslinker with terminal amino groups on the antibody.

The last method of immobilisation involves the indirect covalent linkage of proteins via a spacer or a carrier protein already linked to the surface. Narang *et al*[10] covalently bound an avidin layer onto optical fibres using the chemistry described by Bhatia *et al*[20].

Biotinylated antibodies could then be bound to the avidin layer. Avidin is an egg protein, which has a very strong affinity for the vitamin B6, Biotin[21]. Narang *et al*[10] showed that this method proved more effective than direct covalent linkage of the antibody to the sensor surface.

1.4 Thesis outline and objectives.

The principle objectives of this thesis were as follows (1) The fabrication and characterisation of grating coupled sol-gel waveguides. (2) Their application in the detection of fluorophore labelled antibodies bound to the surface of the waveguide via CCD camera detection. (3) The characterisation of a commercially available Texas Instruments SPR sensor for refractive index sensor applications. (4)The application of this sensor to the monitoring of biomolecular interactions. (5)An investigation of the use of disposable chips for the SPR

Chapter two summarises the theory behind planar waveguides and grating couplers and outlines the characteristics necessary for sensing applications. The fabrication and characterisation of sol-gel derived planar waveguides is presented in chapter three. In chapter 4 the background and procedures for immobilising antibodies onto a waveguide surface are described. The optical and imaging system for the detection of the excited fluorescence is discussed in chapter 5. The theory behind the phenomenon of surface plasmon resonance (SPR) is detailed in chapter 6. This chapter also discusses the use of the commercial SPR refractive index sensor from Texas Instruments, USA, as a liquid refractive index sensor and also for the detection fo biomolecules. The use of disposable sensor chips on this sensor is also discussed.

References

1. Yalow R.S. and Berson S.A., **'Assay of plasma insulin in human subjects by immunological methods'**, Nature, 184, pp1648-1649, 1959.

2. Clark L.C. and Lyons C., **'Electrode systems for continuous monitoring in cardiovascular surgery'**, Ann. N.Y. Acad. Sci; 102, pp29-45, 1962.

3. Liedberg B, Nylander C, Lundstrom I, **Surface plasmon resonance for gas detection and biosensing**, Sensors and Actuators, 4, 299, 1983.

4. Mandenius C.F., Welin S, Danielsson B, Lundstrom I, and Mosbach K, Analytical Biochemistry, 137, pp106, 1984.

5. Schipper E.F., Kooyman R.P.H., Borreman A, Greve J, **'The critical sensor: a new type of evanescent wave immunosensor'**, Biosensors and Bioelectronics, 11, pp295-304, 1996.

6. Duveneck G.L., Pawlak M, Neuschafer D, Bar E, Budach W, Pieles U, Ehrat M, **'Novel bio-affinity sensors for trace analysis based on luminescence excitation by planar waveguides'**, Sensors and Actuators B, 38-39, pp88-95, 1997.

7. Walczak, I.M., **'The application of evanescent wave sensing to a high-sensitivity fluorimmunoassay'**, Biosensors and Bioelectronics, 7, pp39, 1992.

8. Zhou Y, Magill J.V., De La Rue R.M., Laybourn P.J.R., Cushley W, **'Evanescent fluorescence immunoassays performed with a disposable ion-exchanged patterned waveguide'**, Sensors and Actuators B, 11, pp245-250, 1993.

9. Lee D.L., **'Electromagnetic principles of integrated optics'**, Wiley, New York, 1986.

10. Narang U, Anderson G.P., Ligler F.S., Burans J, **'Fiber optic-based biosensor for ricin',** Biosensors and Bioelectronics, Vol 12, No.9-10, pp937-945, 1997.

11. Feldstein M.J., Golden J.P., Rowe C.A., MacCraith B.D., Ligler F.S., **'Array Biosensor: Optical and Fluidics systems'**, Journal of Biomedical Microdevices, 1:2, pp139-153, 1999.

12. Rowe C.A., Tender L.M., Feldstein M.J., Golden J.P., Scruggs S.B., MacCraith B.D., Cras J, Ligler F.S., **'Array biosensor for simultaneous identification of bacterial, viral and protein analysis'**, Analytical Chemistry, 71(17), pp3846-3852, 1999.

13. Brinker C.J., Scherer G.W., **'Sol-gel Science'**, Academic Press, New York, 1990.

14. Raether H, **Surface plasma oscillations and their applications**, Phys. Thin films, 9, 145, 1977.

15. Otto A, **Excitation of nonradiative surface plasma waves in silver by the method of frustrated total reflection**, Z.Phys., 216,398,1968.

16. Kretschmann E, Raether H, **Radiative decay of non-radiative surface plasmons by light**, Z. Naturforsch., 23a, 2135, 1968.

17. Lofas S, Johnsson B, Tegendal K, Ronnberg I, **Dextran modified gold sensors for surface plasmon resonance sensors: immunoreactivity of immobilised antibodies and antibody-surface interaction studies**, Colloids and surfaces B: Biointerfaces, 1, 83-89, 1993.

18. Furlong C.E., Woodbury R.G., Yee S.S., Chinowsky T., Carr R, Elkind J.I., Kukanskis K.A., Bartholomew D, Melendez J.L., **Fundamental system for biosensor characterisation: application to surface plasmon resonance**, SPIE, Vol. 2836, 208-215

19. Polzius R, Schneider Th, Biert F.F., Bilitewski U, **'Optimisation of biosensing using grating couplers: immobilisation on tantalum oxide waveguides'**, Biosensors and Bioelectronics, Vol 11, No. 5, pp503-514, 1996.

20. Bhatia S.K., Shriver-lake L.C., Prior K.J., Georger J.H., Calvert J.M., Bredehorst R., Ligler F.S., '**Use of thiol-terminal silanes and heterobifunctional crosslinkers for immobilisation of antibodies on silica surfaces'**, Analytical Biochemistry 178, pp408-413, 1989.

21. Wilchek M. Bayer E.A., '**Avidin-Biotin technology'**, Methods in Enzymology, vol. 184, 1990, Academic press Inc..

Chapter 2 Waveguide and grating coupler theory.

2.1 Introduction

Four general categories of optical immunosensors have been widely explored. These include planar waveguides[1-3], fibre optic evanescent wave sensors[4], surface plasmon resonance devices[5], and continuous flow immunosensors[6]. This chapter will deal only with planar waveguides. Planar waveguides exploit the same optical phenomena as fiber optics, with some variation.

A waveguide is a material medium that confines and supports a propagating electromagnetic wave. The waveguide structure dealt with in this chapter consists of a thin film dielectric surrounded by lower refractive index media. This is known as step index slab waveguide. The particular configuration of waveguide sensor employed here, is based on evanescent wave excitation and detection of fluorescence. Evanescent field sensing enables the detection of fluorophores exclusively in close proximity to the planar waveguide. The evanescent field penetrates into the surrounding medium, allowing the detection of an analyte, which can be bound to immobilised recognition elements. This chapter will discuss the underlying waveguide theory[7-10].

Light can be coupled into a waveguide by a number of means. The implementation of a surface relief grating coupler embossed onto a sol-gel film was first proposed by Dakss *et al*[11] in 1970. The grating coupler acts as a diffractive element which converts a specific diffractive order into a guided mode of the waveguide structure. The theory of the grating couplers is also described in this chapter.

2.2 Optical waveguide theory

A planar waveguide consists typically of a thin film of refractive index n_2, supported by a substrate with a refractive index n_1, and a cover layer (usually air) with a refractive index n_3 (figure 2.1). This arangement in which the refractive index of the layers surrounding the waveguide are unequal is called an asymmetric waveguide. Light traveling in an optical waveguide is confined by total internal reflection (TIR) at the interface defined

by the waveguide surface. TIR only occurs under a limited set of conditions and is dependent on a number of factors, including the wavelength, incidence angle, and the relative refractive indices of the waveguide and surrounding media. The surrounding media (substrate and cover layer) must be of lower refractive index than the waveguide in order to achieve TIR.

Consider a beam of light incident at an angle θ at the two interfaces respectively (figure 2.1). The critical angles at the waveguide/cover (θ_c^c) and waveguide/substrate (θ_c^s) interfaces are

$$\theta_c^c = Sin^{-1}\left(\frac{n_3}{n_2}\right) \qquad 2.1$$

$$\theta_c^s = Sin^{-1}\left(\frac{n_1}{n_2}\right) \qquad 2.2$$

Since $n_1 > n_3$ (assuming the cover medium is air), it follows that $\theta_c^s > \theta_c^c$. Therefore when $\theta_c^s < \theta < 90°$, the light is confined in the guiding layer by total internal reflections at both the upper and lower interfaces and propagates along the waveguide. This corresponds to a guided mode.

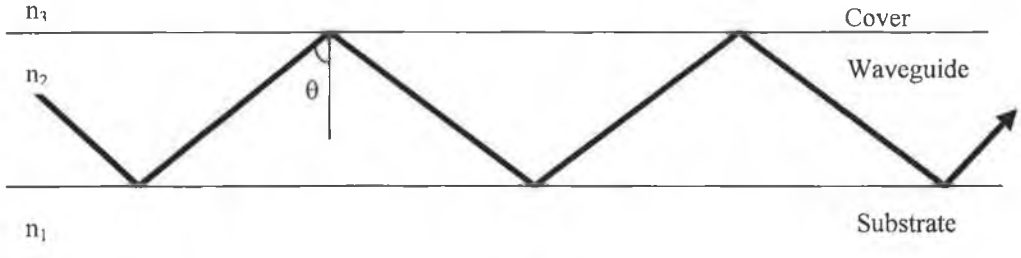

Figure 2.1 A simple dielectric waveguide.

2.2.1 Wave Optics

In order to understand the performance of waveguides, it is necessary to obtain the appropriate solutions to Maxwell's equations[8]. A guided mode is an electromagnetic field distribution which satisfies Maxwells equations when the appropriate boundary conditions are taken into account. Maxwell's equations for a source free isotropic medium are

$$\nabla \times \tilde{E} = -\frac{\partial \tilde{B}}{\partial t} \qquad 2.3$$

$$\nabla \times \tilde{H} = \frac{\partial \tilde{D}}{\partial t} \qquad 2.4$$

where E and H represent, the electric field and the magnetic field of the propagating light, respectively, and B and D the magnetic and electric displacements, respectively. Assuming a lossless medium with a scalar dielectric constant $\varepsilon(\omega)$ and a scalar magnetic permeability μ, we have the constitutive relations

$$D=\varepsilon E \qquad 2.5$$

$$B=\mu H \qquad 2.6$$

A dielectric waveguide is characterised by its dielectric constant

$$\varepsilon=\varepsilon_o n^2(x,y) \qquad 2.7$$

where ε_o is the dielectric permittivity and n(x,y) is the refractive index of the waveguide at the location defined by the coordinates (x,y). For homogenous, isotropic materials n(x,y) is a constant n. Therefore,

$$\nabla \times E = -\mu_o \frac{\partial H}{\partial t} \qquad 2.8$$

$$\nabla \times H = \varepsilon_o n^2 \frac{\partial E}{\delta t} \qquad 2.9$$

In wave optics, modes are generally characterised by propagation constants, whereas they are classified by their incident angle θ in ray optics. The plane wave propagation constant in the wave-normal direction is defined as $k_0 n_2$ as shown in figure 2.2, where $k_0 = 2\pi/\lambda$ and λ is the wavelength in free space. The relationship between the incident angle θ and the propagation constants along the x and z axis are

$$k_x = k_0 n_2 \mathrm{Cos}\theta \qquad 2.10$$

$$k_z = k_0 n_2 \mathrm{Sin}\theta = \beta \qquad 2.11$$

Modes are characterised by the propagation constant β, which is equivalent to the plane wave propagation constant in an infinite medium of refractive index $n_2 \mathrm{Sin}\theta$. The effective indices, N, of modes are defined by

$$\beta = k_0 N, \text{ or } N = n_2 \mathrm{Sin}\theta \qquad 2.12$$

The effective index of a guided mode is a useful concept to characterise guiding conditions. The two extremes of the TIR angle (θ_c^s, 90°) yield effective indices of n_1 and n_2, respectively. In an orthogonal co-ordinate system (x,y,z), we suppose the modes propagate along the z-direction. The electromagnetic field of the mode varies as

$$E = E(x,y) \bullet e^{j(\omega t - k_z z)} \qquad 2.13$$

$$H = H(x,y) \bullet e^{j(\omega t - k_z z)} \qquad 2.14$$

where ω,the angular frequency, is equal to $2\pi c/\lambda$, and c is the light velocity in free space.

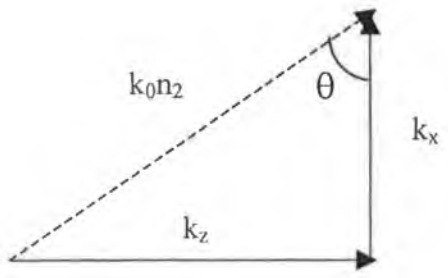

Figure 2.2 Wave-vector diagram

In the waveguide shown in figure 2.2, the electromagnetic fields are independent of y. The solution to Maxwells equations combined with the boundary conditions yield two different modes with mutually orthogonal polarisation states. One is the TE mode, which consists of the field components E_y, H_x, H_z. The other is the TM mode which has field components E_x, H_y, E_z. The field solutions and the boundary conditions at the substrate/waveguide and waveguide/cover interfaces lead to eigenvalue equations that determine the propagation characteristics of the TE and TM modes. Only TE modes will be discussed in this chapter. Maxwell's equations are used to obtain an expression for the guidance condition for TE modes.

2.2.2 TE modes

The form of the field distribution for TE modes in the asymmetric waveguide is assumed to have exponentially decaying fields in regions 1 and 3 and oscillatory behaviour in the core region 2. The electric fields are of the form

$$E_y(x,z) = E_1 e^{-\alpha_1 x} e^{-jk_z z} \qquad \text{Cover} \qquad 2.15$$

$$E_y(x,z) = E_2 \cos(k_x x + \psi) e^{-jk_z z} \qquad \text{Film} \qquad 2.16$$

$$E_y(x,z) = E_3 e^{-\alpha_3 x} e^{-jk_z z} \qquad \text{Substrate} \qquad 2.17$$

where the transverse wavenumbers are defined by the appropriate dispersion relations in each region

$$\alpha_1 = \sqrt{k_z^2 - \omega^2 \mu_1 \varepsilon_1} \qquad 2.18$$

$$\alpha_3 = \sqrt{k_z^2 - \omega^2 \mu_3 \varepsilon_3} \qquad 2.19$$

$$k_x = \sqrt{\omega^2 \mu_2 \varepsilon_2 - k_z^2} \qquad 2.20$$

The general guidance condition is given as

$$2k_x d - \phi_1^{TE} - \phi_3^{TE} = 2p\pi \qquad \text{p=0,1,.....} \qquad 2.21$$

where $\phi_1{}^{TE}$ and $\phi_3{}^{TE}$ are phase shifts resulting from total internal reflection at the upper and lower interfaces, respectively. This condition arises from a constructive interference requirement for the overlapping waves in the waveguide.

Equation 2.21 is a generalisation of the guidance equation. The derivation of this equation is treated in greater detail in Appendix A. This leads to the dispersion relation for the guide which yields the propagation constant β as a function of the frequency ω and film thickness d. To obtain precise values for the asymmetric guide, the dispersion equation has to be evaluated numerically or graphically. In general there is more than one solution, corresponding to different values of p and representing different waveguide modes.

Once the guiding equation has been solved for a particular mode the corresponding fields in all three regions can be obtained by making use of boundary conditions set out in equation A.26 to relate the amplitude coefficients E_1 and E_2 at the substrate/waveguide interface and analogous boundary conditions at the waveguide/cover interface to relate E_2 and E_3. We may then write all the relevant electric fields in terms of E_2 as given below.

$$E_y(x,z) = E_2 Cos(k_x d/2 + \psi) e^{-\alpha_1 (x - d/2)} e^{-jk_z z} \quad \text{Cover} \quad 2.22$$

$$E_y(x,z) = E_2 Cos(k_x d/2 + \psi) e^{-jk_z z} \quad \text{Film} \quad 2.23$$

$$E_y(x,z) = E_2 Cos(k_x d/2 - \psi) e^{-\alpha_3 (x + d/2)} e^{-jk_z z} \quad \text{Substrate} \quad 2.24$$

2.2.3 Dispersion Relation for the Asymmetric Slab Waveguide

Equation 2.21 is the most general guidance condition for the TE mode of a slab waveguide, but can be made more precise by introducing normalisations that combine several guide parameters. Guided TE modes are usually characterised in terms of the following three parameters

$$b = \frac{\varepsilon_{eff} - \varepsilon_s}{\varepsilon_2 - \varepsilon_s} \quad 2.25$$

$$a^{TE} = \frac{\varepsilon_3 - \varepsilon_1}{\varepsilon_2 - \varepsilon_3} \quad 2.26$$

$$V = k_0 d \sqrt{\frac{\varepsilon_2 - \varepsilon_3}{\varepsilon_0}} \quad 2.27$$

The b value is called the normalised waveguide index. The a value is a measure of the asymmetry of a waveguide. The V value is called the normalised frequency parameter, and is a measure of how many modes a waveguide can support. These three prameters are related by the dispersion relation.

$$V\sqrt{1-b} = p\pi + \tan^{-1}\left(\sqrt{\frac{b - a^{TE}}{1-b}}\right) + \tan^{-1}\left(\sqrt{\frac{b}{1-b}}\right) \quad 2.28$$

The dispersion plot for equation 2.28 is shown in figure 2.3. The derivation of equation 2.28 can be found in Appendix A.

If one evaluates the guidance condition for a given waveguide of known thickness and refractive index, a value for the normalised waveguide index, b, can be evaluated. This may then be used to determine the modal effective refractive index.

$$n_{eff} = \sqrt{\frac{\varepsilon_{eff}}{\varepsilon_o}} \qquad 2.29$$

which is the effective refractive index that a mode experiences while propagating along the waveguide film (as described earlier in equation 2.12).

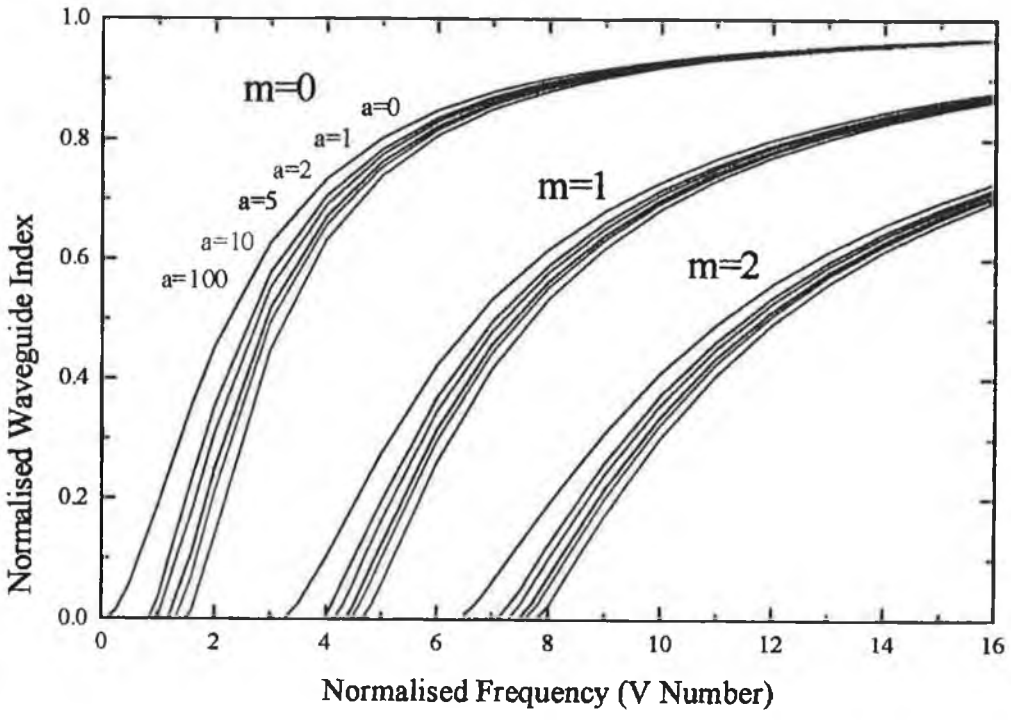

Figure 2.3 Dispersion curve for TE modes in a slab waveguide. Note a^{TE} values are denoted by a.

It is clear from figure 2.3 that there exists a cut-off frequency parameter($V_{cut\text{-}off}$) for each guided mode. This is a critical value of the normalised frequency (V) below which the

waveguide can not support the guided mode. Cut-off occurs when the effective index of the guided mode n_{eff} is equal to or less than the refractive index of the substrate n_1.

2.2.4 Penetration depth

When a beam of light is totally reflected at an interface separating two dielectric media, the reflected beam is physically displaced from the incident trajectory. It appears as though the incident beam enters the medium of lower refractive index through one region of the interface and then emerges from it through a slightly displaced region (figure 2.4).

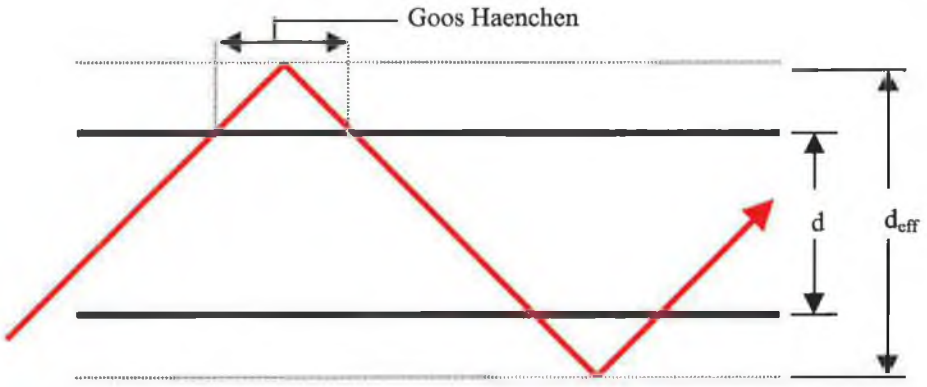

Figure 2.4 Schematic view of the effective guide thickness where the Goos-Haenchen shifts are shown.

This effect is known as the Goos-Haenchen shift. The Goos-Haenchen shift can be seen in figure 2.4. Discussing light-guiding properties in more detail, the power P carried by a TE guided mode per unit waveguide width is given by

$$P = -\int_{-\infty}^{\infty} E_y(x) H_x(x) dx \qquad 2.30$$

which can be expressed as

$$P = \frac{1}{2} E_f H_f d_{eff} \qquad 2.31$$

where

$$d_{eff} = d + \frac{1}{\alpha_3} + \frac{1}{\alpha_1} \qquad 2.32$$

Equation 2.32 indicates that the guided mode is essentially confined to the thickness d_{eff} because it spreads into the substrate and the cover. d_{eff} is the effective waveguide thickness indicated in figure 2.4. The guide modes penetrates to depths of $1/\alpha_1$ and $1/\alpha_3$ in the cover and substrate, respectively. The penetration depths of the evanescent fields are defined by the decay constant reciprocals of the electric field in equations 2.18 and 2.19. Therefore, from equations 2.18, 2.19 and 2.32, the effective refractive index of a guided mode allows for the calculation of the evanescent field penetration depths into the surrounding media

Higher-order guided modes have larger effective waveguide thickness and hence the larger penetration depth. The penetration depth of the evanescent field is one of the major factors, which determines the sensitivity of a waveguide based sensor. The higher the penetration depth the more sensitive the sensing waveguide platform.

2.3 Grating Coupler Theory

Grating couplers, consisting of perturbations or periodic structures, have been shown to possess the ability to couple light from an incident light beam into a thin film waveguide mode[2,5].The grating coupler acts to produce a phase matching between a particular waveguide mode and an unguided optical beam which is incident at an oblique angle on the surface of the waveguide .

It is instructive to consider an optical beam incident at an oblique angle onto a waveguide with no grating (figure 2.5). For coupling to occur, it is necessary that the

components of the phase velocities of the waves in the z direction be the same in both the waveguide (β_{mode}) and the beam (β_{inc}). Thus a phase match condition must be satisfied

$$\beta_{mode} = \beta_{inc} \qquad 2.33$$

where

$$\beta_{mode} = k_0 n_{eff} \qquad 2.34$$

$$\beta_{inc} = k_0 n_a \sin\theta \qquad 2.35$$

In these equations, n_{eff} is the effective refractive index of the guided mode, n_a is the refractive index of the incident medium, θ is the angle of incidence and k_0 is the free-space wavenumber.

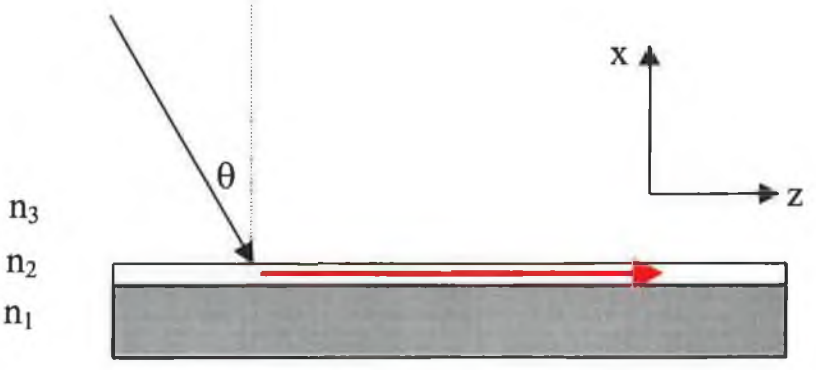

Figure 2.5 Light beam incident on a waveguide with no grating coupler.

If coupling were to occur it would require that $\sin\theta > 1$, since $n_3 < n_1 \leq n_2$ and $n_1 \leq n_{eff} \leq n_2$. This is not possible as equation 2.33 cannot be satisfied under these conditions. If, however, light is incident on a grating embossed onto a waveguide as shown in figure 2.6, the phase matching conditions may be attained. Because of its periodic nature, the grating

perturbs the waveguide modes in the region underneath the grating, and causes each one of them to have a set of spatial harmonics with z-direction propagation constants given by

$$\beta_{mode} = \beta_0 + \frac{m2\pi}{\Lambda} \qquad \text{m=0,±1 ,±2, ±3,±4.....} \qquad 2.36$$

where Λ is the spatial periodicity of the grating and β_0 is the fundamental mode in the perturbed region.

Since all of the spatial harmonics of each mode are coupled to form the complete surface wave field in the grating region, energy introduced from the beam into any one of the spatial harmonics is eventually coupled into the fundamental (m=0) harmonic This fundamental harmonic is very close to and eventually becomes, the β_{mode} mode outside the grating region. Thus, the grating coupler can be used to transfer energy from an optical beam to a particular waveguide mode by properly choosing the angle of incidence. Therefore, the grating coupling condition becomes

$$k_o n_{eff} = k_0 n_3 \sin\theta + \frac{m2\pi}{\Lambda} \qquad 2.37$$

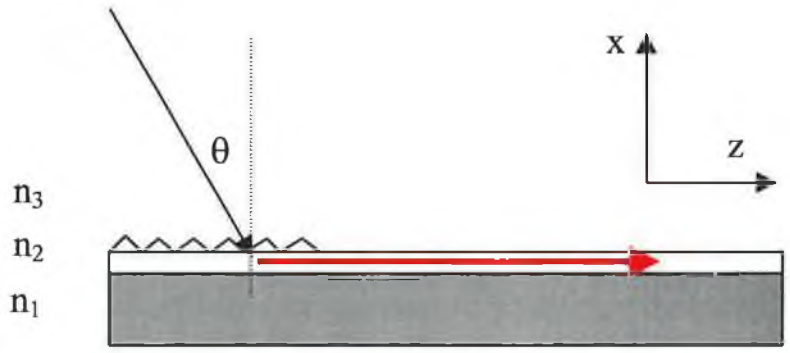

Figure 2.6 Light beam incident on a waveguide with grating coupler.

Hence, for some angle of incidence θ, phase matching of the two propagating constants can be satisfied since m may be positive or negative, and light can be coupled into a waveguide by radiation from the m^{th} diffraction order of the incident radiation.

2.4 Conclusion

In this chapter the basic principles of planar waveguides were introduced. The dispersion relation was derived for transverse electric waveguide modes, and was related to important characteristics of the guided modes such as effective thickness and the penetration depth of the evanescent field into the surrounding media.

The grating coupling equation was derived. This can be used to determine the required angle of incidence of incident light to convert energy from incident radiation into a guided mode.

References

1. Feldstein M.J., Golden J.P., Rowe C.A., MacCraith B.D., Ligler F.S., **'Array Biosensor: Optical and Fluidics systems'**, Journal of Biomedical Microdevices, Vol. 1:2, pp139-153, 1999.

2. Polzius R, Schneider Th, Biert F.F., Bilitewski U, **'Optimisation of biosensing using grating couplers: immobilisation on tantalum oxide waveguides'**, Biosensors and Bioelectronics, Vol 11, No. 5, pp503-514, 1996.

3. Duveneck G.L., Pawlak M, Neuschafer D, Bar E, Budach W, Pieles U, Ehrat M, **'Novel bio-affinity sensors for trace analysis based on luminescence excitation by planar waveguides'**, Sensors and Actuators B, 38-39, pp88-95, 1997.

4. Narang U, Anderson G.P., Ligler F.S., Burans J, **'Fiber optic-based biosensor for ricin',** Biosensors and Bioelectronics, Vol 12, No.9-10, pp937-945, 1997.

5. Lawerence C.R., Geddes N.J., Furlong D.N., **'Surface plasmon resonance studies of immunoreactions utilising disposable diffraction gratings'**, Biosensors and Bioelectronics, Vol 11, No.4, pp389-400, 1996.

6. Kusterbeck A.W., Wemhoff G.A., Charles P, Bredehorst R, Ligler F.S., **'A continuous flow immunoassay for rapid and sensitive detection of small molecules'**, Journal of Immunological Methods, Vol. 135, pp191-197, 1990.

7. Nisihara H, Haruna M, Suhara T, **'Optical integrated circuits'**, McGraw-Hill, New York, 1989.

8. Lee D.L., **'Electromagnetic principles of integrated optics'**, Wiley, New York, 1986.

9. Tamir T, **'Integrated Optics'**, Vol.7, Springer-Verlag, New York, 1979.

10. Hunsperger R.G., ' **Integrated Optics: Theory and technology'**, 3rd edition, Springer-Verlag, New York, 1991.

11. Dakss M.L., Kuhm L, Heidrich P.F., Scott B.A., **'Grating coupler for efficient excitation of optical guided waves in thin films'**, Applied Physics Letters, Vol. 16, pp523-525, 1970.

Chapter 3 Waveguide Fabrication and Characterisation.

3.1 Introduction

In this chapter the fabrication of low-loss asymmetric planar waveguides via a sol-gel dip-coating process is described. The procedures employed to determine the physical characteristics of the waveguide, such as thickness, refractive index and propagation losses, are presented.

3.2 Sol-gel process

The preparation of materials by the sol-gel process generally involves the use of metal alkoxides which undergo hydrolysis and condensation polymerisation reactions to give gels. Generally the silica is fabricated by mixing a metal alkoxide (eg $Si(OC_2H_5)_4$ or Tetraethoxysilane) water, a solvent and a catalyst. The first metal alkoxide was prepared from $SiCl_4$ and alcohol in 1845 by Eberman[1], who found that the compound gelled on exposure to the atmosphere. But it was not until the 1930's that Geffchen recognised that alkoxides could be used in the preparation of thin films for optical purposes[2].

The sol-gel process typically involves a solution consisting of a metal alkoxide, water which acts as a hydrolysis agent, alcohol as a solvent and either an acid or base catalyst. These are mixed together to achieve chemical homogeneity on the molecular scale. At low temperatures the metal compounds undergo hydrolysis and polycondensation reactions to produce a "sol", which is a suspension of colloidal particles. Further reaction connects the particles to produce a disordered branched network, "the gel", which is interpenetrated by liquid. Low temperature curing removes any of the remaining solvents and leaves a porous oxide. Further densification, by means of high temperature annealing, can produce glass capable for use in waveguiding applications. Film parameters such as porosity, thickness and hydrophobicity can be optimised through appropriate changes in the sol-gel process.

One of the most common precursors employed in the sol-gel process is tetraethoxysilane (TEOS, $Si(OC_2H_5)_4$). TEOS consists of a central silicon atom surrounded by four ethoxy groups. Other types of precursors known as organoalkoxysilanes, which contain one or more organic ligands may also be used. An example of such precursors is methyltriethoxysilane (MTES, $CH_3(C_2H_5O)_3Si$)

3.2.1 Hydrolysis and Condensation

The first step in the sol-gel process is hydrolysis. The hydrolysis reaction replaces alkoxide groups (OR) on the precursor with hydroxyl groups (OH) by the nucleophilic attack on silicon atoms by oxygen.

$$\equiv Si - OR + H_2O \Leftrightarrow \equiv Si - OH + ROH \qquad 3.1$$

The condensation reactions occur via a nucleophilic condensation reaction and produce siloxane bonds, Si – O – Si, along with by-products of alcohol (ROH), or water.

$$\equiv Si - OR + HO - Si \equiv \Leftrightarrow \equiv Si - O - Si \equiv + ROH \qquad 3.2$$

$$\equiv Si - OH + HO - Si \equiv \Leftrightarrow \equiv Si - O - Si \equiv + H_2O \qquad 3.3$$

In the sol-gel process, the condensation reactions continue to build up long polymeric chains of Si – O – Si molecules which, with time, interlink to become a three dimensional network which is known as a gel.

3.2.2 Ormosils

Ormosils, or organically modified silicates, are a relatively new family of materials in which organic and inorganic components are linked by chemical bonds to form a non-crystalline network [3]. The addition of an organic component to a sol-gel structure enables the fabrication of crack-free sol-gel derived thin films of up to 2 μm in thickness compared to 0.5-1μm with TEOS only[4]. It is also possible to control the porosity of sol-gel derived material by controlling the type and concentration of the organic groups [5]. Typically, the hybrid organic-inorganic gels are less porous and

denser in nature than the standard inorganic gels [4]. This allows the possibility for the fabrication of thick sol-gel derived films which may be densified to produce high quality low-loss waveguiding layers for integrated optical applications.

Generally standard alkoxides, like TEOS, produce films with hydrophilic surfaces which are due to the surface hydroxyl groups, which allow the adsorption of water molecules. This moisture sensitivity is a major obstacle for many sensing applications. Enhancing the hydrophobicity of the sensing surface by chemical means is one solution to this problem. The surface of TEOS-based films have a large concentration of hydroxyl (-OH) groups which readily react with water in the film environment. These can be replaced with hydrophobic methyl (CH_3) groups by employing a modified silicon alkoxide precursor such as methyltriethoxysilane (MTES, $CH_3(C_2H_5O)_3Si$)

3.3 Fabrication of MTEOS sol gel waveguides.

This section of the chapter details the preparation of sol-gel derived thin film waveguides using Methyltriethoxysilane (MTES) as a precursor, and the embossing technique for the fabrication of surface relief gratings. In addition, the conditioning of slides, sol-gel preparation and the dipcoating process are discussed.

3.3.1 Preparation of slides

In order to obtain good quality films on microscope slides it was necessary to obtain a clean surface onto which the sol-gel film was deposited. The glass microscope slides used were Select MicroSlides (Chance Propper Ltd, UK) with a refractive index n=1.512. They were first cut to size, 40mm in length and 15mm in width. The slides were first rinsed in deionised water after which they were dried with lens tissue and placed in a beaker of methanol. The slides were individually rinsed in methanol and dried as before. This procedure was repeated with acetone before finally rinsing the slides again in deionised water. The glass substrates were then conditioned by soaking the slides in deionised water at 70°C overnight. This was considered to have the effect of increasing the concentration of silanol (SiOH) groups on the surface of the glass and thereby improving the adhesion of the sol-gel film to the surface. The slides were stored in deionised water in a sealed beaker at room temperature until use.

3.3.2 MTEOS Sol preparation

All reagents used were purchased from Sigma-Aldrich. The sol was prepared by mixing 8ml of ethanol, 4ml of methyltriethoxysilane, 2 ml of titanium(IV) tetrabutoxide ($Ti(OBu)_4$) and 0.4mls of silicon (IV) chloride[6]. Simple silica precursor-based sols typically produce thin films of refractive index 1.43. Even at full densification, the highest refractive index that can be achieved with silica is 1.46. For waveguiding to occur the refractive index of the waveguide layer must be higher than that of the surrounding media and the substrate (1.512). High refractive index films were achieved by the addition of the precursor titanium(IV) tetrabutoxide $Ti(OBu)_4$ into the sol. This is a precursor for titania and has a high refractive index (>2). Preparation of the sol in anhydrous conditions can reduce propagation losses. The silicon alkoxide (MTES) hydrolyses relatively slowly, hence the need for an acid or a base catalyst. Titanium alkoxides, such as $Ti(OBu)_4$, hydrolyse at a much faster rate. Addition of acidified water as the catalyst (e.g. HCl) to the mixture will result in faster hydrolysis of the titania precursor and thus the formation of titania and silica rich sites in the sol. This leads to inhomogeneity in the waveguide layer and increases guided mode scattering. Silicon tetrachloride ($SiCl_4$) has been successfully used as the catalyst, to produce homogeneous sol-gel films[6]. Except for trace amounts of water, which were probably introduced during the mixing of the sols components, the $SiCl_4$ catalysis was carried out under anhydrous conditions. The catalyst was uniformly mixed with the two precursor components without hydrolysis and condensation taking place simultaneously.

The silicon(IV) chloride acts as a catalyst for the reaction and the ethanol is a solvent. The sol was stirred for 2 hours at room temperature. The resultant sol was homogenous, transparent and light yellow in colour. The sol was then passed through a 0.45μm disposable syringe filter to remove any large particles that could reduce film quality. It was then left for 24 hours at room temperature in a sealed glass vial prior to use.

3.3.3 Thin film fabrication

In dip coating, the substrate is immersed in a solution and is then withdrawn vertically at a constant speed. The dipping apparatus, shown in figure 3.1, enabled the glass slide to be held rigidly while the solution was fixed onto a moving stage. The stage was drawn away from the sample. The stage was controlled by computer, which set the direction and speed of coating. Coating rates ranging from 0.5mm/sec to 3mm/sec were selected depending on the required thickness. Typically, the higher the speed, the thicker the film produced. This is an unusual rheological property of sols.

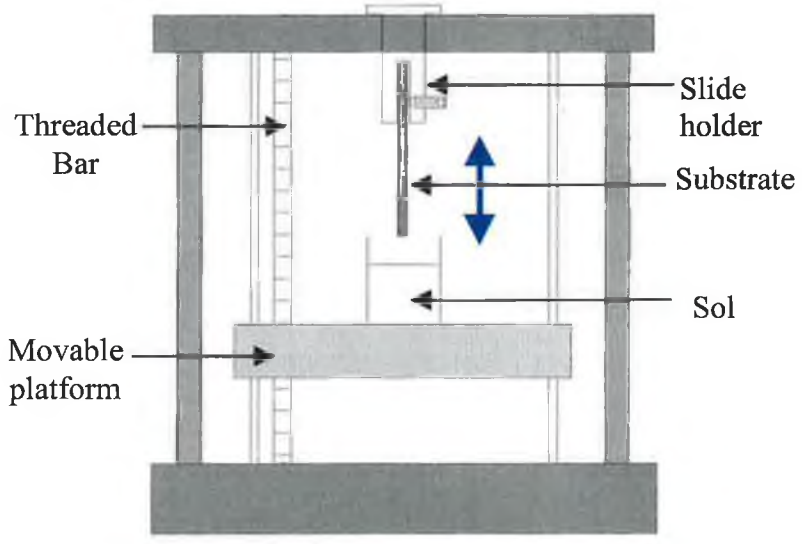

Figure 3.1 Dip coating apparatus

A coating rate of 2.8mm/sec was used for all waveguides reported here. Before coating, the conditioned slides were taken from the deionised water and dried with lens tissue. Once slides were coated they were stored for 20 minutes at room temperature to dry. Then they were either coated again for a thicker film or annealed in an oven at 500°C for 15 minutes. The films were then stored in sealed glass vials for 24 hours before embossing grating couplers on. Only single-sided films were made here. This was achieved by masking one side of the glass substrate with insulating tape prior to coating.

3.3.4 Embossing technique for fabrication of surface relief gratings

A series of aluminium-coated surface relief gratings (Edmund Scientific, USA) of varying periodicity were used to produce the embossed grating couplers. The couplers were fabricated by first dipping the end of the waveguide into MTES sol and withdrawing it at a constant rate of approximately 1mm/sec. The dipcoated film was immediately placed in the embossing apparatus (see figure 3.2). The master grating was then manually pressed onto the dipcoated end of the film and left for 2 minutes. After 2 minutes the pressure was released. The embossed film, observed as a negative imprint of the surface relief grating, was left to dry at room temperature for up to 5-7 days prior to use. The master grating periods used here were specified as 600, 1200 and 2400 lines/mm, respectively. The embossing procedure can be seen in figure 3.3.

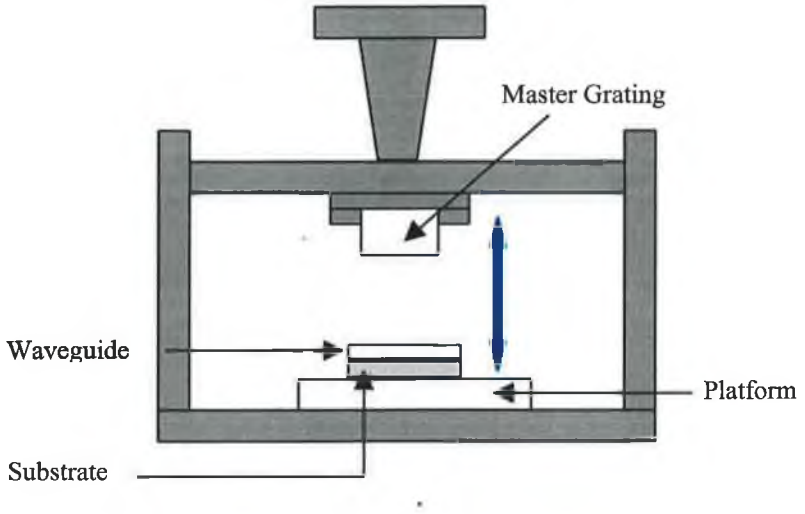

Figure 3.2 Embossing apparatus

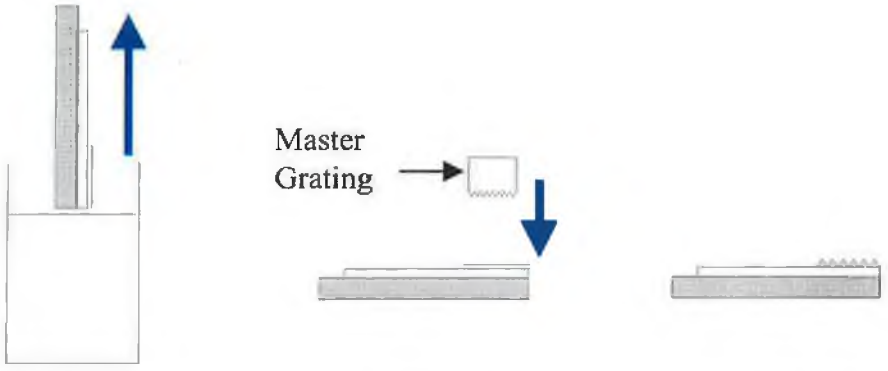

Figure 3.3 Embossing procedure.

3.4 Characterisation of waveguides

A series of experiments was carried out on all waveguides for characterisation purposes and to ensure that all waveguides used in experimental work were of the same quality and characteristics.

3.4.1 Thickness and refractive index measurements

Thickness and refractive indices of the waveguides were determined from transmission spectra of the films using a UV-Vis spectrometer. In spectral analysis the refractive index is determined from the absolute value of transmittance peaks, while the thickness is related to the wavelengths of the transmittance peaks, as shown in equations 3.4 and 3.5,

$$n = 1.52 + \frac{\Delta}{62.5} \qquad 3.4$$

$$t = \frac{m}{2n\left(\frac{1}{\lambda_1} - \frac{1}{\lambda_2}\right)} \qquad 3.5$$

where m is the order of extrema separation, Δ is equal to the difference of the max. transmission peak and min. transmission peak and λ_1 & λ_2 are the wavelengths where these peaks appear.

Sol-gel films were coated on both sides of the glass slide for these measurements to be taken. Both single layered and double layered waveguides were measured. A single coating of MTES/$Ti(OBu)_4$ sol was coated onto a glass substrate at a speed of 2.8mm/sec and densified at 500°C for twenty minutes, to gave a thickness of approximately 340nm and a refractive index in the region of 1.6. For a double coated waveguide coated at the same speed and annealed at the same temperature, a thickness of approximately 710nm and a refractive index in the region of 1.57 was found typically.

3.4.2 Attenuation of waveguides

In an optical waveguide, a guided mode continuously loses a small part of its power by scattering. This scattered power is proportional to the total guided power. Thus the scattered light decrease may be used to image the propagation losses of the guided mode.

The experimental setup to observe the scattered light is shown in figure 3.4. The waveguide is mounted on a rotation stage and rotated until the coupling angle has been reached and the light from the incident beam is coupled into the waveguide. A streak of light is observed propagating along the waveguide. A 632.8nm He-Ne laser was used in this experiment. Only the attenuation of the TE_0 mode was measured. A CCD camera (Hitachi, KP-M1) was used to image the light streak. The camera is interfaced to the computer via a MV-200 framegrabber so the image can be displayed on the screen. IDL software was used to analyse these images and to plot an intensity profile of the scattered light against the propagation length. A least mean squares fit of the measured data to this decreasing exponential function was then used to calculate the propagation losses using equation 3.6

$$\alpha = \frac{-10}{L}\left\{\log\frac{p_f}{p_i}\right\} \qquad 3.6$$

where L is the propagation length, and p_f and p_i are the final and initial powers scattered from the waveguide respectively.

The measured attenuation coefficients ranged form 0.3dB/cm to 6dB/cm. Only waveguides with attenuation coefficients ranging from between 0.3dB/cm and 2 dB/cm were used in experiments here. The relationship between the attenuation coefficient which is expressed in dB/cm and the actual percentage of power lost as the guided mode propagates along a unit length of the waveguide is illustrated in figure 3.5. As can be seen from this figure a 6dB/cm loss is equivalent to a 75% loss in power over 1cm of propagation. Such waveguide power losses are too large and are not acceptable for this application. Waveguides must be able to support guided modes over propagation distances of the order of two centimetres without large power losses. This is one major drawback in the development of these sensors as waveguides can differ significantly from sample to sample despite identical laboratory fabrication techniques.

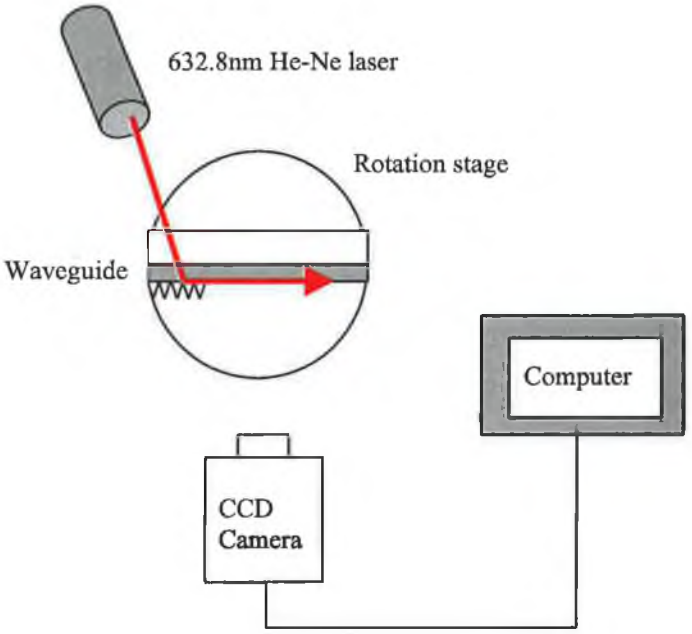

Figure 3.4 Experimental setup for attenuation measurement

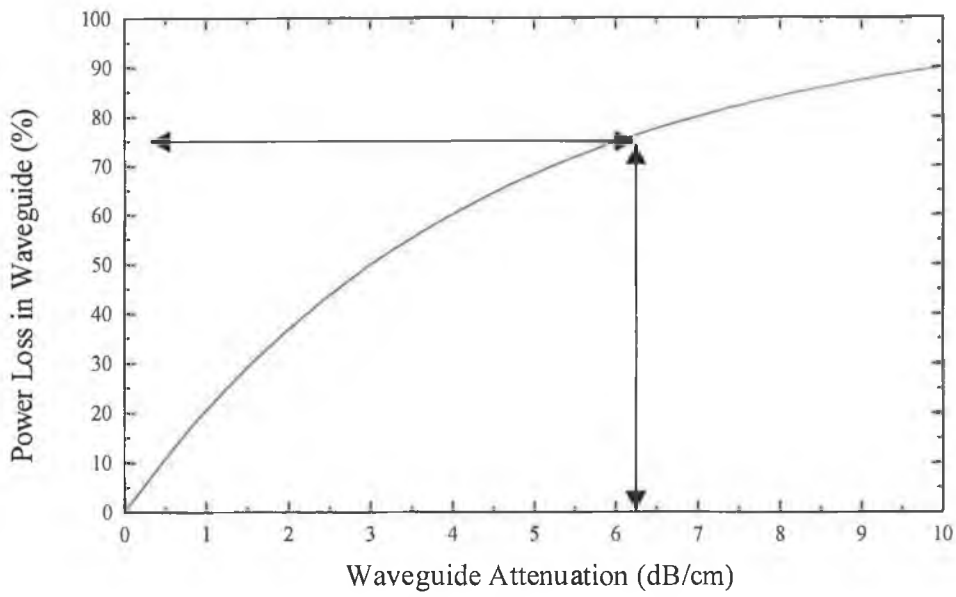

Figure 3.5 Power loss over 1cm versus attenuation coefficient

3.4.3 Efficiency of gratings

The grating coupler efficiency η was determined by mounting the waveguide onto a rotation stage and directing a 632.8nm He-Ne laser beam on to the embossed grating coupler. The experimental set up is shown in figure 3.6. When the coupling conditions had been reached and a mode was visible, the light intensity incident (I_i) on the grating was measured using a laser power meter, as were the transmitted intensity (I_t) and the reflected intensity (I_r). The coupling efficiency, η, is then calculated using the equation[7]

$$\eta = \frac{I_i - I_r - I_t}{I_i} \qquad 3.7$$

The assumption made here is that incident light, which is not reflected or transmitted is coupled into the waveguide/coupler combination. Typical efficiencies range from 1 % to 25%. Of course the higher the efficiency the better the waveguide. Only waveguides with efficiencies of 10% or greater were used in experiments.

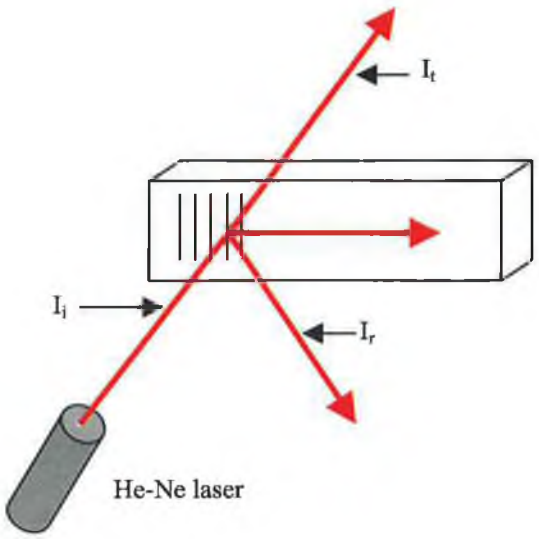

Figure 3.6 Experimental setup used to determine efficiency

3.4.4 Incoupling angle

Practical measurements for the incoupling angles of TE_0 modes were made using a 632.8nm He-Ne laser. The waveguide was mounted onto a rotation stage. The laser beam was incident on the grating and the waveguide was rotated until coupling conditions had been met. Three different grating periodicities were used on waveguides: 600lines/mm, 1200 lines/mm, 2400lines/mm. Table 1 shows a comparison of theoretical predictions and practical measurements of the incoupling angle of TE modes. The theoretical predictions were obtained using the theory outlined in Chapter 2.

Λ (lines/mm) Grating Period	**θ_{TE} Theoretical**	**θ_{TE} Experimental**
600	56.34°	56°
1200	50.54°	51°
2400	1.58°	1.5°

Table 3.1. Incoupling characteristics for three waveguides using different periodicities.

3.5 Conclusion

The processes involved in the fabrication of sol-gel planar waveguides have been discussed, including sol preparation and substrate preparation. The procedure for the fabrication of grating couplers on the waveguide for incoupling of incident radiation has also been presented. Methods for measuring the physical characteristics of the planar waveguides and grating coupler, such as thickness, refractive index, propagation loss and grating efficiency were discussed.

Waveguides, used in the subsequent experiments typically had a thickness of ~350nm, a refractive index of ~1.6, a propagation loss of 0.3-2dB/cm and a grating efficiency of between 10% and 25%.

References

1 Ebelman M, **'Annales de Chemie et de Physique'**, Vol. 57, No.3, pp319-355, 1846.

2. Brinker C.J., Scherer G.W., **'Sol-gel Science'**, Academic Press, New York, 1990.

3. Hoshino Y, MacKenzie J.D., **'Viscosity and structure of Ormosils solutions'**, Journal of Sol-gel Science and Technology, 5, pp83-92, 1995.

4. Innocenzi P, Abdirashid M.O., Gugleilmi M, **Structure and properties of sol-gel coatings from Methyltriethoxysilane and tetraethoxysilane'**, Journal of Sol-gel Science and Technology, 3, pp47-55, 1994.

5. Sakka S, **'The current state of Sol-Gel Technology'**, Journal of Sol-gel Science and Technology, Vol. 3, pp69-81, 1994.

6. Yang L, Saavedra S.S., Armstrong N.R., Hayes J, **'Fabrication and characterisation of low-loss, sol-gel planar waveguides'**, Analytical Chemistry, Vol. 66, pp1254-1263, 1994.

7. Gong Q, Assanto G, Zanoni R, Stegeman G.I., Burzynski R, Prasad P.N., **'Efficient grating coupling to poly-4BCMU optical waveguides'**, Applied Optics, Vol.29, pp3887-3890, 1990.

Chapter 4 Biomolecule Immobilisation

4.1 Introduction

A biosensor is an analytical device employing an immobilised biological material (enzyme, antibody, antigen, organelles, DNA, cells or tissues) in contact with or integrated within a transducer, which ultimately converts a biological signal into an electrical or optical signal. Sensor action is generally based on the specificity of response of the biological material to a target material. An important factor in the production of biosensors is the immobilisation technique employed for stabilising biomolecules and binding them to the surface of the transducer. The usual aim is to produce a thin film of immobilised biologically active material on or near the transducer surface. An emerging trend is the use of sensor arrays for the purpose of multi-analyte sensing. Planar waveguides can be patterned with immobilised capture antibodies, enabling simultaneous identification and detection. The aim here is to produce a pattern of different capture antibodies on the waveguide, allowing a multi-channel flow cell to be used to perform different assays on one waveguide at the same time.

In this chapter procedures undertaken to immobilise IgG antibodies onto sol-gel waveguides via the avidin-biotin affinity technique, using a two-channel flow-cell, are described. Basic steps leading to the development of multianalyte biosensors are also reported.

4.2 Covalent immobilisation

Attachment of antibodies to sensor substrates can be achieved via a number of different routes: adsorption[1], covalent attachment[2] and avidin-biotin bridges[3]. Antibodies immobilised by adsorption suffer partial denaturation and tend to leach or wash off the surface. Covalent binding, however, is a preferred method of attaching an antibody to a surface due to the strong, stable linkage. Bhatia *et al*[2] described in detail the immobilisation chemistry for direct covalent binding of antibodies to a silica surface. The procedure involves three steps: (1) A clean silica surface is coated with a silane film. (2) A

heterobifunctional crosslinker with different reactive groups on each end is coupled to a thiol group on the silane, through its maleimide region. (3) The free succinimide end of the crosslinker forms an amide bond with terminal amino groups on the antibody.

It has been documented that antibodies can denature or lose a significant portion of their activity when covalently immobilised directly onto surfaces[3,13]. Narang *et al*[3] found that antibodies bound indirectly to a surface, using an avidin-biotin bridge, had advantages over those immobilised using the direct covalent method: (1) An avidin-biotin bridge is very specfic, forming a very stable complex. (2) Avidin provides a passivation layer over the substrate which subsequently prevents adsorption of the antibody to the surface, thereby cutting down on non-specific binding. (3) Avidin-coated substrates will bind practically any biotinylated antibodies. (4) Avidin is multivalent for biotin. Narang *et al*[3] covalently bound an avidin layer onto optical fibres using the chemistry described by Bhatia *et al*[2]. Biotinylated antibodies could then be bound to the avidin layer.

4.3 Proteins

In the following section, a brief description of the bio-molecules used in this work is presented. Avidin is a protein found in egg white and is combined with the vitamin B6 (Biotin) to immobilise immunoglobulin G (IgG) onto the sol-gel based waveguides, described earlier.

4.3.1 Immunoglobulin G

Antibodies, proteins in a class called immunglobulins (Ig), are the most important molecules of the vertebrate immune system. They are produced on B-lymphocytes after the organism is invaded by a "foreign body" or "antigen", and responds with an immunoreaction. Because of their specificity and affinity for antigens, antibodies have been widely used in biological research and in clinical testing to detect molecules of interest.

There are five classes of immunoglobulins, IgA, IgG, IgM, IgD, and IgE, and within these classes there are subclasses. Each class or subclass is specific for one type of antigen. The work reported here employed only immunoglobulin G (IgG). IgG antibodies have a

molecular weight of 150,000 Da. The general structure of an antibody of the IgG type is given in figure 4.1. Antibodies consist of four chains: two identical "heavy" chains and two identical "light" chains, consisting of 440 and 220 amino acids, respectively.

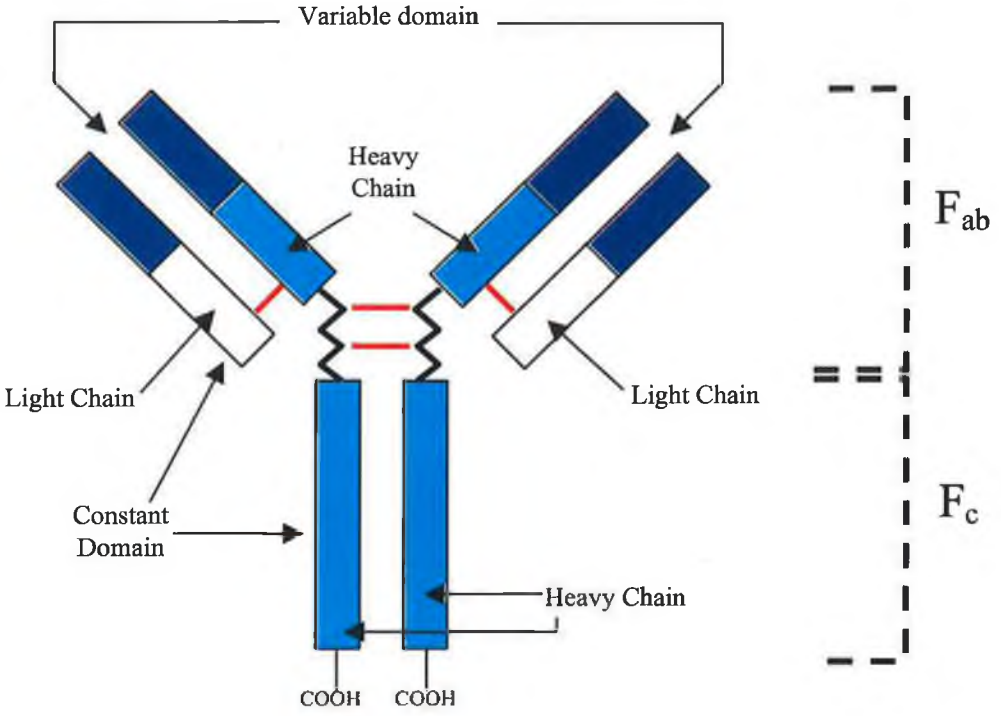

Figure 4.1 General structure of an antibody of the IgG type composed of two heavy and two light chains. Disulfide bonds are indicated in red.

These chains are linked by disulfide bonds, forming a molecule of approximately 10nm in length. Antibodies, for convenience, are regarded as Y-shaped molecules. The "arms" of the Y contain the specific antigen binding sites, which are responsible for the recognition process of sensors using such molecules as sensing elements. The two arms are identical and if the antibodies are cleaved enzymatically, fragments containing these binding sites are obtained separately, and are named "fragments antigen binding" (F_{ab}). The specificity of one antibody over another is achieved by slight variations in the amino acid sequence in small parts of the arms, which are therefore called the variable region. The remaining "core" of the antibody molecule can be crystallised and is referred to as F_c,

"fragment crystallising". The F_c fragment contains carboxy terminal amino acids, which can be used for immobilisation onto solid supports. It has no antigen binding properties.

4.3.2 Avidin-Biotin

The Avidin-Biotin system has many uses in both research and technology[5]. Its major distinguishing feature is the high affinity ($10^{-15}M^{-1}$) between the water-soluble vitamin B6 (biotin) and the egg-white protein avidin. Its interaction is so strong that even biotin coupled to proteins, is available for binding by avidin. If a biologically active compound, such as an antibody, is chemically modified with biotin, the biological and physiochemical properties of the biotin-modified molecule are still available for interaction with avidin. Avidin has four binding sites for biotin. If avidin can be attached to a sensor surface of some sort, then the avidin can be made available for direct interaction with the biotinylated antibody (figure. 4.2).

Avidin is a tetrameric protein with four identical subunits. Biotin is relatively polar and can be coupled to antibodies under very mild conditions with little disruption to their structure. Biotin is a vitamin which is required in very small quantities for a variety of cellular processes whereas avidin's biological role is that of a scavenger, inhibiting bacterial growth in egg white[6]. Avidin proved to be a minor constituent of egg white that could induce a nutritional deficiency in rats by forming a very stable non-covalent complex with what was subsequently proved to be biotin, vitamin B6[5].

Both avidin and streptavidin are readily available commercially at little cost. The disadvantage of using avidin, is its extremely basic nature, which can cause it to bind nonspecifically by electrostatic forces[7]. Streptavidin, a binding protein isolated from *Streptomyces*, is an alternative to avidin. It has four identical chains but amino acid analysis show that streptavidin has only half the number of basic amino acids. For this reason it has a much less basic isoelectric point and therefore exhibits much reduced non-specific binding[5].

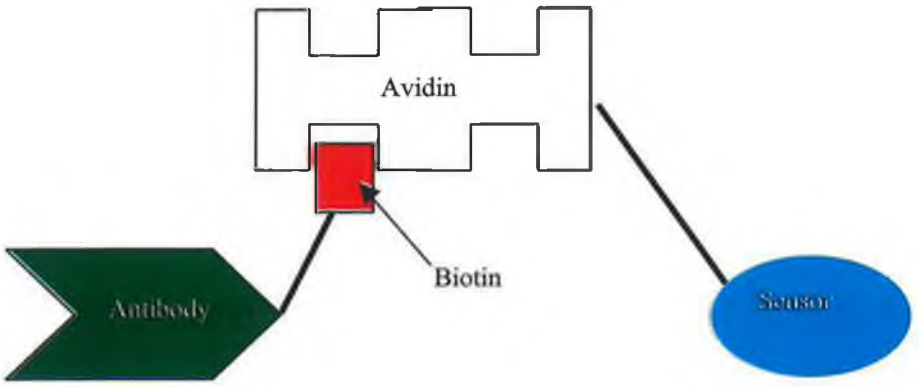

Figure 4.2 The avidin-biotin system.

4.4 Fluorophores

A fluoroimmunosensor combines the step of selective analyte recognition by means of an immobilised antibody, with signal generation via a fluorescently labelled antibody, near or on the surface of a transducer. There are two basic types of heterogeneous immunoassays. The first is called a competitive immunoassay, involving competition between an analyte and a labelled analyte for a limited number of antibody binding sites. The second, a sandwich assay, involves two antibodies directed toward the one antigen forming an antibody sandwich trapping the antigen in the middle (figure 4.3). The first antibody is immobilised. Subsequently the antigen molecules are reacted with and bind to the immobilised antibody. The second antibody, fluorescently labelled, is also specific for the antigen and binds only to an antigen that has previously bound to the immobilised antibody. The signal generated by the label is proportional to the antigen concentration.

Fluorescent molecules can absorb energy, for example in the form of radiation or through a chemical reaction, and emit this as photons. Absorbed light excites the electron field of the molecule from its ground state singlet to a higher state[8]. Energy may be lost from non-radiative conversion, by radiative transition to the ground state (fluorescence) or through a semi-stable triplet state (phosphorescence).

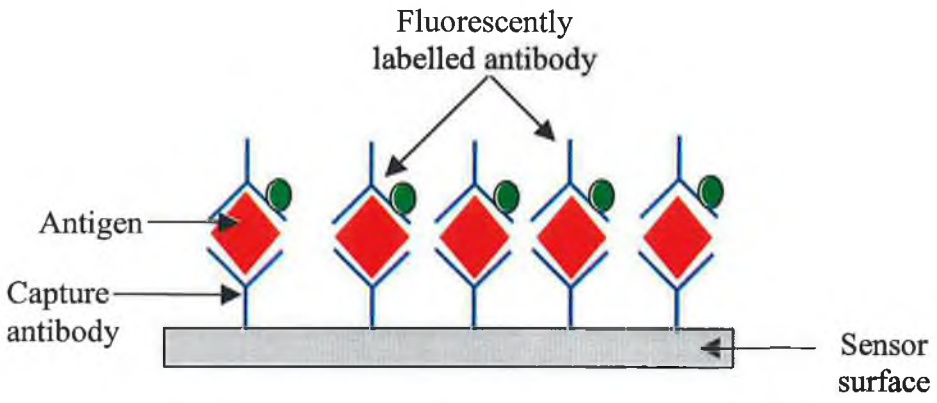

Figure 4.3 Sandwich assay

The wavelength of emitted light is always longer than that of the excited energy because of energy losses before emission. This wavelength difference (the "Stokes shift") is generally small – in the region of 30-50nm for fluorescent organic molecules- but is greater for phosphorescent molecules (150nm). Decay times of fluorescent molecules are also important. For phosphorescence, the decay time is approximately 1μs to 10s, while those for fluorescent molecules are much shorter ranging from 2 to 20ns typically. Fluorescent molecules can also be classified in terms of quantum yield (the ratio of emitted to absorbed light energy).

The sensitivity of fluorescence measurements can be interfered with due to light scattering, background fluorescence and quenching of the fluorescent molecule. Light scattering causes high background readings from solutions containing proteins or small colloidal particles. Background fluorescence arises from natural fluorescence of proteins or other reagents used in an assay. Background fluorescence from biological samples usually arises between 350-600nm and overlaps with the emission spectrum of many fluorophores. Fluorophores can also be influenced by relatively minor changes in their environment. For example, pH or polarity (solvent effects) can cause enhancement or quenching of the signal and influence the emission wavelength.

Fluorophores used in immunoassays should have a high fluorescent intensity, giving a signal easily distinguishable from the background. To achieve this, it must have a high

molar absorptivity with as high a quantum yield as possible. The binding of the fluorophore to the protein should not adversely affect its properties. Using fluorophores with excitation wavelengths greater than 600nm and with Stokes shifts of over 40nm can reduce both light scattering and background fluorescence[9]. Furthermore, for covalent coupling to antibodies, the fluorophore must posses a suitable functional group (hydroxyl, organic amine or sulphonic acid residue). Reaction intermediates that have been used for linkage include esters, N-hydroxysuccinimides, isocyanates, isothiocyanates and maleimides.

Fluorophores that have been widely used in immunoassays are fluorescein[10] and rhodamine. These have limitations associated with them. They both have Stokes shifts of only 28-35nm and both absorb and emit in the region of 300-600nm, which is the same region as the natural fluorescence of biological material.

There is only a small number of chemical compounds that exhibit significant absorption and fluorescence in the red, far-red and near IR spectral regions (600-1000nm). These include a group of cyanine reagents.

Cyanine (Cy) reagents have been shown to be useful as fluorescent labels for biological compounds[1,3,11,12]. These dyes are water soluble and highly fluorescent, providing significant advantages over other existing fluorescent labels such as fluorescein or rhodamine. They produce high signals due to a high molar extinction coefficient (absorptivity) and relatively high quantum efficiency when bound to proteins. Their high water-solubility allows easy labelling reactions. They are pH insensitive over a broad range, unlike fluorescein, which loses fluorescence below a pH of 8.

Cy dyes range from those emitting in the green to those emitting in the near infra red region. The dye employed in the work reported here is Cy 5 dye (Amersham Life Sciences, UK). This dye has an absorption maximum at 649nm and a fluorescence maximum at 670nm, which gives a Stokes shift of 21nm. Figure 4.4 shows the Cy5 emission spectra. Cy5 has a high molar extinction coefficient ($250{,}000 M^{-1}cm^{-1}$) and a quantum yield of 0.28 when bound to protein. Another advantage of Cy dyes is their compatibility with low cost laser diodes.

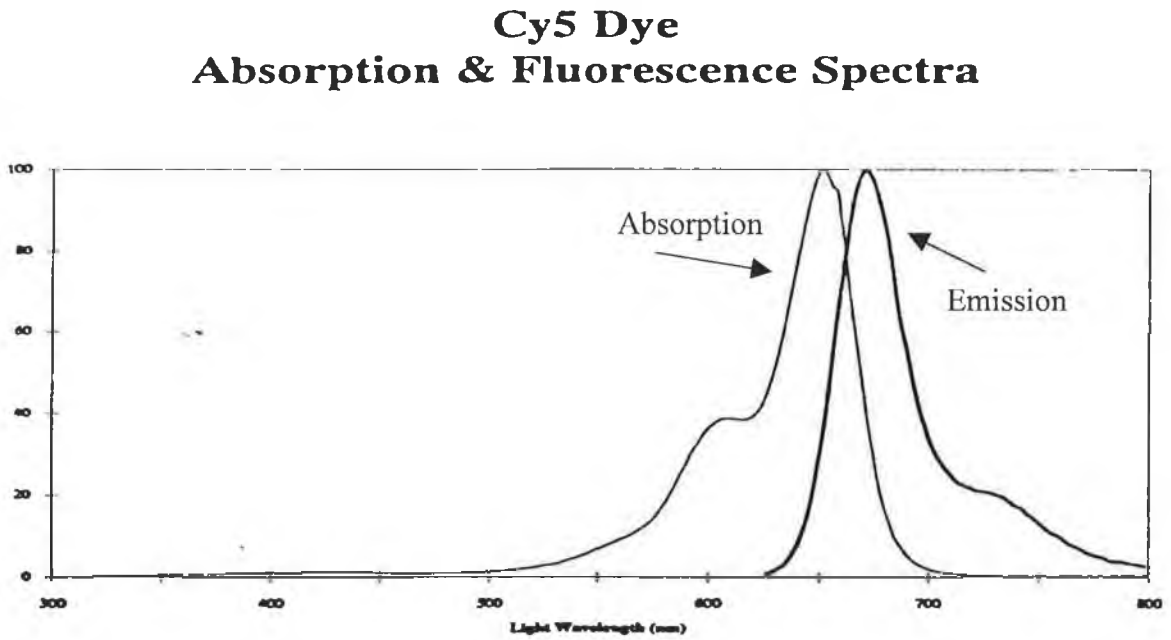

Figure 4.4 Absorption and Emission spectra of Cy5 dye.

4.5 Biological materials and methods

The following section details the procedures employed in the fluorescent labelling and biotinylation of rabbit IgG, together with the process involved in immobilising streptavidin and the antibodies onto sol-gel waveguides.

4.5.1 Antibody labelling with CyDye.

The antibody used in all of the following experiments was rabbit IgG. The antibody was made up to a 10mg/ml solution in a 50mM solution of Phosphate buffer saline (PBS).

1ml of the protein solution was added to 1ml of a coupling buffer (1M sodium carbonate, pH 9.3) and mixed thoroughly by inverting the capped vial 10-15 times. The coupling buffer was needed to raise the pH of the coupling reaction to 9.3 as it has been shown that optimal coupling takes place at this pH [2,3]. After mixing, the mixture of protein and coupling buffer was added to a vial containing 0.5mg of the Cy5 dye. The mixture was

allowed to react for 30 minutes at room temperature with additional mixing every 10 minutes.

The labelled protein was separated from the un-conjugated dye using a gel-filtration column. The column was equilibrated with 13ml of elution buffer (PBS, pH 7.2) and the reaction mixture added to the column. Once this had passed into the column, 2ml of elution buffer was added. By the time the reaction mixture entered the column the labelled protein had separated from the un-conjugated dye and was flowing faster through the column. This could be seen as a blue-green band. A further 2.5ml of buffer was added to the column and the faster blue-green band was collected from the column. The labelled protein was entirely eluted by the time the 2.5ml of buffer had entered the column.

Molar concentrations of the dye and the protein were measured by firstly measuring the absorbency of the dye at 635nm (A_{635}) and of the protein at 280nm (A_{280}) and using equations 4.1 and 4.2.

$$[Cy5] = \frac{A_{635}}{\varepsilon_{dye@635}} \qquad 4.1$$

$$[\mathrm{Pr}otein] = \frac{A_{280} - (0.2 \cdot A_{635})}{\varepsilon_{protein@280}} \qquad 4.2$$

where ε_{635} and ε_{280} stand for the extinction coefficients of the dye at 635nm (250,000 $M^{-1}cm^{-1}$) and of the protein at 280nm (107,142 $M^{-1}cm^{-1}$) respectively, and A_{280} and A_{635} are the absorbance values of the protein at 280nm and of the dye at 635nm respectively. The value for A_{280} had to be corrected, as part of the value for A_{280} was due to the Cy dye absorbing at 280nm. This worked out at approximately one fifth of the absorbance of the dye at 635nm and was subtracted from A_{280} as indicated in equation 3.2. All absorbances were measured using a UV-Vis spectrophotometer.

The final Dye/Protein ratio was found using the equation:

$$\frac{D}{P}_{final} = \frac{[Cy5]}{[\mathrm{Pr}otein]} \qquad 4.3$$

All labelled antibodies used in the experiments described in chapter 5 had a final dye/protein ratio of between 2-4, i.e. 2-4 dye molecules to every antibody. The exact ratio will be stated where appropriate.

4.5.2 Biotinylation of rabbit IgG

The following procedure describes the preparation of biotinylated IgG. The antibodies were labelled with the fluorescent dye Cy5, as described previously. The molar ratio in the reaction mixture was 10:1 of biotinylation reagent (BAC-SulfoNHS, MW=556.8) to IgG (MW=150,000). The immobilisation of biotinylated, fluorescently labelled antibodies onto waveguides was used to evaluate the optical imaging performance of the sensor system.. This can not be used as a sensor.

A 10mg/ml solution of BAC-SulfoNHS was made up, by mixing 5mg of the reagent with 30µl of dimethylsulfoxide (DMSO) and making the solution up to 0.5ml with Phosphate Buffer Saline (PBS). DMSO was used to dissolve the biotinylation reagent. A 38µl sample of the reagent was added to 1ml of a 10mg/ml IgG solution. This sample was incubated with gentle stirring for 20 minutes at room temperature.

The biotinylated protein was separated from any un-reacted reagent by a fast gel-filtration step. The gel-filtration column, which is packed with Sephadex G-25M, was supported over a beaker and was equilibrated with 30ml of PBS. The reaction mixture was then added to the column. The reaction mixture was then eluted with 10ml of PBS, collecting 1ml fractions. The presence of the protein was monitored by measuring the absorbance at 280nm. An elution profile was obtained (figure 4.5). The fractions containing the protein were pooled and the concentration of the final mixture was obtained by measuring A_{280} of the protein.

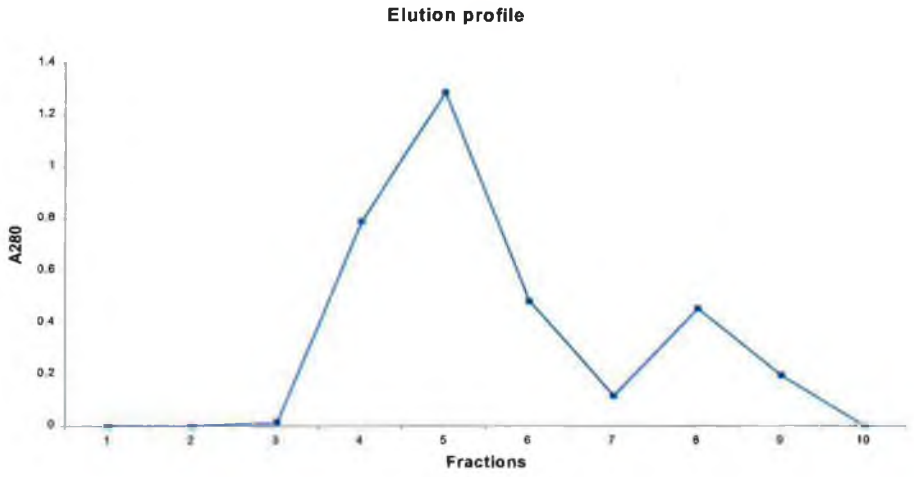

Figure 4.5 Elution profile-Protein concentration v's Fraction

The extent of biotinylation and the ratio of biotin to protein was determined by an avidin-HABA assay[8]. The protein concentration and the biotin content have to be determined in order for the ratio to be calculated.

To determine the protein concentration, a 0.1ml sample of the pooled protein, as described above, was diluted to 1ml by adding 0.9ml of PBS. The A_{280} of this sample was found using a 1cm-path length cuvette and an UV-Vis spectrophotometer. This was labelled "Protein Sample". To determine the biotin concentration, the avidin-HABA assay was used. HABA (4'-Hydroxyazobebzene-2-carboxylic acid) is a dye, which binds to avidin resulting in increased absorption of the dye at a wavelength of 500nm. The absorption of the avidin-HABA complex decreases proportionally with increased concentration of biotin as the HABA dye is displaced from avidin due to the higher affinity of avidin for biotin. Another 0.1ml sample of the biotinylated protein was incubated with 10µl of pronase, for 1.5 hours at 37°C. This sample was labelled "biotin sample". The reason for the pronase is to prevent steric hindrance of biotin to avidin and non-specific binding of the dye to the biotinylated protein. An avidin-HABA solution was made up by adding 0.1ml of 10mM HABA solution to 3.2ml of 10mM avidin solution. 0.1ml of the biotin sample was mixed with 0.9 ml of the avidin-HABA solution (Biotin sample). 0.1ml

of PBS was mixed with 0.9 ml of the avidin-HABA solution as a control. The absorbance of the biotin sample and the control at 500nm (A_{500}) was found. As the HABA dye is displaced from the avidin due to the higher affinity of avidin for biotin the absorption of avidin-HABA complex at 500nm can be seen to decrease. The corrected A_{500} was calculated by subtracting the value for A_{500} of the biotin sample, from A_{500} of the control sample. Protein and biotin concentrations in nmol/ml were calculated as follows:

$$\text{Protein (nmol/ml)} = \frac{A_{280} \times 10(dilution\ \_factor) \times 10^6}{E_{280}} \qquad 4.4$$

$$\text{Biotin (nmol/ml)} = \frac{Corrected\ \_A_{500} \times 10 \times 10^6}{E_{500}} \qquad 4.5$$

where the extinction coefficient E_{280} of IgG is107142 $M^{-1}cm^{-1}$ for a 1M solution and E_{500} is the extinction coefficient of the avidin-HABA complex and is equal to 34,000 for a 1M biotin solution.10^6 is the conversion factor from mol/l to nmol/ml. The final Biotin/Protein ratio was calculated using equation 4.6:

$$\frac{Biotin(nmols/ml)}{\text{Pr}\,otein(nmols/ml)} \qquad 4.6$$

All biotinylated antibodies used in the experiments described in chapter 4 have a final biotin/protein ratio of between 4-6. The exact ratio will be stated where appropriate.

4.5.3 Immobilisation of avidin to waveguides

The immobilisation process illustrated in figure 4.6 involves three steps: (1) A clean silica surface was coated with a silane film. (2) A heterobifunctional crosslinker with different reactive groups on each end was coupled to the thiol group on the silane, through its maleimide region. (3) The free succinimide end of the crosslinker forms an amide bond

with terminal amino groups on the avidin molecule. All the following work was carried out in a fume hood. The waveguides were numbered with an etching pen on the same side of the glass slide as the waveguide. All the slides were handled with a tweezers once the cleaning process had started so as not to disrupt the silanisation and patterning of the slides.

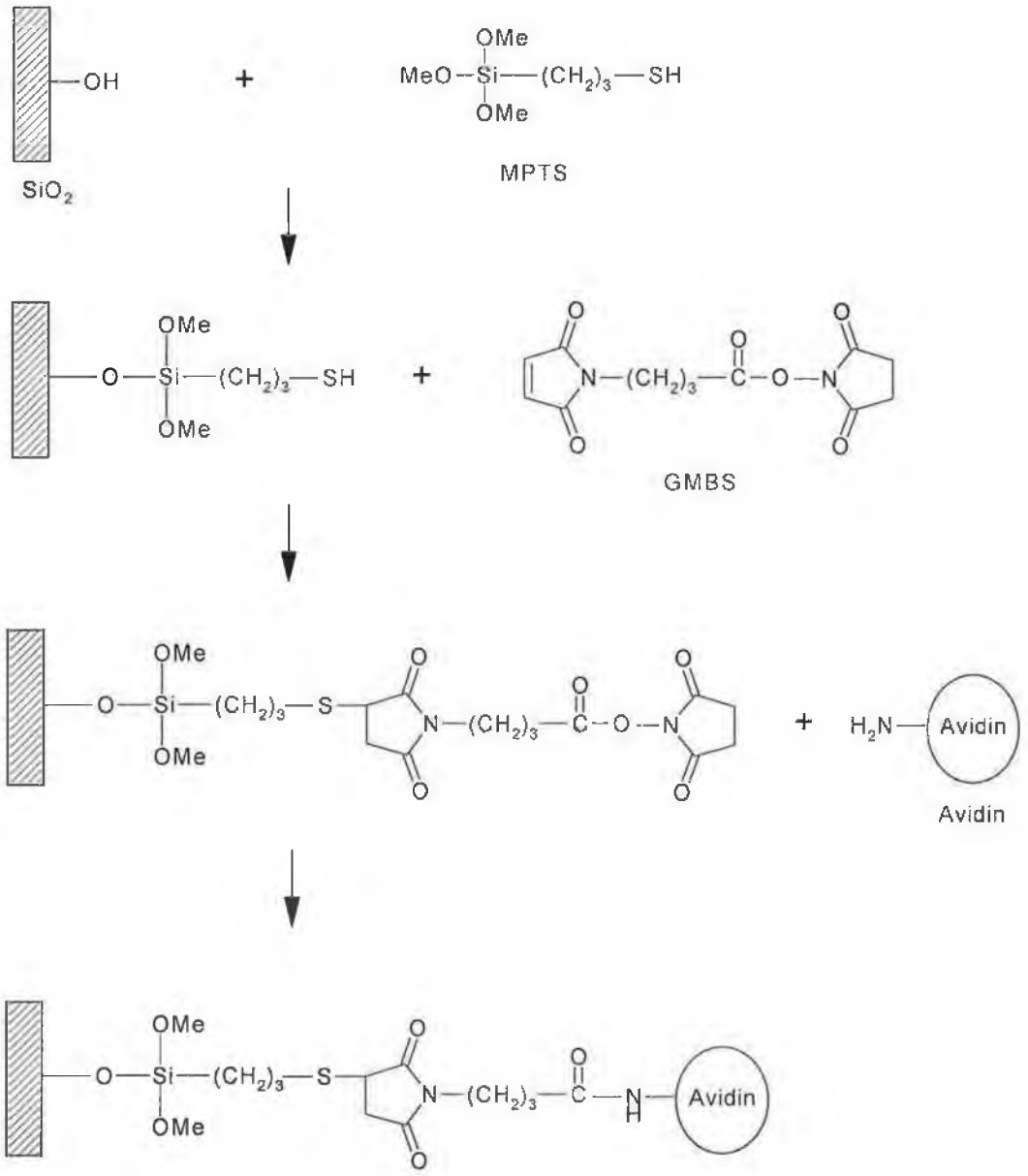

Figure 4.6 Immobilisation procedure for covalent attachment of avidin to silica surface.

1. Cleaning of waveguides and silanisation.

The waveguides were first acid-cleaned by immersion for twenty minutes in a 1:1 mixture of concentrated hydrochloric acid and methanol followed by rinsing in deionised water. The silanisation process started, by drying the slides with nitrogen and putting them into a clean beaker, containing a 2% solution of 3-mercaptopropyltrimethoxysilane (MPTS) in anhydrous toluene for 2 hours. The slides were then removed from the solution and rinsed three times in anhydrous toluene and allowed to air-dry face up on lint free tissue.

2. Heterobifunctional crosslinker

The organic crosslinking reagent, N-γ-maleimidobutyryloxy succinimide ester (GMBS), was dissolved (25mg) in 0.5ml of dimethylsulfoxide (DMSO) and then diluted with ethanol to a 2mM solution. The slides were left sitting in this solution for a half-hour and then washed in deionised water.

3. Immobilisation of Avidin.

A 3% streptavidin solution was made up by Adding 1ml of a 1mg/ml streptavidin solution in PBS to 30 ml of PBS-0.1% sodium azide (NaN_3) solution. The slides were left in this solution overnight at approximately 4°C. The slides were then removed and placed in a clean jar containing PBS-0.01% NaN_3 and stored at 4°C until use.

4.5.4 Patterning of slides

The following was the procedure employed for the patterning of waveguides with biotinylated labelled IgG. The set-up for the immobilisation process is shown in figure 4.7. The waveguide was fixed to a two-channel flow-cell using a clamp, and the relevant solutions were flowed through the channels. The channels were circular in shape with a 0.6cm diameter. With the rubber O-rings inserted to prevent any leaking, the active width of both channels becomes 0.3cm. Both channels have inlet and outlet tubes, which have a bore diameter of 0.1cm.

The slides were removed from PBS solution just before being clamped to the flow cell. Care was taken to avoid placing either of the channels over the grating coupler embossed onto the waveguide. A Gilson minipuls3 peristaltic pump was used to flow PBS-0.01%NaN_3 into both channels, in order to keep the avidin coating wet.

Antibody solution concentrations used in the following experiment ranged from between 10μg/ml to 50μg/ml. These were made up by diluting the biotinylated, Cy5 labelled, antibody solutions with PBS.

The antibody solutions were introduced to both channels of the flow cell, and were allowed to recirculate at a rate of 0.4ml/min for 2 hours. After this step, the channels were washed out using a PBS-0.001%Tween/20 solution followed by a 1mg/ml Bovine Serum Albumin (BSA) solution. The PBS/Tween was purely for washing away any unbound antibodies and the BSA was to help reduce non-specific binding. The next step was to dry the slides. A drying solution was introduced to the channels. The drying solution used was a low phosphate buffer, which consisted of 50mM sodium phosphate/100mM trehalose. The low phosphate buffer did not contain NaCl, which does not help the drying process. The trehalose is a sugar and provides a sugar coating over the bound antibodies to protect them. The drying solution was left static in the channels for 30 minutes. The slide was then removed from the flow cell and left to dry in air. Once dry, the slides were kept in the dark at 4°C until used.

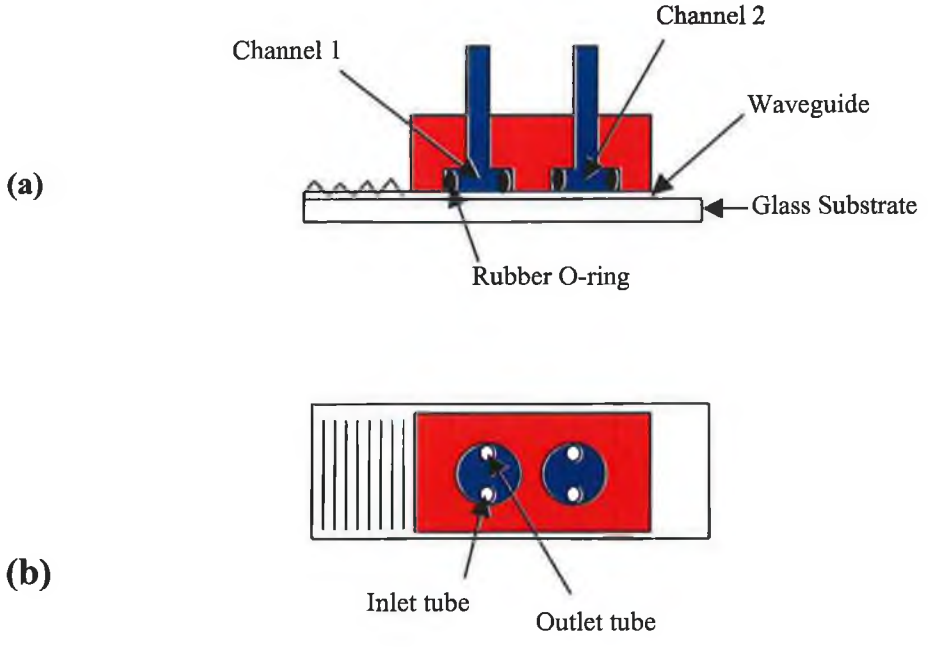

Figure 4.7 Flow cell used for Immobilisation of antibodies: (a) View from side; (b) View from top.

Channel one was always used as the control channel, in which an antibody concentration of 40μg/ml was used in all experiments. The second channel was used for a variety of concentrations, ranging from 10μg/ml to 50μg/ml. Once the slides were dried, two circular patches, approximately 0.3cm in diameter, corresponding to the two patches of immobilised antibodies were visible. The patches were more noticeable when the sugar coatings protected them.

4.6 Conclusion

Rabbit IgG was biotinylated with a final biotin/protein ratio of 4-6, i.e. approximately 4-6 biotin molecules are attached to every molecule of the antibody. The molar ratio of Cy5 fluorescent label to the same IgG was calculated to be 2-4. Sol-gel waveguides were coated with a layer of avidin using a covalent binding technique employing a heterobifunctional crosslinker. These waveguides were patterned with two spots of biotinylated antibodies which were also fluorescently labelled.

References

1. Duveneck G.L., Pawlack M, Neushafer D, Bar E, Budach W, Pieles U, Ehrat M, **'Novel bioaffinity sensors for trace analysis based on luminescence excitation by planar waveguides'**, Sensors and Actuators B, 38-39, pp88-95, 1997.

2. Bhatia S.K., Shriver-lake L.C., Prior K.J., Georger J.H., Calvert J.M., Bredehorst R., Ligler F.S., **'Use of thiol-terminal silanes and heterobifunctional crosslinkers for immobilisation of antibodies on silica surfaces'**, Analytical Biochemistry 178, pp408-413, 1989.

3. Narang U, Anderson G.P., Ligler F.S., Burans J, **'Fiber optic-based biosensor for ricin',** Biosensors and Bioelectronics, vol 12, 9-10, pp937-945, 1997.

4. Polzius R, Schneider Th, Bier F.F., Bilitewski U, **'Optimization of biosensing using grating couplers: immobilisation on tantalum oxide waveguides'**, Biosensors and Bioelectronics, vol. 11, 5, pp503-514, 1996.

5. Wilchek M. Bayer E.A., **'Avidin-Biotin technology'**, Methods in enzymology, vol. 184, 1990, Academic press Inc..

6. Gyorgy Y., **'The Vitamins'**, vol.1, p527, Academic press Inc., New York, 1954.

7. Newman D.J., Olabiran Y, Price C.P., **'Chapter 3: Bioaffinity agents for sensing systems'**, Handbook of biosensors and electronic noses, 59-86, 1997, CRC Press Inc..

8. Wood P, Barnard G, **'Chapter 16: Fluoroimmunoassay'**, Principles and practice of immunoassay 2nd edition, p389, Macmillan Ref. Ltd, 1997.

9. Diamardis E.P., **'Immunoassay with time resolved fluorescence spectroscopy: Principles and applications'**, Clin. Biochem., 21, 139, 1988.

10. Zhou Y, Magill J.V., De La Rue R.M., Laybourn P.J.R., Cusley W, **'Evanescent fluorescence immunoassays performed with a disposable ion-exchanged patterned waveguide'**, Sensors and Actuators B, 11, pp245-250, 1993.

11. Mujumdar R.B., **'Cyanine dye labeling reagents: Sulfoindocyanine Succinimidyl Esters'**, Bioconjugate Chemistry, 4(2), 105-111, 1993.

12. Southwick P.L., **'Cyanine dye labeling reagents: Carboxymethylindocyanine Succinimidyl Esters'**, Cytometry, 11, 418-430, 1990.

13. Taylor R.F., **'Protein immobilisation: fundamentals and applications'**, Marcel Dekker, New York, 1987.

Chapter 5 Optical System and Imaging

5.1 Introduction

Planar waveguide sensors are ideally suited to multianalyte sensing. On a single sensor chip, many different chemical reactions can be monitored simultaneously. The techniques involved in the local immobilisation of antibodies on such surfaces have been developed[1,2,3]. Such arrays can be used to perform multiple analyte measurements, or in a pattern scheme, where each immobilised receptor patch is specific for a defined analyte. Planar waveguides are more attractive than fibre optics, because they are easier to coat with a reagent layer[4] for use in an array sensor. Moreover, the 2-dimensional surface of the waveguide lends itself to spatial patterning of multi-analyte array elements.

Both mono-mode[5,6] and multi-mode[1,2] waveguides have been used for immunosensing. Polzius *et al* [5] and Duveneck *et al* [6] have described the immobilisation of biomolecules on the surface of tantalum oxide waveguides. The immobilisation included a variety of strategies, e.g. covalent attachment, avidin-biotin bridges and adsorption. Both groups reported the use of these sensors for bio-affinity analysis. Feldstein *et al* [1] reported the use of low cost, disposable multi-mode planar waveguides patterned with immobilised capture antibodies using a physically isolated patterning (PIP) method. This method enabled simultaneous deposition of several antibodies and completely circumvented cross immobilisation problems encountered with other approaches. This resulted in an optical and fluidics system that was able to perform fluorescence assays with an array of capture molecules. Another array immunosensor for the detection of multiple analytes was reported by Rowe *et al* [2] . The sensor was able to perform simultaneous assays for viruses, bacteria and toxins, indicating that it could be used to detect very different types of analytes on a single substrate.

In this chapter, the imaging of a variety of concentrations of fluorescently labelled antibodies immobilised onto a waveguide is described. The optical system reported here employs a non-inverting 2 dimensional graded index (GRIN) lens array (Nippon Sheet

Glass) to provide a 1:1 image of an evanescently excited fluorescent pattern onto a CCD array. The sensor platform is a mono-mode sol-gel planar waveguide described earlier.

5.2 Optical System

5.2.1. Waveguide Excitation

Fluorescently labelled antibodies immobilised onto a waveguide surface were optically interrogated using the evanescent wave of a guided mode resulting from the injection of light from a 633nm-laser diode. The laser beam was launched onto the edge of the embossed grating nearest the immobilised antibodies. Once coupling conditions were reached, a streak of light was visible propagating along the waveguide, in the direction away from the grating (figure 5.1).

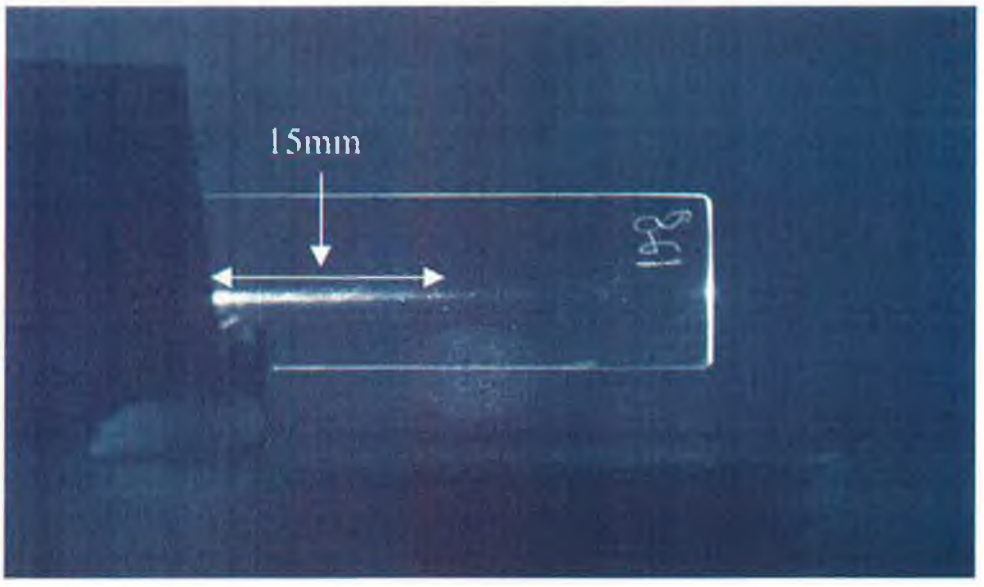

Figure 5.1 Camera image showing coupled mode propagating left to right along waveguide.

This streak was used to evanescently excite the fluorescent spots on the waveguide. The width of the streak was the same as the width of the laser spot (≈ 2-3mm). Only waveguides that produced streaks between 10-15mm in length were used in the following experiments. The laser diode was permanently mounted on an optical bench. Its beam was incident on the grating coupler of the waveguide. The imaging system was rotated relative to the laser beam until coupling conditions were met. The rotation stage was then clamped at this fixed angle, so as no more adjustments to the laser diode were required before imaging the sensing surface.

5.2.2 Imaging system.

The evanescently excited fluorescent spots were imaged (figure 5.2) onto a thermoelectrically cooled charge coupled device (CCD) imaging array (Sensicam PCO CCD, Pulse Electronics, U.K.). A cooled camera was used so as to detect the low fluorescent light levels emitted by the fluorescent antibodies. Exposure times on the cooled CCD camera could be selected in the range from 1 millisecond to 1000 seconds.

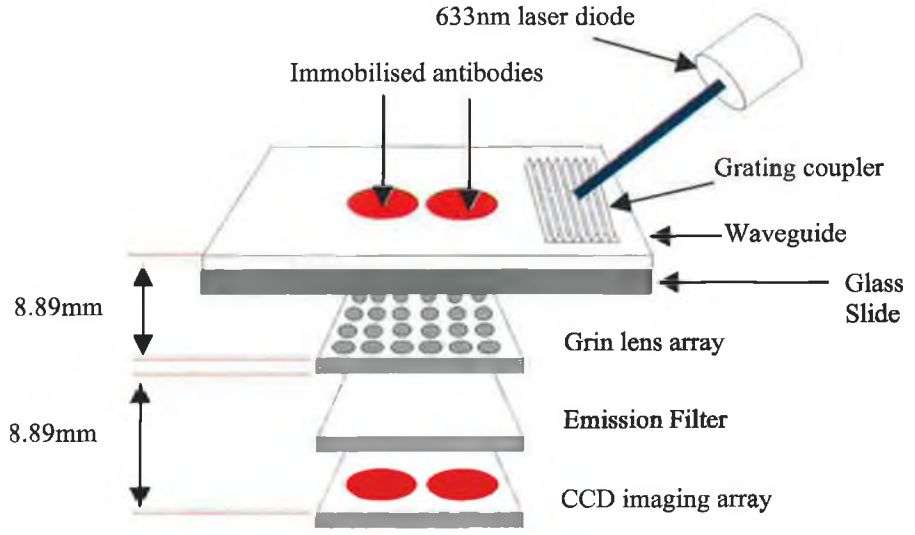

Figure 5.2 Imaging system showing laser diode excitation and a graded index (GRIN) lens array (GRIN).

A bandpass filter (Omega Optical, U.K.) with a centre wavelength of 670nm and a bandpass of 40nm, was used to discriminate between excitation and emission light. A non-inverting 2 dimensional graded index (GRIN) lens array (Nippon Sheet Glass, Japan) was used to image (1:1 ratio) the fluorescent emission from the spots onto the CCD camera [1].

GRIN (GRadient INdex) lenses are rod lenses in which the index of refraction varies in a parabolic fashion with a maximum index at the centre. The propagation paths in such lenses are illustrated in figure 5.3. By manufacturing such lenses with the correct length, they can smoothly and continually redirect light rays towards a point of focus (figure 5.3). The internal structure of this index "gradient" can dramatically reduce the need for tightly controlled surface curvatures and results in a simple, compact lens geometry [2]. Furthermore, 2-D arrays of such lenses have only recently become available. The important features of such lens arrays are the planar orientation of the arrays and also the short operating distance (equivalent to focal length), which make them ideal for use in a compact optical imaging system.

Three benefits were derived from the use of a GRIN lens array: (1) Each lens produced an erect image at the focal plane, in contrast to standard lens arrays. (2) The short focal length and high numerical aperture of each lens, provided enhanced fluorescence capture efficiency. (3) The compact size of the lens array was critical for keeping the sensor system small. The focal length of the lens array used in these experiments was 8.89mm.

The imaging system was mounted on a rotation stage that was fixed to an optical bench. The waveguide was clamped perpendicular to the stage. The coated side of the glass substrate was facing towards the camera. The GRIN lens array was mounted at a fixed distance of 8.89mm from the waveguide (figure 5.2). A slot was machined into the stage to facilitate the 670nm bandpass filter, in-between the waveguide and the lens array. The CCD camera was fixed to the opposite end of the stage. This was mounted onto a translation stage, which was used to adjust the distance between the lens array and CCD array to the optimum length of 8.89mm.

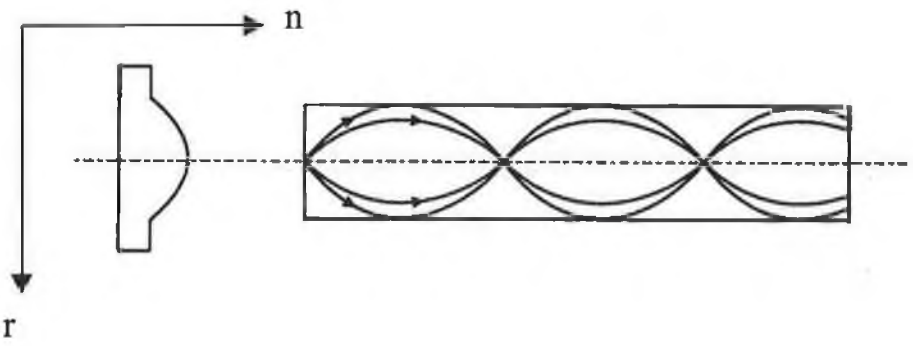

Figure 5.3 Refractive index profile of GRIN lens.

5.2.3 Camera operation.

The CCD camera was controlled and images displayed on the monitor in a Windows environment by using the "Sensicontrol" software, which is provided by the cameras manufactures. The recorder function allowed the user to record single images or image sequences and to display them on the monitor (figure 5.4).

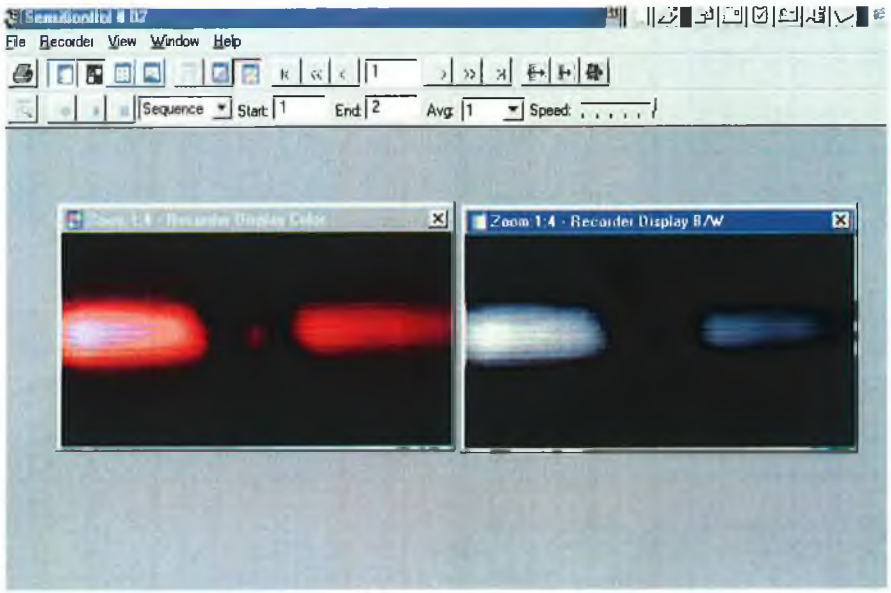

Figure 5.4 Sensicam software window showing an image in colour and in black and white.

The sensor type is a CCD-interline progressive scan. It has 1280 horizontal (H) × 1024 vertical (V) pixels on an array area of 8.6mm × 6.9mm. The camera is cooled to a temperature of -12°C by a 2-stage peltier cooler with forced air-cooling. The benefit of a cooled CCD camera is its reduction of thermal noise and its consequent ability to detect lower light levels. The peltier-cooled CCD used provided noticeable improvements over a room temperature camera employed previously as it had a lower and more stable electronic background..

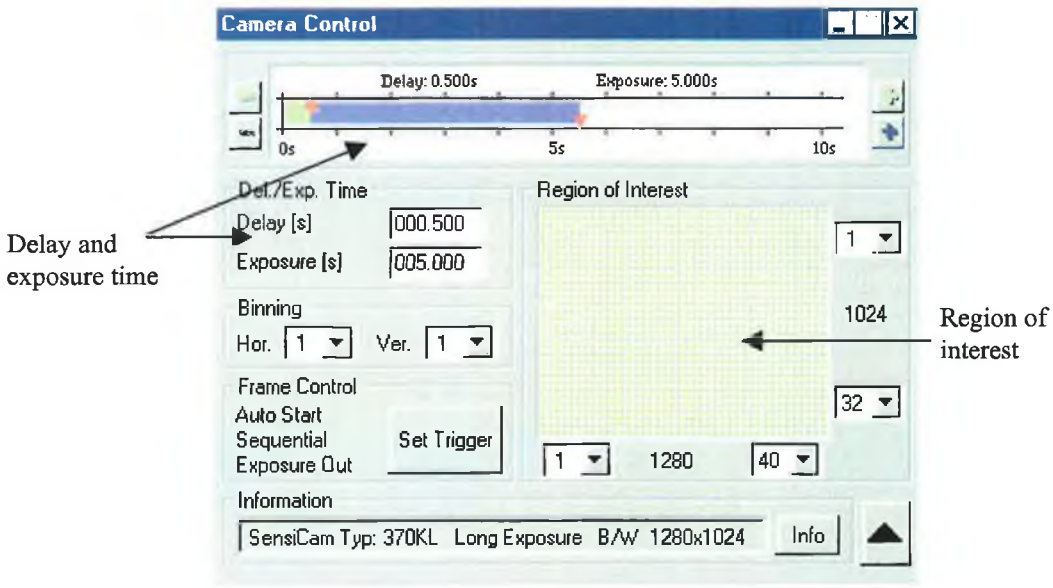

Figure 5.5 Camera control window

The camera settings can be controlled via the camera control window (figure 5.5). The camera control window allows the user to select exposure times by a sliding bar (blue bar) or by direct input with the keyboard. There is also a delay option (green line), in which the camera can be delayed before taking an image. This also has a range of 1ms to 1000s. The camera control window also enables the user to select the imaging area, as long as this is within the CCD array area. Figure 5.5 shows the region of interested highlighted in green. This shows that the whole area of the array is exposed. The area can be selected by mouse or by keyboard input.

Because a range of antibody concentrations was immobilised onto the waveguide surfaces investigated, exposure times varied depending on the fluorescence intensity. Ten seconds was the standard exposure time. For strong signals, exposure times as low as 0.5secs were used, whereas for weak signals, images were collected for 30secs.

5.2.3 Image analysis

The images taken with the camera were in a 12-bit format. However, when the images were exported from the camera software they were converted to an 8-bit image. Images were subsequently viewed in Adobe Photoshop 5.0.

Images were taken of a series of waveguides. Each had two immobilised spots. One was a reference spot, which had a fluorescently labelled antibody concentration of 40μg/ml and the other, the signal spot, had one of a series of concentrations ranging from 5μg/ml to 50μg/ml. A square covering an area of 2500 pixels was highlighted on each spot as in figure 5.6. The mean pixel intensity for each spot and the adjacent background intensity, indicated in fig 5.6 as the dark region, were extracted from each image using the histogram function in Photoshop. The mean fluorescent signal (MFS) for each of the spots was calculated by subtracting the background pixel intensity from the mean pixel intensity of the spot.

The fluorescence intensity of the signal spot was also corrected for the propagation loss of the waveguide. The relationship between the attenuation coefficient which is expressed in dB/cm and actual percentage of power lost as the guided mode propagates along a unit length of the waveguide was presented earlier in chapter 3. This issue is important because the two spots on the waveguide are excited by two different excitation powers, and consequently cannot be compared without correction.

To correct the signal fluorescence level, the 670nm bandpass filter was removed and the excitation light, i.e. the guided mode, was imaged using an exposure time of 1.5seconds. It was noted that although the excitation light was exciting fluorescence, the amount of fluorescence was considered negligible. The propagation loss of the waveguide was then calculated as described previously. Using this value, the % power loss over 1cm can then

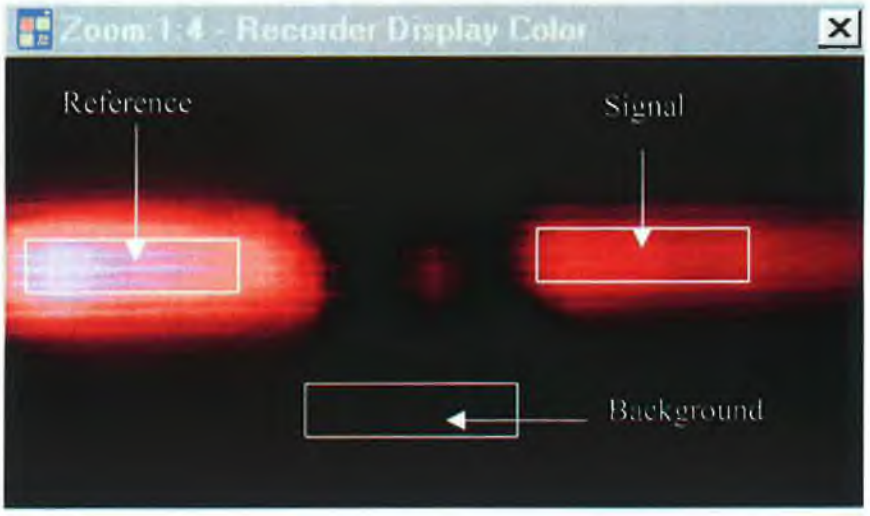

Figure 5.6 Fluorescence image of antibody spots on a waveguide. Mean fluorescence intensity values extracted were from the areas highlighted.

be evaluated from figure 3.5 in chapter 3. Assuming that the power level of the excitation light is proportional to the fluorescence excited, the fluorescence intensity level at the signal spot can be normalised. Essentially this adjusts the fluorescence level up to the fluorescence level that would be emitted if the spot was excited with the same intensity of excitation light as that of the reference spot.

Once the signal intensity has been evaluated, a normalised intensity for the signal spot was calculated by dividing the MFS for the signal spot by that of the reference spot. This corrects for variations between waveguides,

5.3 Results

Seven different concentrations of labelled antibodies were immobilised on waveguides, with each waveguide having a different propagation loss and grating efficiency. Figure 5.6 shows a typical image of evanescently excited fluorescence from the spots. On the left is the reference spot consisting of immobilised fluorescently labelled IgG,

that had an antibody concentration of 40μg/ml, and on the right is a spot of immobilised IgG, with a concentration lower than that of the reference spot.

A series of control experiments was carried out to determine whether the 670nm discriminating filter was rejecting the excitation light sufficiently so that only fluorescence was being detected. Images were taken of waveguides with: (a) No immobilised antibodies on either spot. (b) Immobilised antibodies (not fluorescently labelled) on both spots. (c) Immobilised Cy5 labelled antibodies on one spot and non-labelled antibodies on the other. For (a) and (b), images showed, after an exposure time of 20 secs in each case, no fluorescence and only a very small background level. For (c), images showed fluorescence on the spot covered by labelled antibodies and none on the second spot (figure 5.7). From these tests one could conclude that the light being detected by the CCD was evanescently excited fluorescence from the antibody spots.

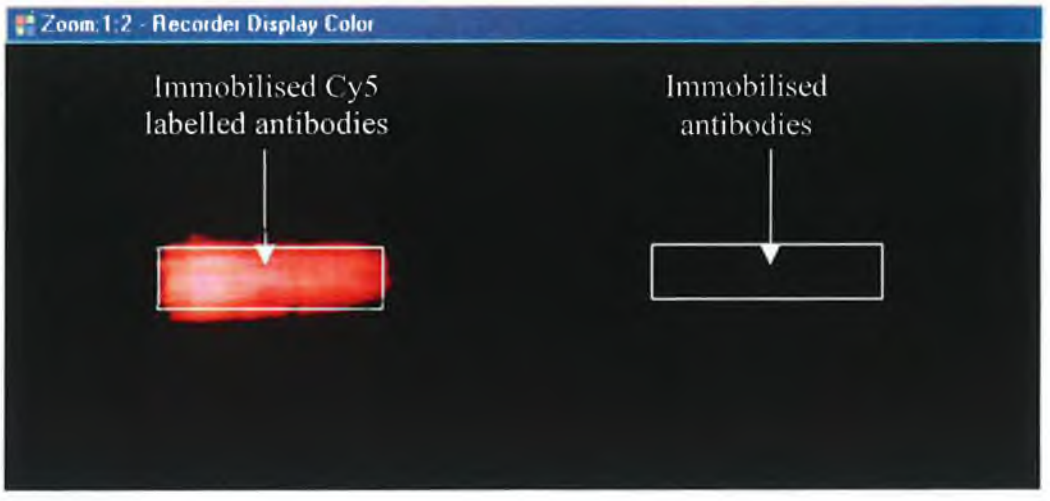

Figure 5.7 Control experiment (c)

Figure 5.8 shows normalised fluorescence data obtained from the different concentrations of immobilised fluorescently labelled antibodies. The intensities of 7 different concentrations of antibodies were calculated using the method described earlier.

The different concentrations of antibodies all had the same dye/protein ratio. The graph shows the normalised corrected signal of evanescently excited fluorescence at various concentrations. The observed signal for each concentration was normalised by a 40μg/ml antibody sample signal and represents the mean fluorescence intensity over a fixed area of the spot (± Standard Deviation).

Figure 5.8 showed that different concentrations of fluorescently labelled antibodies immobilised to the waveguide surface could be detected using the image detection system described. Although the experiments described were not real immunoassays, the approximate linearity of the curve suggest that the system could be used in real assays.

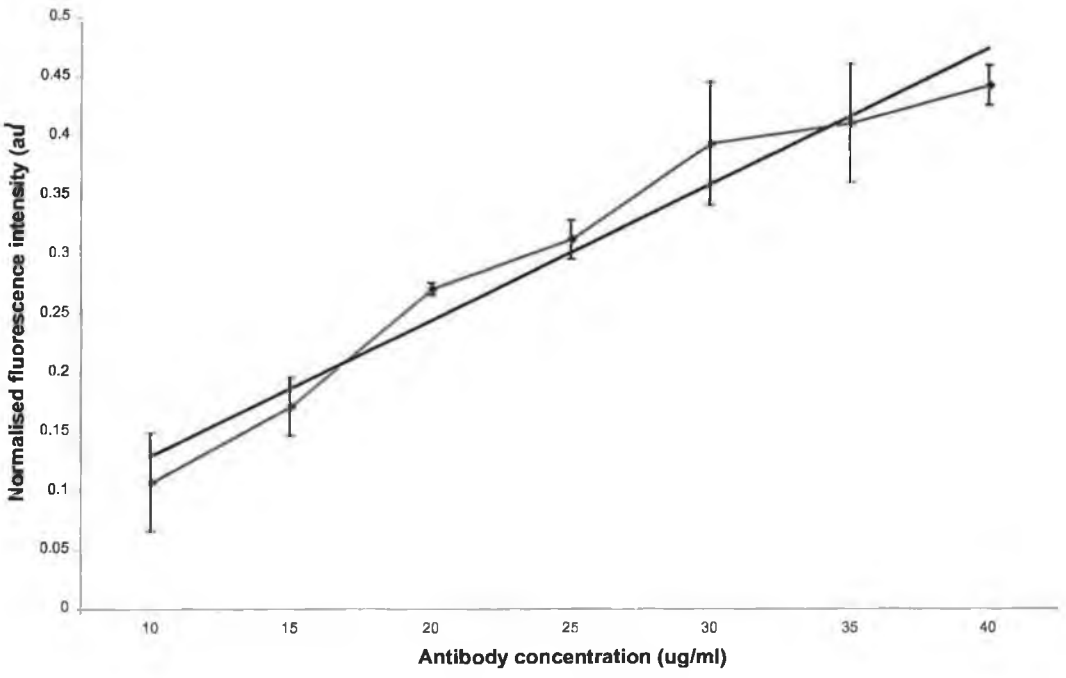

Figure 5.8 Calibration curve of immobilised antibodies.

The fluorescent intensities were directly related to antibody concentrations, as all antibodies used had the same dye/protein ratio.

This measurement system exhibits a number of problems, however. Fig 5.19 shows an image of a guided mode in a typical waveguide. The image was taken with an exposure time of 0.05 seconds with no filters in place. It is evident that there is a significant amount of scattered light, due to dust particles within the waveguide itself. The propagation loss of the intensity, as described earlier, is clear. But, it can also be seen that the intensity is not uniform over the width of the propagating mode, resulting in streaks of light. This is also evident in figure 5.6, where the fluorescent intensity of both the reference and signal spots are not uniform across the width of the spot. These "streaks" cause problems in the measurement of fluorescence intensities from waveguide to waveguide.

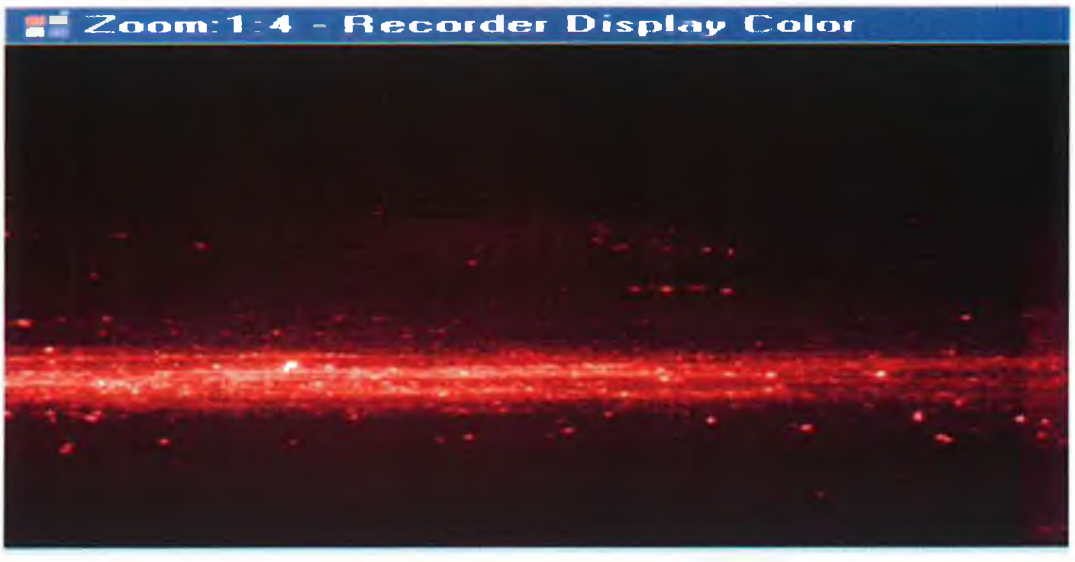

Figure 5.9 Image of guided mode, showing non-uniformity of intensity across width of propagating mode.

References

1. Feldstein M.J., Golden J.P., Rowe C.A., MacCraith B.D., Ligler F.S., **'Array Biosensor: Optical and Fluidics systems'**, Journal of Biomedical Microdevices, 1:2, pp139-153, 1999.

2. Rowe C.A., Tender L.M., Feldstein M.J., Golden J.P., Scruggs S.B., MacCraith B.D., Cras J, Ligler F.S., **'Array biosensor for simultaneous identification of bacterial, viral and protein analysis'**, Analytical Chemistry, 71(17), pp3846-3852, 1999.

3. Zhou Y, Magill J.V., De La Rue R.M., Laybourn P.J.R., Cushley W, **'Evanescent fluorescence immunoassays performed with a disposable ion-exchanged patterned waveguide'**, Sensors and Actuators B, 11, pp245-250, 1993.

4. Rabbany S.Y., Donner B.L., Ligler F.S., **'Optical Immunosensors'**, Critical reviews in biomedical engineering, 22(5/6), pp307-346, 1994.

5. Polzius R, Schneider Th, Biert F.F., Bilitewski U, **'Optimisation of biosensing using grating couplers: immobilisation on tantalum oxide waveguides'**, Biosensors and Bioelectronics, Vol 11, No. 5, pp503-514, 1996.

6. Duveneck G.L., Pawlak M, Neuschafer D, Bar E, Budach W, Pieles U, Ehrat M, **'Novel bio-affinity sensors for trace analysis based on luminescence excitation by planar waveguides'**, Sensors and Actuators B, 38-39, pp88-95, 1997.

Chapter 6 Sensing with Surface Plasmon Resonance

6.1 Introduction

A surface plasmon is an electromagnetic field charge density oscillation that can exist at a metal-dielectric interface. This phenomenon occurs as a result of total internal reflection of incident light on the metal-dielectric interface. It propagates as a bound non-radiative surface electromagnetic mode along the metal-dielectric interface, and is resonantly excited by p-polarised light once momentum conditions are satisfied. Upon excitation of the surface plasmons, an electromagnetic field is formed which decays exponentially with the distance from the metal film surface into the interfacing medium. When resonance occurs, the reflected light intensity from the metal surface goes through a minimum at a defined angle of incidence, known as the plasmon resonance angle. The plasmon resonance angle depends on the optical properties of the incident medium, the type and thickness of the metal, the wavelength of the incident radiation and the refractive index of a thin layer adjacent to the metal surface, which is within sensing distance of the plasmon field. This last factor is exploited in surface plasmon resonance sensors.

SPR was first demonstrated in 1968 by Otto [1] using the prism/air-gap/metal configuration shown in figure 6.1a. He showed that, at a specific angle of incidence, the internal reflection of the light beam from the inner surface of a prism was significantly attenuated if a silver film was brought close to the prism surface. The problem with this configuration, however, is the difficulty of maintaining a small and precise separation between prism and metal [2] . A more favoured configuration is the Attenuated Total Reflection (ATR) method, proposed by Kretschmann and Raether [3], shown in figure 6.1b, in which the air gap is replaced by the metal itself.

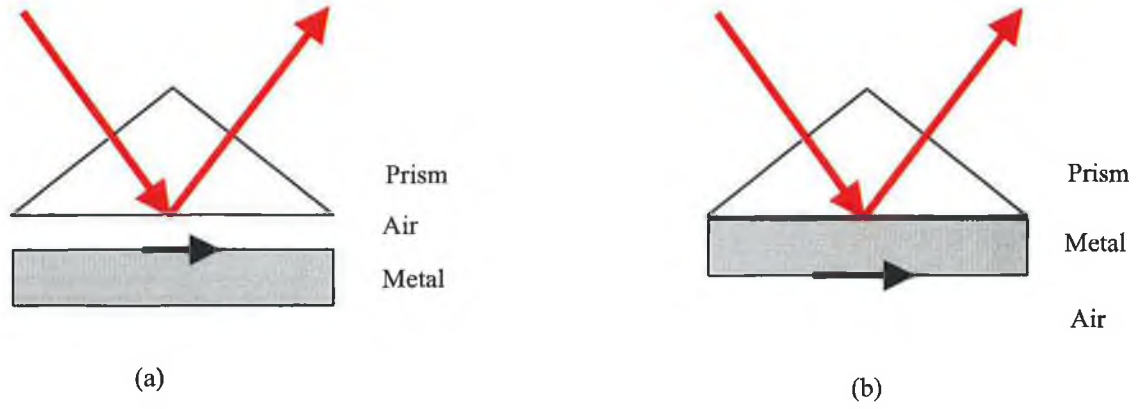

Figure 6.1. (a) Otto configuration; (b) Kretschmann and Raether configuration

SPR was first employed in a sensing device by Nylander et al [4], who showed that a gas sensor could be constructed from a prism coated with silver, the outer surface of which was covered with an overlayer of silicone oil. When monochromatic, p-polarised light was incident internally on the silver films, the reflectivity exhibited a dip at angles for which a the surface plasmon wave was excited. The exact position of this dip was characteristic of the refractive index of the oil. When a mixture of halothane gas and nitrogen was passed over the oil surface, halothane was adsorbed. As a result the refractive index of the overlayer was altered, thereby changing the reflectivity plot and hence indicating the presence of the gas. A linear relationship between the angle of minimum reflectivity and the concentration of halothane was found.

Later, Liedberg and Nylander[5] used a similar version of the gas sensor (Kretschmann configuration) to study antibody-antigen interactions at the surface of the silver film. Gamma-globulin IgG was adsorbed on the silver surface and used to sense various concentrations of anti-gamma globulin IgG. As the anti-gamma-globulin IgG bound to the layer of gamma-globulin IgG on the silver surface, a shift in the plasmon angle was observed. Since this work there have been many studies carried out using SPR for the studies of interactions between biomolecules [6-11].

Recently a real-time immunosensor has become commercially available (BIAcore^{TM}, Pharmacia Biosensor AB, Uppsala, Sweden). The biosensor group from Pharmacia have reported the use of SPR for the detection of various proteins on a sensor

chip consisting of a thin gold film deposited on a glass support and covered with a carboxymethyl-dextran hydrogel matrix [12]. This matrix provides covalent linkage sites for antibody binding and also protects the film from non-specific protein adsorption. This commercial biosensor makes use of a flow injection cell, which permits kinetic measurements over a wide dynamic range, and significantly reduces the incubation time required for interaction analyses compared with static solid-liquid sensing. This flow-injection technology also simplifies handling of the biosensor surface. The BIAcore ™ has its refractive index resolution optimized to about 3×10^{-7} refractive index units (RIU). This is an example of a bulk prism based SPR sensor. The sensor, coupled with an advanced detection system and angle measurement algorithm, results in a high performance sytem which enables high resolution measurements. Its large size and cost, however, limits its use to laboratory applications.

Miniaturised SPR sensors using the ATR method have been developed as an alternative to laboratory SPR systems. These have been developed as compact and cost effective sensing devices with potential for field applications. One such sensor, developed by Texas Instruments[13], integrates a light source, a detector and an optical system for excitation and interrogation of surface plasmon waves into a single sensor chip. The system relies on the detection of the angular position of surface plasmon resonance by measuring the reflection of a divergent light beam, using a 128 pixel linear Si detector array. It includes a temperature sensor and exhibits a resolution of 1×10^{-5} RIU [13].

This chapter, discusses the use of this Texas Instruments SPR sensor as a liquid refractive index sensor and a sensor for the detection of biomolecules. Work was also carried out on the fabrication of gold coated glass slides for use as disposable sensor chips on the TI SPR sensor.

6.2 Theory of Surface Plasmon Resonance

SPR excitation occurs when photons are incident on a metal/dielectric interface at an angle above the critical angle. The evanescent wave which penetrates the metal layer interacts with free oscillating electrons in the metal, and creates a propagating wave. This wave will propagate over distances of approximately a few microns, exhibiting an evanescent wave which is perpendicular to the interface which penetrates the adjacent media. Figure 6.2 shows plane polarised monochromatic light incident on a smooth interface between two media, both of which are lossless and nonmagnetic (i.e. the magnetic permeablity, μ, for all layers is equal to μ_0). The light strikes the interface at some arbitrary angle θ, and is partially transmitted into the second medium, while the remaining light is reflected.

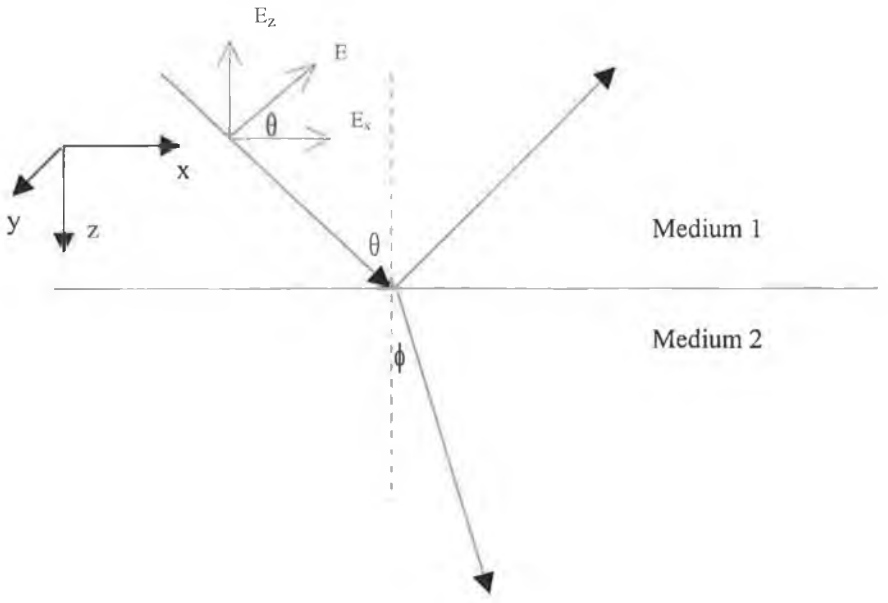

Figure 6.2 TM light incident on a planar interface at an incident angle θ, producing a transmitted and reflected beam.

The light is linearly polarized, with its electric (E) field vector parallel to the plane of incidence. This is said to be p-polarized (Transverse Magnetic). In this case there is an E-field component perpendicular to the interface such that $E_z = |E|.\mathrm{Sin}(\theta)$. As both media

on either side of the interface have differing refractive indices, they also have differing dielectric permitivities $\varepsilon_1=(n_1)^2$ and $\varepsilon_2=(n_2)^2$.

The permittivity of a metal changes with the frequency of the incident electromagnetic waves. This dependence is described by the dispersion relation. For an ideal metal consisting of undamped free-electrons, the optical permittivity of the material is dictated by what is known as the plasma frequency, ω_p, the value of which is characteristic of a given metal, and which represents the highest frequency at which its electrons can oscillate. The can be expressed as

$$\varepsilon_{metal} = 1 - (\frac{\omega_p}{\omega})^2 \qquad 6.1$$

where ω is the frequency of the incident radiation

To examine SPR in more detail it is necessary to apply Maxwell's electromagnetic wave equations to the behavior of the light at the interface. For the resonant wave propagation in the x-direction, the surface plasmon wave can be described by the equation

$$E_z(x,z,t) = E_x^{\ 0}(z)\exp(i\omega t - ik_x x) \qquad 6.2$$

where k_x is the x-component of the wavevector k. When all boundary conditions are met they result in the expression [2]

$$\frac{\varepsilon_1}{k_{z1}} = \frac{\varepsilon_2}{k_{z2}} \qquad 6.3$$

where k_{z1} and k_{z2} are the z-components of the wavevector k, in medium 1 and 2 respectively. The wavevector is in the same direction as the propagating light, and can be split into separate x- and z-components such that

$$k_{x1} = (\varepsilon_1)^{1/2} \cdot k \cdot \sin(\theta) = k_x \qquad 6.4$$

$$k_{z1} = (-k_x^2 + \varepsilon_1 \cdot k^2)^{1/2} \qquad 6.5$$

$$k_{z2} = (-k_x^2 + \varepsilon_2 \cdot k^2)^{1/2} \qquad 6.6$$

Substituting equation 6.5 and 6.6 into equation 6.3 gives us the expression for the propagation constant of the surface plasmon wave[1]

$$k_{sp} = \frac{\omega}{c}\left(\frac{\varepsilon_1 \cdot \varepsilon_2}{\varepsilon_1 + \varepsilon_2}\right)^{1/2} \qquad 6.7$$

where ω is the frequency of the propagating wave and c is the speed of light. This expression is the dispersion relation for the surface plasmon, propagating along the interface between a metal with a complex permittivity, and a dielectric with a real permittivity. This expression can be illustrated in figure 6.3 as line no. 2. If a propagating resonant mode k_x is real, then $|\varepsilon_2| > \varepsilon_1$. However a real metal possesses an imaginary component of its permittivity, such that $\varepsilon_2 = \varepsilon_{2r} + i \cdot \varepsilon_{2i}$, and this makes k a complex quantity ($k_x = k_{xr} + i \cdot k_{xi}$).

It is not possible, however, to set up a surface plasmon at the interface by using a direct reflection technique, i.e. with light incident from a less dense medium, because k_{sp} in equation 6.7 will always be larger than the wavevector k_x in the incident medium which is given as

$$k_x = \left(\frac{\omega}{c}\right)(\varepsilon_1)^{1/2} \sin\theta_{sp} \qquad 6.8$$

This problem is clearly illustrated in figure 6.3, where the dispersion relation for the incident light in the dielectric at an angle θ, always lies to the left of the dispersion relation for the surface plasmon. Excitation of the surface plasmon requires momentum in excess of the maximum which may be supported in medium 1, and it is therefore impossible for incident light to couple directly to the surface plasmon.

One way to overcome this problem with the mismatch between the wavevectors is to employ the ATR configuration shown in figure 6.4 where the metal layer is deposited onto a high index prism or glass slide such that $\varepsilon_1 > \varepsilon_3$. The wavevectors for the surface plasmon and the incident light are given as

$$k_{sp} = \frac{\omega}{c}\left(\frac{\varepsilon_2\varepsilon_3}{\varepsilon_2+\varepsilon_3}\right)^{1/2} \qquad 6.9$$

$$k_x = \left(\frac{\omega}{c}\right)(\varepsilon_1)^{1/2}\sin\theta_{sp} \qquad 6.10$$

The relation that must be reached for SPR to occur is to match the wavevector k_x of the incident light to that of the surface plasmon k_{sp}. From fig. 6.3 we see immediately that a part of the dispersion relation of k_{sp} lies to the left of that of k_x. If the angle θ, measured in the medium ε_1, is varied from zero to higher values, total reflection starts at $\sin\theta = 0$ or $k_x = \omega/c$ and continues up to $\text{Sin}\ \theta = 1$ or $k_x = (\omega/c)(\varepsilon_1)^{1/2}$. Between these two limits the wavevector for the incident light k_x meets that of the surface plasmon k_{sp}. Thus plasmons that lie on the line to the left of the light line can be excited by photons coming from the medium ε_1 whose momenta have increased by a factor of $\varepsilon^{1/2}$. If the dispersion relation is fulfilled, a drop is seen in the intensity of the totally reflected light. Absorption takes place, and the reflectance drops from a value of one to smaller values. This represents attenuated total reflection, and is found in all metals due to the finite value of their imaginary part.

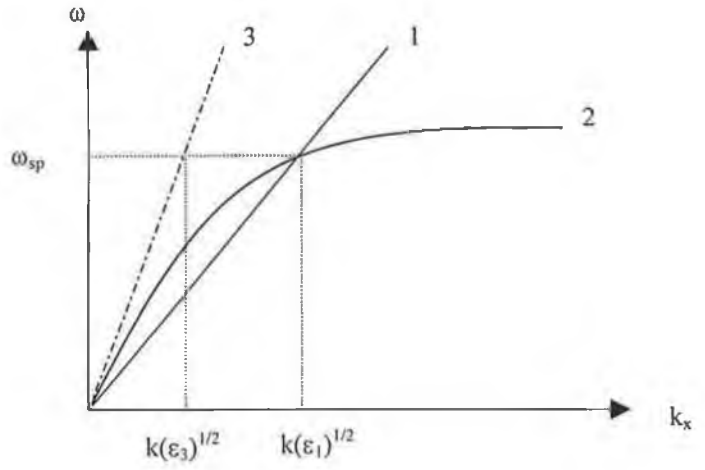

Figure 6.3 Dispersion relations for (1) Light in Glass; (2) Surface plasmons; (3) Light in air. SPR occurs at the intercept of 1 and 2.

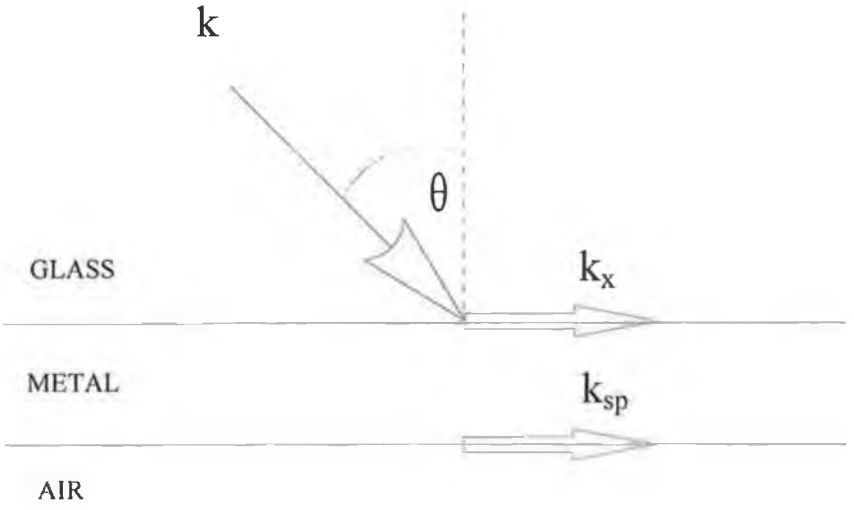

Figure 6.4 Schematic illustration of the ATR configuration. The surface plasmon is excited at the metal/air interface.

6.2.1 Fresnel Coefficients

The thickness of the metal film is very important with respect to the excitation of a surface plasmon wave. A thick metal film would act as a mirror, reflecting all light, incident upon it, and no light would be able to penetrate to the medium on the other side. If the metal layer were too thin then the two interfaces, glass/metal and metal/air would interfere with each other. The metal layer must be thick enough to prevent this interference, and to ensure that the surface plasmon wave excited at the air/metal interface is independent of the parallel glass/metal interface. By increasing the metal layer thickness, the evanescent field that penetrates through to the air/metal interface is also reduced. To optimise the excitation, a balance is needed between the metal thickness and the magnitude of the evanescent field. Examination of the dispersion relation (permittivity vs frequency) of various metals shows that the permittivity of the metal layer changes with thickness. Consequently, if one examines the dispersion relation of various metals, only a few metals can support sharp, well defined surface plasmon waves. The most commonly used metals are silver, gold, platinum and aluminium. For the purposes of the experiments reported in this work, gold was used. It can be shown that the optimum thickness for surface plasmon excitation in gold is approximately 50nm. This optimum thickness can be calculated theoretically by considering the complex Fresnel coefficients on the three-layer system of glass, metal and air [15-16].

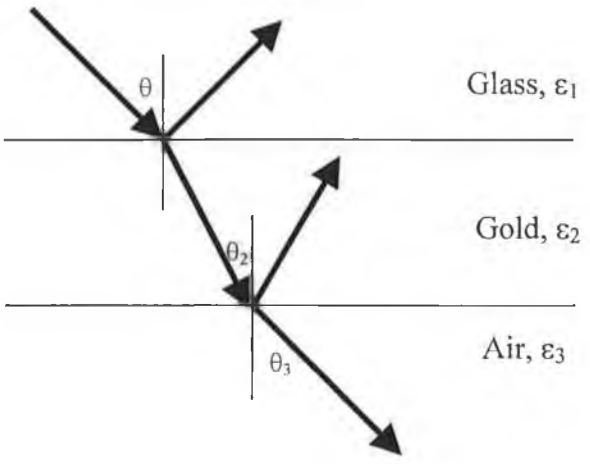

Figure 6.5 Three layer system, showing the reflected and transmitted rays.

The complex Fresnel coefficients of the two interfaces shown in figure 6.5 are given by

$$r_{12} = \frac{\varepsilon_2^{1/2} \cdot Cos\theta_1 - \varepsilon_1^{1/2} \cdot Cos\theta_2}{\varepsilon_2^{1/2} \cdot Cos\theta_1 + \varepsilon_1^{1/2} \cdot Cos\theta_2} \qquad 6.11$$

and

$$r_{23} = \frac{\varepsilon_3^{1/2} \cdot Cos\theta_2 - \varepsilon_2^{1/2} \cdot Cos\theta_3}{\varepsilon_3^{1/2} \cdot Cos\theta_2 + \varepsilon_2^{1/2} \cdot Cos\theta_3} \qquad 6.12$$

where the subscripts 12 and 23 denote the glass/metal and the metal/air interfaces, respectively. The angles θ_2 and θ_3 can be found using the relationships,

$$Cos\theta_2 = \sqrt{1 - \frac{\varepsilon_1}{\varepsilon_2} \cdot Sin^2\theta_1} \qquad 6.13$$

and

$$Cos\theta_3 = \sqrt{1 - \frac{\varepsilon_1}{\varepsilon_3} \cdot Sin^2\theta_1} \qquad 6.14$$

Therefore the reflected amplitude can be found using the expressions,

$$R = \frac{r_{12} + r_{23} \cdot \exp(2i\delta)}{1 + r_{12}r_{23} \cdot \exp(2i\delta)} \qquad 6.15$$

and

$$\delta = 2\pi\sqrt{\varepsilon_2} \cdot Cos\theta_2 \frac{d}{\lambda} \qquad 6.16$$

where d is the thickness of the metal layer and λ is the wavelength of the incident radiation.

The absolute values of the two coefficients represent the ratios of the amplitudes of the electric field in the reflected and transmitted beam to that of the incident beam. Above the critical angle for total internal reflection, the transmitted beam becomes the evanescent wave.

The optimum thickness of a gold layer for surface plasmon resonance to occur can then be calculated, using equations 6.12-6.17. The permittivities of the glass layer (ε_1) and air (ε_3), and the incident radiation (λ) are all known values and can be kept constant. By varying the complex permittivity of the gold layer (ε_2) and the thickness over a range of angles, a model of a surface plasmon curve can be plotted (figure 6.6). As the optimum thickness approaches the curve gets deeper and narrower. Once the optimum thickness has passed, the curve stays narrow but the dip in the curve is reduced.

6.2.2 Theoretical model of SPR curves

Appendix B. contains a program written in Mathematica®3.0 (Wolfram Research) to model the SPR curves that might occur in practice using the TI SPR sensor. The program uses Fresnel's coefficients to predict the SPR curves. The parameters of the gold layer and the sensor included in the program are as follows:

Permittivity of substrate:	2.28 (Refractive Index of glass substrate = 1.512)
Permittivty of gold layer:	-21 + 0.99i
Permittivity of sensing layer:	1.75 (Refractive Index of water = 1.333)
Incident angle range:	58° - 76°
Wavelength of light:	830nm

The program was run for a series of different thicknesses and gold permittivities to illustrate the behaviour of the surface plasmon wave due to the change in thickness and permittivities of the gold layer (figure 6.6)

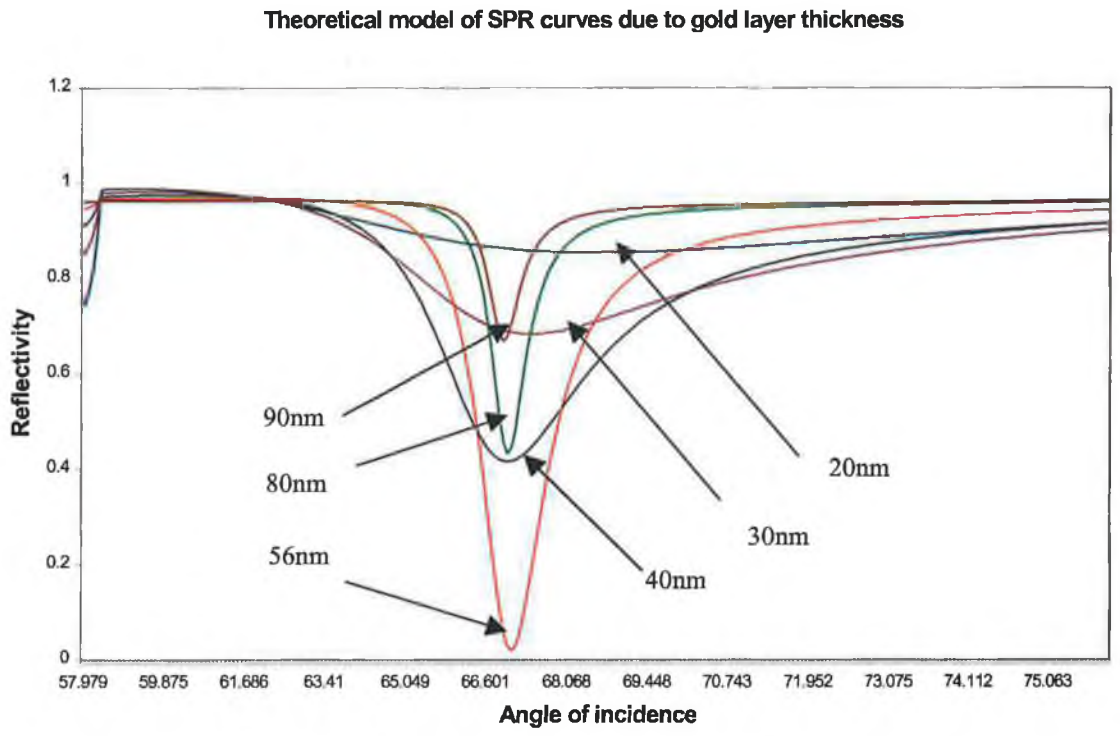

Figure 6.6 Theoretical data of SPR curves for gold layers with different thickness

6.3 Texas Instruments Surface Plasmon Resonance sensor.

The SPR measurement system used in the following experiments was developed by Texas Instruments Inc., Dallas, Texas, USA. It is a pre-commercial sensing system, distributed to research labs for evaluation. The system comprises an integrated miniature, surface plasmon resonance device interfaced to a computer. The sensor combines all the necessary electro-optical components to excite a surface plasmon wave and to quantify the resonance minimum position within a single platform as shown in figure 6.7.

A narrow band LED, which emits light with a peak wavelength of 830nm, is used to excite the surface plasmon wave. This light source is attached to the substrate and is enclosed in an absorbing, apertured box. On top of the apertured box is a polarising film, which removes the transverse electric component of the light, which cannot excite the plasmon wave. The light emitted by the LED falls directly on the underside of the SPR layer (thin gold film) over a range of angles. The light is reflected from the SPR layer onto the reflecting mirror on top of the device, which serves to direct the light onto a linear

detector array. The output signal from the array is connected to a readout electronics box, which is interfaced to a computer. All the analysis is carried out

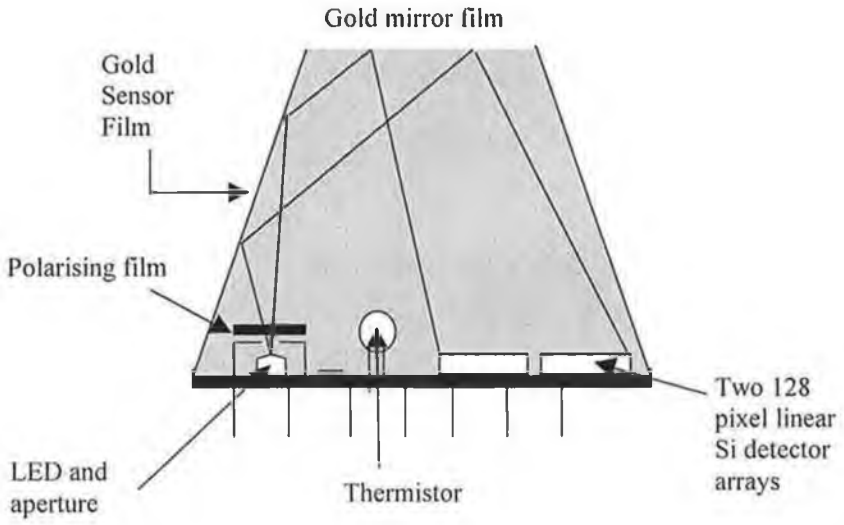

Figure 6.7 Schematic diagram of TI SPR sensor.

using proprietary TI SPR software. The whole assembly is encased in clear epoxy and the side-walls are coated with an opaque film to block out external light.

The angle at which a ray of light is incident upon the thin film is directly mapped onto a specific point on the photodiode array. Depending upon the refractive index of the medium next to the thin gold film, the reflected light intensity will experience a minimum at a particular angle corresponding to where the SPR occurs. Figure 6.10 shows a typical SPR curve measured with this system.

6.3.1. Sensor orientation.

The SPR active surface of the sensor is the long slim surface shown in figure 6.8. The active region is a strip approximately 4.5mm long and 0.025mm wide on the face of the sensor. This region must be completely immersed in the analyte for the sensor to operate properly.

Measurements can be taken by immersing the active sensor surface into a beaker or by dropping a bead of analyte onto the surface. However, for the purpose of the experiments reported here, a flow cell developed by Texas Instruments Inc, Dallas, Texas, USA, was used (figure 6.9).

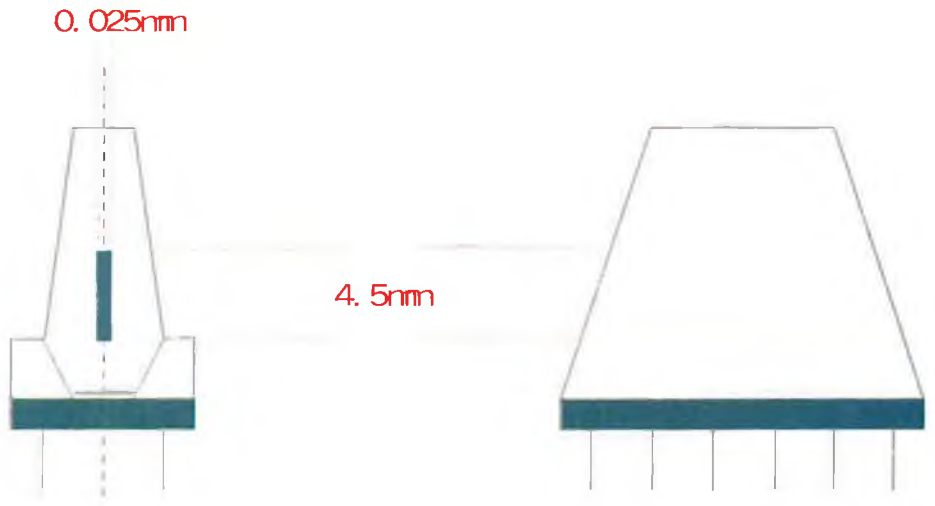

Figure 6.8. Schematic of TI-SPR sensor showing active surface of gold layer.

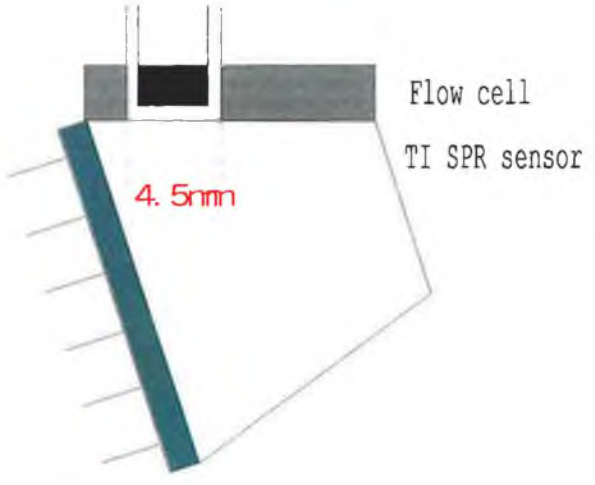

Figure 6.9. TI SPR sensor with flow cell.

6.3.2 Sensor and software operation.

The TI SPR sensor can work in two different modes: (a) single measurement mode; (b) continuous monitoring. There are three measurements that must be made before refractive index measurements can take place. 1. Initialization (In air); 2. Background; 3. Calibration.

Initialization of the sensor in air prepares the sensor for liquid measurements by varying the LED intensity and photodiode integration times to maximize the sensor signal without saturating the output. The records air reference data and verifies that the reflectivity values are close to unity. This air reference is taken while the sensor is dry. Since the index of refraction of air (≈1) is outside the measurement range of the sensor, there will be no resonance curve. The second measurement is the background reference. This is performed with the LED turned off and is necessary because in the dark, the photodiode array has a small response which must be subtracted from all measurements. Background light can come from light entering the sensor through the semi opaque thin gold film. The third measurement is the calibration of a liquid with a liquid of known refractive index. The SPR program can store calibration points. For all measurements taken in the following experiments, the sensor was first calibrated with water, which has a refractive index of ≈1.33.

All three measurements are necessary for the reflectivity to be evaluated. The reflectivity is a measure of the reflected light from the thin gold layer onto the photodiode array. It is calculated using the formula

$$R = \frac{S - B_s}{A - B_a} \qquad 6.17$$

where R is the reflectivity, A is the air reference, and $B_{S/A}$ is the signal background and air background respectively. A plot of signal magnitude (when normalised) vs. pixel position is produced by the program. If an SPR condition exists as in figure 6.10, a minimum will be seen in such a plot. This minimum is calculated by the program using one of four analysis

methods. The position of the SPR curve minimum is the best indicator of the refractive index.

The analysis method used in all the experiments described in this chapter was a method which performs a polynomial fit about the minimum. Figure 6.10 shows the analysis region giving an example of the analysis method which is shown in the top left hand corner.

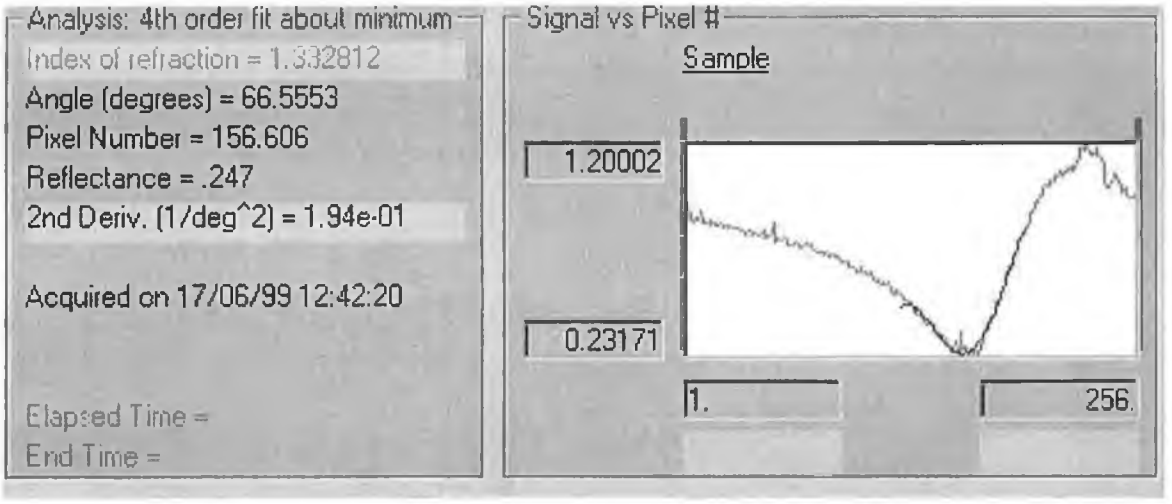

Figure 6.10 Example of SPR curve using TI SPR software.

The polynomial fit about the minimum method makes a first pass of the SPR curve to find the approximate location of the minimum of the resonance. Next it performs an n-th order polynomial least squares fit (using a selectable number of points about the minimum) to interpolate the position of the minimum.

This method is not susceptible to y-axis shifting of the SPR curve. However, since it only uses a relatively small number of points on the curve it can be susceptible to what points are included in the calculation. The order of the polynomial fit is 4 and the number of points in the fit on each side of the minimum was 35 for all experiments.

6.4 Experimentation

A series of experiments was carried out using the Texas Instruments Surface Plasmon Resonance sensor chip. The first objective in these experiments was to calibrate the sensor against a commercial refractometer (Milton Roy tabletop Abbe refractometer 3L) using a range of glycerol fractions in water. The second objective was to observe a change in the refractive index of the layer above the gold layer due to biomolecules binding to it using real time analysis. The possibility of using disposable gold coated chips on the sensor by coating thin glass slides with gold and using them for sensing was also investigated. A theoretical mathematical model was compared with experimental data from these disposable slides and hence the thickness and dielectric permittivities calculated.

6.4.1 Liquid sensing

Glycerol solutions were made up by mixing fixed quantities of glycerol with deionised water. The percentage solutions used in experiments were 50%, 25%, 12.5%, 6.25%, 3.2%, 1.6%, 0.8%, and 0.4%. The solutions were mixed using a magnetic stirrer and stored in closed vials at room temperature when not being used. Prior to use the solutions were stirred again if they had not been used in a while.

The orientation of the sensor chip was as shown in figure 6.11. The sensor chip was plugged into the socket connected to the readout electronics box, and clamped in a retort stand so that the active gold surface was parallel to the bench. The flow cell was then fixed to the sensor chip.

Before any refractive index measurements were taken, the initialisation (in air), background, and calibration (in water) measurements were recorded. All measurements were taken with static samples in this experiment.

Using a 1ml syringe, 0.5ml of a glycerol solution was injected into the flow cell. After introducing the sample to the cell, the inlet and outlet tubes were clamped, in order to prevent any air bubbles entering the cell. A sample measurement was taken and the refractive index of the sample was recorded. Between each two measurements, the flow cell was washed out with deionised water by injecting 2-3mls through the cell.

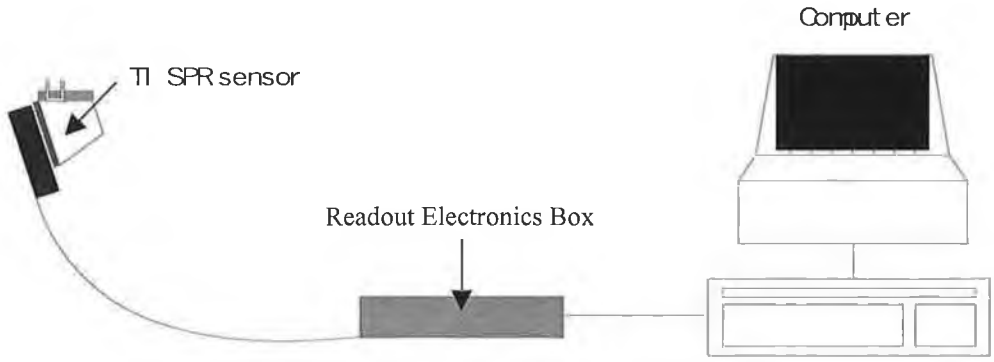

Figure 6.11 TI SPR sensor setup

This procedure was carried out for each of the eight glycerol samples. Twenty measurements of each sample were taken and the average calculated. The refractive index of the same samples was also measured using a Abbe refractometer, and the two sets of results compared with each other. Table 6.1 shows the refractive index values of the glycerol solutions measured by the two systems. Figure 6.12 shows a graph of the two sets of results. The graph shows good agreement in the refractive indices of the glycerol solutions. An important feature is the repeatability of the TI SPR sensor. The refractive indices for the glycerol solutions were reproducible up to the 5^{th} decimal place. This compares well with the commercial Biacore SPR sensor which has a resolution of 3×10^{-7} refractive index units (RIU)[17].

Figure 6.13 shows a real time plot of refractive index of glycerol solutions measured with the TI-SPR. The percentage solutions used were, 0%, 1.25%, 2.5%, 5%, 10%, 20%, 30%, and 40%. These solutions were made up in the same way as before. The plot illustrates the signal to noise ratio, stability and the speed of response of the system. The sensor could not sense any solutions with a refractive index above 1.5 as this was outside the operational range of the sensor.

% Glycerol Solution	TI SPR sensor	Abbe Refractometer
0	1.332348	1.3323
0.4	1.332685	1.3328
0.8	1.333345	1.3335
1.6	1.334026	1.3339
3.2	1.335794	1.3368
6.25	1.339843	1.3398
12.5	1.347738	1.3473
25	1.363942	1.3637
50	1.39174	1.3921

Table 6.1 Refractive Indices of glycerol solutions

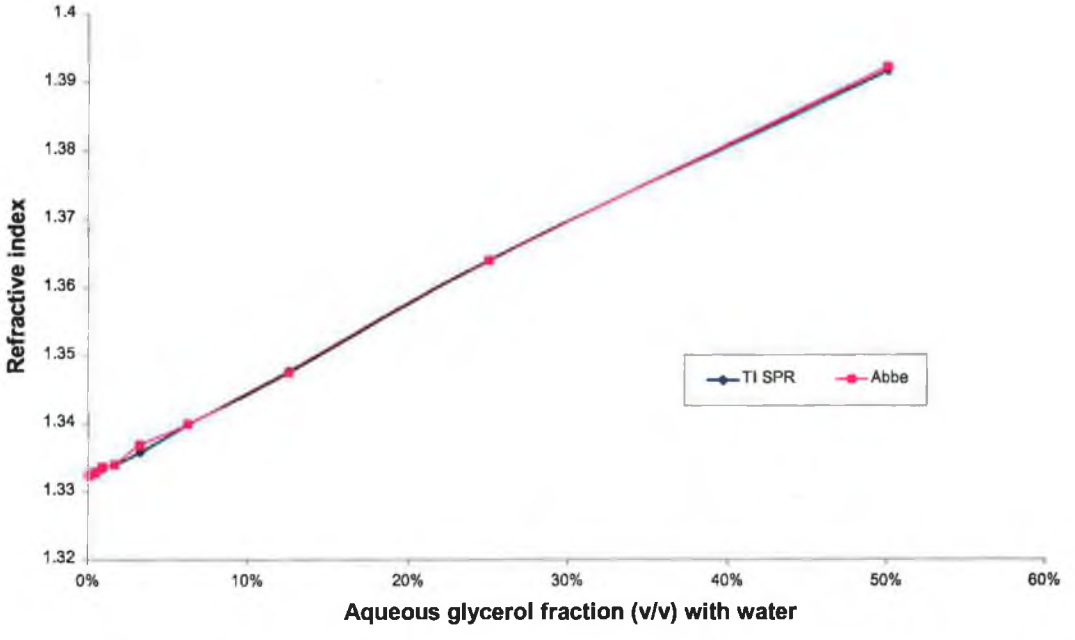

Figure 6.12 Comparison of TI SPR data v's Abbe refractometer data

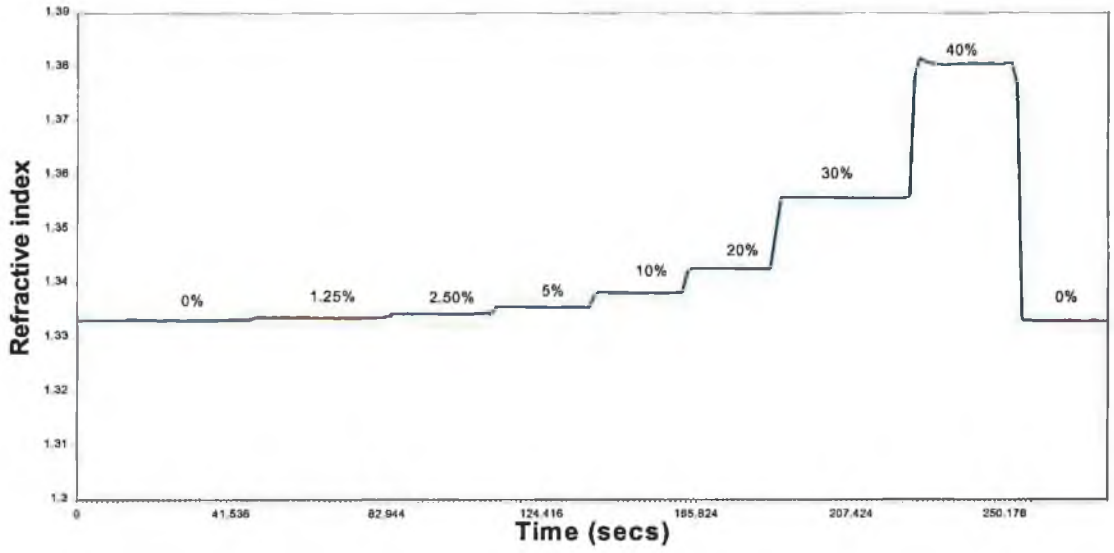

Figure 6.13 Real time analysis of aqueous glycerol fractions in water.

6.4.2 Biomolecule sensing

In the study of immunoreactions[11], a novel hydrogel matrix has been used on the previously mentioned Biacore SPR based sensor. In this case one of the interactants is immobilised on the surface and allowed to interact with compounds flowing over the surface. It is utilised to increase the number of receptors bound to the sensor surface and to increase their activity. In an attempt to examine biomoleculer interactions with the TI-SPR, this type of surface was produced on the gold active surface of the TI SPR in conjunction with Dr John Quinn, School of Biological Sciences, Dublin City University. In this method, carboxymethylated dextran chains are attached, forming a non-crosslinked and flexible hydrogel-like layer. This allows the covalent binding of proteins in a thin layer in the vicinity of the surface rather than immobilisation on the solid surface[12] (figure 6.14).

In summary, the gold film was first modified with a monolayer of 16 mercaptohexadecan-1-ol under conditions of self-assembly. This layer was further

derivatised by epichlorohydrin reaction and coupling of dextran T500 (Pharmacia AB), followed by carboxymethylation with bromoacetate under basic conditions.

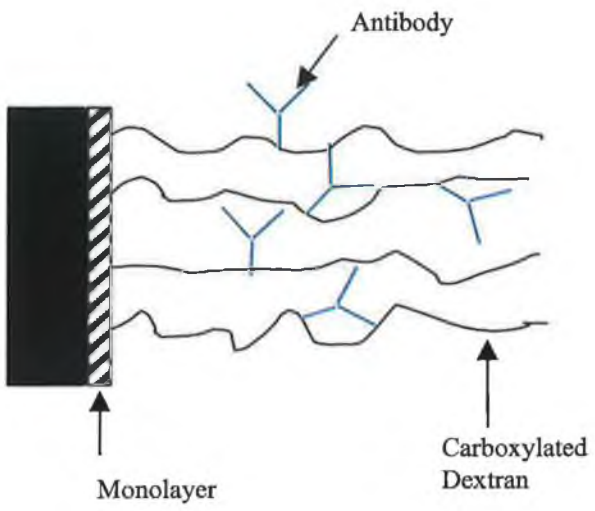

Figure 6.14 Schematic diagram of the modified sensor surface, showing antibodies bound to the dextran hydrogel.

A protein will bind to the dextran matrix if it is in suitable conditions. The protein used in this test was Bovine Serum Albumin (BSA). It was made up with sodium acetate (10mM) and to a pH of 4.5 with acetic acid. The regeneration solution was Phosphate Buffer Saline (PBS) and was made up with deionised water. 0.3M NaCl and some 0.05% tween were added. The BSA at pH 4.5 is positively charged while the COO^- on the dextran matrix is negatively charged. The two are attracted to each other via an electrostatic interaction. The BSA will preconcentrate onto the matrix forming an ionic bond with the dextran matrix. This increases the mass on the layer and thereby increases the refractive index of the layer. The high salt concentration of the PBS will increase the pH in the area, and will change the polarity of the BSA, which will then dissociate from the dextran matrix.

The experiment was performed by injecting static samples into the flow channel while looking at the real time output (figure 6.15). 1ml of deionised water was injected into the flow cell and used as the baseline. After 1min, 0.5ml of the BSA solution was injected into the cell. As the BSA molecules are attracted to the matrix the mass on the gold surface increased, indicated by the change in refractive index on the graph. Once it started to reach a plateau, 1ml of the regeneration solution was injected into the cell. The increase in pH in the flow cell caused the BSA to dissociate from the matrix and this was indicated in the decrease in refractive index. Water again was injected into the system and the output returned to baseline.

Figure 6.15 shows a small change in refractive index between the time the BSA is injected and when it dissociates from the matrix, due to a change in mass on the gold surface. The baseline refractive index for water was higher than 1.333. This was due to the dextran matrix linked to the gold surface.

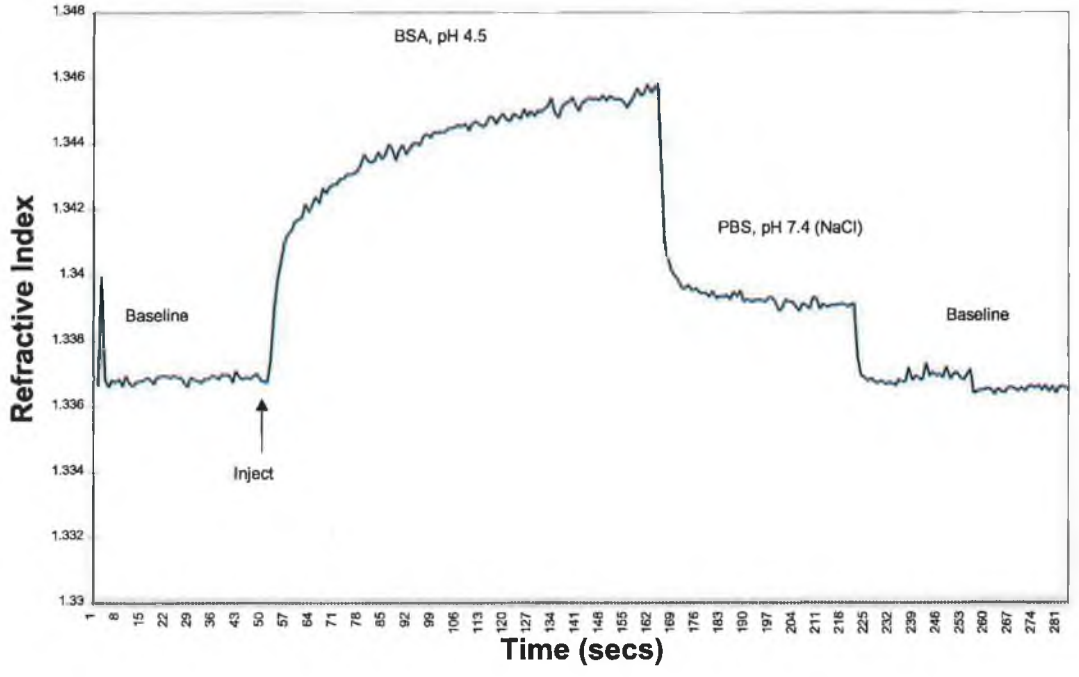

Figure 6.15 Sensorgram of Bovine Serum Albumin concentrating onto hydrogel dextran matrix.

There is a problem with this method of immobilising biomolecules to the sensor surface. The gold layer is adhered to the sensor substrate via a 5nm thick chromium layer. The chromium layer is thin enough to allow the incident light to penetrate to the gold layer. The chemistry involved in adhering the dextran layer, can cause the gold layer to wash off the sensor surface.

6.4.3 Disposable sensor chips

In order to overcome the problem of gold removal, a set of microscope coverslips which were coated with gold for use as disposable chips were examined on the TI SPR sensor. Firstly the gold coating on the TI SPR sensor was removed by polishing with calcined aluminium oxide powder (Logitech, 3 microns). The powder was made into a paste by adding water and mixing. Using Q-tips dipped in the paste, the gold and chromium layers were removed.

6.4.3.1 Coating of slides

The microscope coverslips were 45μm thick and were conditioned sequentially in deionised water, methanol, and acetone. They were stored in deionised water. Prior to coating they were removed from the water and dried at 70°C for 10 minutes.

A thin layer of chromium had to be applied as an adhesion layer. This was evaporated onto the slides using a electron beam evaporator (Edwards Auto 306 vacuum system). Chromium chips (Alfa) were used. These chips were placed in a crucible in the evaporating chamber. The chamber was pumped down to a pressure of 7×10^{-7} mbar. Once the pressure had reached the desired level, the power of the evaporator was turned up to a level of 3kV and 50milliamps. Once the chromium chips had been heated up, the screen was removed and the chromium was evaporated onto the slides above. Chromium was evaporated until the thickness monitor showed a change of 5-10 nm.

The slides were then removed and placed into a sputterer (Edwards S150B cool Sputter Coater) to apply the gold layer. As there was no thickness monitor on the apparatus, a series of slides was coated with gold using different time lengths. SPR curves obtained from the slides were fitted to a theoretical curve in order to determine the gold thickness.

The sputterer was set to a power level of 20kV and 20 milliamps each time. The time lengths were 2, 3, 5, and 7 minutes. The longer the time length the thicker the gold layer. The coated slides were left overnight before use.

6.4.3.2. Comparison of Experimental and Theoretical Data

The gold coated slides were fixed to the TI SPR sensor as previously described for the flow cell. To obtain an SPR curve for the slide, the sensor was used to sense for the refractive index of water. An SPR curve was obtained for each slide. The procedure for this is as previously described.

The coated slides were cut to size to fit over the active area of the TI SPR sensor (5mm × 18mm). They were then fixed to the flow cell using silicone rubber around the edges to prevent any leaks. The side with the gold layer was set facing up into the flow cell. After drying, the flow cell was then fixed to the sensor using a refractive index matching oil.

The Mathematica program was then used to fit a curve to the experimental curve to obtain an estimate of the thickness of gold layer. The thicknesses of the gold layer for the slides coated under the different time lengths 2,3,5, and 7 minutes were found to be 24, 28.5, 33, and 35.3nm respectively. In general the experimental curves were found to be broader than the theoretical curves. This is because the permittivities of the gold layers were not fitted exactly to the experimental curves. This could be due to dependence of the width of the curve on the imaginary component of the dielectric permittivity of the gold layer, which in the Mathematica program was set as -21+0.99i . Even though the sputterer applied a thicker layer as the time length increased, the amount applied per minute was not constant.

6.5 Conclusion

The use of the Texas Instruments Surface Plasmon Resonance sensor as a sensor for liquids and biomolecules was investigated. The sensor is easy to use and can be used to good effect as a refractive index sensor for liquids in the range from 1.2 to 1.5. It gives reproducible results up to the 4^{th} decimal place. It was also shown to be capable of detecting biomolecular interactions due to biomolecules associating themselves onto the surface. The use of disposable sensor chips was also investigated. Gold-coated slides were fixed onto the sensor and it was showed that these could produce useful SPR curves.

References.

1. Otto A, **Excitation of nonradiative surface plasma waves in silver by the method of frustrated total reflection**, Z.Phys., 216,398,1968.

2. Lawerence C.R., Geddes N.J., **Chapter 7: Surface plasmon resonance for biosensing**, Handbook of biosensors and electronic noses, 149-168, 1997, CRC Press, Inc.

3. Kretschmann E, Raether H, **Radiative decay of non-radiative surface plasmons by light**, Z. Naturforsch., 23a, 2135, 1968.

4. Nylander C, Liedberg B, Lind T, **Gas detection by means of surface plasmon resonance**, Sensors and Actuators, 3, 79, 1982/82.

5. Liedberg B, Nylander C, Lundstrom I, **Surface plasmon resonance for gas detection and biosensing**, Sensors and Actuators, 4, 299, 1983.

6. Lawerence C, Geddes N, Furlong D, Sambles J, **Surface plasmon resonance studies of immunoreactions utilising disposable diffraction gratings**, Biosensors and Bioelectronics, Vol 11., No.4, 389-400, 1996.

7. Daniels P.B., Deacon J.K., Eddowes M.J., Pedley D.G., **Surface plasmon resonance applied to immunosensing**, Sensors and Actuators, 15, 11-18, 1988.

8. Liedberg B, Lundstrom I, Stneberg E, **Principles of biosensing with an extended coupling matrix and surface plasmon resonance**, Sensors and Actuators B, 11, 63-72, 1993.

9. Morgan H, Taylor D.M., **A surface plasmon resonance immunosensor based on the streptavidin-biotin complex**, Biosensors and Bioelectronics, 7, 405-410, 1992.

10. Lofas S, Malmquist M, Ronnsberg I, Stenberg E, Liedberg B, Lundstrom I, **Bioanalysis with surfacce plasmon resonance**, Sensors and Actuators B, 5, 79-84, 1991.

11. Geddes N.J., Lawerence C.R., **Chapter 16: Monitoring immunoreactions with SPR**, Handbook of biosensors and electronic noses, 349-368, 1997, CRC Press, Inc.

12. Lofas S, Johnsson B, Tegendal K, Ronnberg I, **Dextran modified gold sensors for surface plasmon resonance sensors: immunoreactivity of immobilised antibodies and antibody-surface interaction studies**, Colloids and surfaces B: Biointerfaces, 1, 83-89, 1993.

13. Furlong C.E., Woodbury R.G., Yee S.S., Chinowsky T., Carr R, Elkind J.I., Kukanskis K.A., Bartholomew D, Melendez J.L., **Fundamental system for biosensor characterisation: application to surface plasmon resonance**, SPIE, Vol. 2836, 208-215

14. Raether H, **Surface plasma oscillations and their applications**, Phys. Thin films, 9, 145, 1977.

15. Boardman A.D., **Chapter 2: Attenuated total reflection analysis of surface polaritons**, Physics Programs, 47-78, John Wiley + Sons Ltd, 1980.

16. Olney R.D., Romagnoli J, **Optical effects of surface plasma waves with damping in metallic thin films**, Applied Optics, Vol. 26, No. 11, 1987.

17. Homola J, Yee S.S., Gauglitz G, **Surface Plasmon Resonance sensors: review**, Sensors and Actuators B, 54, 3-15, 1999.

Chapter 7 Conclusion

Two optical sensor platforms based on evanescent wave interactions for detection of biomolecules are presented. The first describes the immobilisation of fluorescently labelled antibodies onto a mono-mode sol-gel planar waveguide. A compact optics system was also described for the imaging of the evanescently excited fluorescence. Work leading to the use of disposable sensor chips on a pre-commercial surface plasmon resonance (SPR) was also presented.

The theory behind the operation of planar waveguides and grating couplers was presented. The dispersion relation was derived for transverse electric waveguide modes, and was related to important characteristics of the guided modes. These include effective thickness and the penetration depth of the evanescent field into the surrounding media which are important parameters for the use of waveguides in a sensor system. The grating coupling equation was also derived. This was used to determine the required angle of incidence of incident light to convert energy from incident radiation into a guided mode.

The fabrication techniques to produce the waveguides via the sol-gel process were described. The waveguides were fabricated by dip coating a glass slide with a high refractive index sol. The resulting waveguides exhibited low losses while the embossed grating couplers exhibited high coupling efficiencies.

The procedure for the immobilisation of antibodies to the surface of a waveguide was presented. Sol-gel waveguides were coated with a layer of avidin using a covalent binding technique employing a heterobifunctional crosslinker. These waveguides were patterned with two spots of biotinylated antibodies, which were also fluorescently labelled.

The planar waveguides were optically interrogated with a 633nm laser diode. The guided mode evanescently excited the immobilised fluorescently labelled antibodies. The emitted fluorescence was imaged using a compact optical system, employing a GRIN lens array for 1:1 imaging of the fluorescent spots onto a large area, cooled CCD array. Different concentrations of antibodies were immobilised close to a reference spot of a fixed concentration of the same antibody. The resulting images showed two fluorescent spots,

indicating that the immobilisation of the antibodies via the avidin-biotin bridge was a success. The system was calibrated by measuring the fluorescence intensity of signal spot and normalising it against the reference spot. Results indicated almost linear calibration. This data provides evidence of the potential of this technique in assays.

Finally, the theory behind the phenomena of surface plasmon resonance was discussed in detail. Fresnel equations were used to theoretically calculate the optimum thickness of the metal layer, which is very important with respect to the excitation of a surface plasmon wave. The theoretical model of gold layer thickness was discussed and it showed that the optimum thickness was 56nm. A pre-commercial surface plasmon resonance sensor from Texas Instruments was used for liquid refractive index sensing. Results showed good agreement with results from a commercial Abbe refractometer. The sensor was also used in a preliminary investigation of its application to monitoring biomoleculer interactions. Disposable sensor chips were fabricated by coating gold layers onto microscope coverslips and these were characterised in terms of thickness on the TI SPR sensor. SPR curves obtained from the disposable chips were successfully matched to theoretical curves in order to predict their thickness.

Future work based on the results presented in this thesis include obtaining a guided mode with uniform intensity across its width. This could be done by improving the embossing technique, or producing a waveguide free of particles which can cause light to be scattered out of the waveguide.

Future work would also include the performing of assays on the waveguide using the optical system for the detection of evanescently excited fluorescence. This would involve the immobilisation of an antibody (not fluorescently labelled) onto the waveguide surface. Once the analyte has bound to the capture antibody, a fluorescently labelled antibody could then be used as the signal generator in the assay.

Finally, with regard to the surface plasmon resonance sensor, results show that disposable chips do work on the sensor chip. Work should be carried out to produce a chip with gold layer thickness of ≈50nm. Assay should then be performed.

Appendix A Derivation of guidance condition

Since $\partial/\partial t = j\omega$ then

$$\nabla \times \vec{E} = -\mu \frac{\partial H}{\partial t} = -j\mu\omega H \qquad \text{A.1}$$

The curl of the electric field is expressed as

$$(\vec{\nabla} \times \vec{E})_x = \left(\frac{\partial E_z}{\partial y} - \frac{\partial E_y}{\partial z} \right) \qquad \text{A.2}$$

$$(\vec{\nabla} \times \vec{E})_y = \left(\frac{\partial E_x}{\partial z} - \frac{\partial E_z}{\partial x} \right) \qquad \text{A.3}$$

$$(\vec{\nabla} \times \vec{E})_z = \left(\frac{\partial E_y}{\partial x} - \frac{\partial E_x}{\partial y} \right) \qquad \text{A.4}$$

Because transverse electric modes have zero longitudinal electric field along the z axis (E_z=0) then

$$(\vec{\nabla} \times \vec{E})_x = \left(-\frac{\partial E_y}{\partial z} \right) \qquad \text{A.5}$$

$$(\vec{\nabla} \times \vec{E})_y = \left(\frac{\partial E_x}{\partial z} \right) \qquad \text{A.6}$$

$$(\vec{\nabla} \times \vec{E})_z = \left(\frac{\partial E_y}{\partial x} - \frac{\partial E_x}{\partial y} \right) \qquad \text{A.7}$$

Electromagnetic fields in this case are independent of y so $\partial/\partial y$=0. Therefore equations A.5-A.7 become

$$(\vec{\nabla} \times \vec{E})_x = \left(-\frac{\partial E_y}{\partial z} \right) \qquad \text{A.8}$$

$$(\vec{\nabla} \times \vec{E})_y = \left(\frac{\partial E_x}{\partial z} \right) \qquad \text{A.9}$$

$$(\vec{\nabla} \times \vec{E})_z = \left(\frac{\partial E_y}{\partial x} \right) \qquad \text{A.10}$$

Also since $\partial/\partial z = -jk_z$

$$(\vec{\nabla}\times\vec{E})_x = jk_z E_y \qquad \text{A.11}$$

$$(\vec{\nabla}\times\vec{E})_y = -jk_z E_x \qquad \text{A.12}$$

$$(\vec{\nabla}\times\vec{E})_z = \left(\frac{\partial E_y}{\partial x}\right) \qquad \text{A.13}$$

Therefore equations A.11-13 become,

$$-j\omega\mu H_x = jk_z E_y \qquad \text{A.14}$$

$$-j\omega\mu H_y = -jk_z E_x \qquad \text{A.15}$$

$$-j\omega\mu H_z = \frac{\partial E_y}{\partial x} \qquad \text{A.16}$$

Now we assume exponentially decaying fields in regions 1 and 3, and oscillatory behaviour in the case of region 2. These fields are of the form

$$E_y(x,z) = E_1 e^{-\alpha_1 x} e^{-jk_z z} \qquad x>d/2 \qquad \text{A.17}$$

$$E_y(x,z) = E_2 \cos(k_x x + \psi) e^{-jk_z z} \qquad |x| \le d/2 \qquad \text{A.18}$$

$$E_y(x,z) = E_3 e^{-\alpha_3 x} e^{-jk_z z} \qquad x<-d/2 \qquad \text{A.19}$$

where the transverse wavenumbers are defined by the appropriate dispersion relations in each region.

$$\alpha_1 = \sqrt{k_z^2 - \omega^2 \mu_1 \varepsilon_1} \qquad \text{A.20}$$

$$\alpha_1 = \sqrt{k_z^2 - \omega^2 \mu_3 \varepsilon_3} \qquad \text{A.21}$$

$$k_x = \sqrt{\omega^2 \mu_2 \varepsilon_2 - k_z^2} \qquad \text{A.22}$$

Note that each region has a different permeability. This is because the introduction of this will enable the TM mode solutions to be obtained by duality. The constant ψ is present in equation A1.18 because solutions in general are neither even nor odd. Its relationship to the amplitude coefficients E_1,E_2,E_3 is determined from the requirement of continuity of tangential E and H at x=±d/2. From equation A.16 the tangential component of H is obtained from Maxwell's curl equation,

$$H_z(x,z) = \frac{j}{\omega\mu_m}\frac{\partial E_y(x,z)}{\partial x} \qquad m=1,2,3 \qquad \text{A.23}$$

Therefore for x>d/2

$$H_z(x,z) = \frac{-j\alpha_1}{\omega\mu_1} E_1 e^{-\alpha_1 x} e^{-jk_z z} \qquad \text{A.24}$$

For $|x| \leq d/2$

$$H_z(x,z) = \frac{-jk_x}{\omega\mu_2} E_2 Sin(k_x x + \psi) e^{-jk_z z} \qquad \text{A.25}$$

For x<d/2

$$H_z(x,z) = \frac{j\alpha_3}{\omega\mu_3} E_3 e^{\alpha_3 x} e^{-jk_z z} \qquad \text{A.26}$$

Applying the boundary conditions at x=d/2 for both electric and magnetic fields gives ($E_y(x,z)$ for region 1 = $E_y(x,z)$ for region 2)

E_{tan}: $E_1 e^{-\alpha_1 d/2} = E_2 Cos(k_x d/2 + \psi)$ A.27

H_{tan}: $\frac{-j\alpha_1}{\omega\mu_1} E_1 e^{-\alpha_1 d/2} = \frac{-jk_x}{\omega\mu_2} E_2 Sin(k_x d/2 + \psi)$ A.28

which becomes after rearranging,

H_{tan}: $E_1 e^{-\alpha_1 d/2} = \frac{\mu_1 k_x}{\mu_2 \alpha_1} E_2 Sin(k_x d/2 + \psi)$ A.29

The left hand side in both equations A.27 and A.29 are equal. Therefore taking the ratio of these equations yields

$$\frac{E_1 e^{-\alpha_1 d/2}}{E_1 e^{-\alpha_1 d/2}} = \frac{E_2 Cos(k_x d/2 + \psi)}{\frac{\mu_1 k_x}{\mu_2 \alpha_1} E_2 Sin(k_x d/2 + \psi)} \qquad \text{A.30}$$

which yields

$$\tan(k_x d/2 + \psi) = \frac{\mu_2 \alpha_1}{\mu_1 k_x} \qquad \text{A.31}$$

Similarly, matching of boundary conditions at x=-d/2 gives us

$$\tan(k_x d/2 - \psi) = \frac{\mu_2 \alpha_3}{\mu_3 k_x} \qquad \text{A.32}$$

Note that tan x = tan(x±nπ) where n is an integer. Therefore equations A.31 and A.32 can be written as

$$\tan(k_x d/2 + \psi \pm n\pi) = \frac{\mu_2 \alpha_1}{\mu_1 k_x} \quad \text{A.33}$$

$$\tan(k_x d/2 - \psi \pm m\pi) = \frac{\mu_2 \alpha_3}{\mu_3 k_x} \quad \text{A.34}$$

Alternatively the above two equations can be written as

$$k_x d/2 + \psi = \tan^{-1}\left(\frac{\mu_2 \alpha_1}{\mu_1 k_x}\right) \pm n\pi \quad \text{A.35}$$

$$k_x d/2 - \psi = \tan^{-1}\left(\frac{\mu_2 \alpha_3}{\mu_3 k_x}\right) \pm m\pi \quad \text{A.36}$$

or

$$k_x d/2 + \psi = \frac{1}{2}\phi_1^{TE} \pm n\pi \quad \text{A.37}$$

$$k_x d/2 - \psi = \frac{1}{2}\phi_3^{TE} \pm m\pi \quad \text{A.38}$$

where

$$\phi_1^{TE} = 2\tan^{-1}\left(\frac{\mu_2 \alpha_1}{\mu_1 k_x}\right) \quad \text{A.39}$$

$$\phi_3^{TE} = 2\tan^{-1}\left(\frac{\mu_2 \alpha_3}{\mu_3 k_x}\right) \quad \text{A.40}$$

Adding equations A.37 and A.38 to eliminate ψ gives (treating the two as simultaneous equations)

$$2k_x d - \phi_1^{TE} - \phi_3^{TE} = 2p\pi \qquad \text{p=0,1,.....} \quad \text{A.41}$$

For TE modes, by direct substitution for k_x, k_z,ϕ_1^{TE},ϕ_3^{TE},α_1 and α_3 into the guidance equation gives

$$2d\sqrt{\omega^2\mu_2\varepsilon_2 - k_z^2} - 2\tan^{-1}\left(\frac{\mu_2\sqrt{k_z^2 - \omega^2\mu_1\varepsilon_1}}{\mu_1\sqrt{\omega^2\mu_2\varepsilon_2 - k_z^2}}\right) - 2\tan^{-1}\left(\frac{\mu_2\sqrt{k_z^2 - \omega^2\mu_3\varepsilon_3}}{\mu_3\sqrt{\omega^2\mu_2\varepsilon_2 - k_z^2}}\right) = 2p\pi \quad \text{A.42}$$

But $k_z = \omega(\mu\varepsilon_{eff})^{1/2}$, therefore the above equation gives us

$$2d\sqrt{\omega^2\mu_2\varepsilon_2-\omega^2\mu_2\varepsilon_{eff}}-2\tan^{1}\left(\frac{\mu_2\sqrt{\omega^2\mu_2\varepsilon_{eff}-\omega^2\mu_1\varepsilon_1}}{\mu_1\sqrt{\omega^2\mu_2\varepsilon_2-\omega^2\mu_2\varepsilon_{eff}}}\right)-2\tan^{1}\left(\frac{\mu_2\sqrt{\omega^2\mu_2\varepsilon_{eff}-\omega^2\mu_3\varepsilon_3}}{\mu_3\sqrt{\omega^2\mu_2\varepsilon_2-\omega^2\mu_2\varepsilon_{eff}}}\right)=2p\pi \quad \text{A.43}$$

We can now assume that all three regions are magnetically equivalent, i.e. $\mu_1=\mu_2=\mu_3$. Therefore equation A.43 becomes

$$2d\omega\sqrt{\mu}\sqrt{\varepsilon_2-\varepsilon_{eff}}-2\tan^{-1}\left(\sqrt{\frac{\varepsilon_{eff}-\varepsilon_1}{\varepsilon_2-\varepsilon_{eff}}}\right)-2\tan^{-1}\left(\sqrt{\frac{\varepsilon_{eff}-\varepsilon_3}{\varepsilon_2-\varepsilon_{eff}}}\right)=2p\pi \quad \text{A.44}$$

After rearranging this becomes

$$d\omega\sqrt{\mu}\sqrt{\varepsilon_2-\varepsilon_{eff}}=p\pi+\tan^{-1}\left(\sqrt{\frac{\varepsilon_{eff}-\varepsilon_1}{\varepsilon_2-\varepsilon_{eff}}}\right)+\tan^{-1}\left(\sqrt{\frac{\varepsilon_{eff}-\varepsilon_3}{\varepsilon_2-\varepsilon_{eff}}}\right) \quad \text{A.45}$$

The first normalisation to be introduced is the parameter b, which is the normalised guide index

$$b=\frac{\varepsilon_{eff}-\varepsilon_s}{\varepsilon_2-\varepsilon_s} \quad \text{A.46}$$

or this can be represented as

$$\frac{b}{1-b}=\frac{\varepsilon_{eff}-\varepsilon_s}{\varepsilon_2-\varepsilon_{eff}} \quad \text{A.47}$$

Substituting this equation into equation A.45 gives us

$$d\omega\sqrt{\mu}\sqrt{\varepsilon_2-\varepsilon_{eff}}=p\pi+\tan^{-1}\left(\sqrt{\frac{\varepsilon_{eff}-\varepsilon_1}{\varepsilon_2-\varepsilon_{eff}}}\right)+\tan^{-1}\left(\sqrt{\frac{b}{1-b}}\right) \quad \text{A.48}$$

The second normalisation introduced is the parameter a. this is a measure of the asymmetry of the waveguide. The parameter a ranges in value from zero for perfect symmetry and to infinity for strong asymmetry.

For a TE mode

$$a^{TE}=\frac{\varepsilon_3-\varepsilon_1}{\varepsilon_2-\varepsilon_3} \quad \text{A.49}$$

Combining this with equation A.47 gives

$$\frac{b+a^{TE}}{1-b}=\frac{\varepsilon_{eff}-\varepsilon_1}{\varepsilon_2-\varepsilon_{eff}} \quad \text{A.50}$$

Introducing this into equation A.48 gives

$$d\omega\sqrt{\mu}\sqrt{\varepsilon_2 - \varepsilon_{eff}} = p\pi + \tan^{-1}\left(\sqrt{\frac{b - a^{TE}}{1-b}}\right) + \tan^{-1}\left(\sqrt{\frac{b}{1-b}}\right) \quad \text{A.51}$$

The normalised frequency and film thickness is given by[3]

$$V = k_0 d\sqrt{\frac{\varepsilon_2 - \varepsilon_3}{\varepsilon_0}} \quad \text{A.52}$$

Since $k_0 = \omega(\mu\varepsilon)^{1/2}$

$$V = d\omega\sqrt{\mu}\sqrt{\varepsilon_2 - \varepsilon_3} \quad \text{A.53}$$

Using equations A.47 and A.49 we find that

$$V\sqrt{1-b} = d\omega\sqrt{\mu}\sqrt{\varepsilon_2 - \varepsilon_{eff}} \quad \text{A.54}$$

Therefore equation A.54 can be written as

$$V\sqrt{1-b} = p\pi + \tan^{-1}\left(\sqrt{\frac{b - a^{TE}}{1-b}}\right) + \tan^{-1}\left(\sqrt{\frac{b}{1-b}}\right) \quad \text{A.55}$$

This equation fully describes the properties of any guided mode propagating in a planar waveguide.

Appendix B Mathematica Program listing for theoretical model of SPR curves

$\theta_1 = Table[x + 0.069, \{x, 57.979, 75.72, 0.069\}]$ (*Setting incident angle range*)

$\theta_{1a} = \frac{(\theta_1 \times 3.14159)}{180}$ (*Convert degrees to radians*)

$W = Cos[\theta_{1a}]$ (*Finding the Cosine of θ_1*)

$\varepsilon_1 = 2.28$ (*Setting the permittivity of the substrate layer*)

$\varepsilon_2 = -21 + 0.99i$ (*Setting the permittivity of the gold layer*)

$\varepsilon_3 = 1.75$ (*Setting the permittivity of the sensing layer*)

$c = 2.99792458 \times 10^8$ (* The speed off light in vacuum*)

$\lambda = 830 \times 10^{-9}$ (*Wavelength of incident light*)

$\omega = 2 \times \pi \times \frac{c}{\lambda}$ (*Frequency of incident light*)

$d = 56 \times 10^{-9}$ (*Thickness of gold layer*)

$Y = \sqrt{(1 - (\frac{\varepsilon_1}{\varepsilon_2} \times Sin^2[\theta_{1a}])}$ (*Calculating Cos θ_2*)

$Z = \sqrt{(1 - (\frac{\varepsilon_1}{\varepsilon_3} \times Sin^2[\theta_{1a}])}$ (*Calculating Cos θ_3*)

$\delta = 2 \times \pi \times \sqrt{\varepsilon_2} \times Y \times \frac{d}{\lambda}$

$r_{12} = \frac{\sqrt{\varepsilon_2} \times W - \sqrt{\varepsilon_1} \times Y}{\sqrt{\varepsilon_2} \times W + \sqrt{\varepsilon_1} \times Y}$ (*Fresnel first coefficient*)

$$r_{23} = \frac{\sqrt{\varepsilon_3} \times Y - \sqrt{\varepsilon_2} \times Z}{\sqrt{\varepsilon_3} \times Y + \sqrt{\varepsilon_2} \times Z}$$ (*Fresnel second coefficient*)

$$R = Abs\left[\frac{r_{12} + (r_{23} \times Exp(2 \times i \times \delta))}{1 + (r_{12} \times r_{23} Exp(2 \times i \times \delta)}\right]^2$$ (*Calculating the reflectivity*)